Universidade de Lisboa

Faculdade de Farmácia

Effect of tableting-related parameters on the manufacture of oral solid dosage forms containing biologicals

Rúben Martins Fraga

Dissertation supervised by Prof. Dr. João F. Pinto and Prof. Dr. Amrit Paudel

Master in Pharmaceutical Engineering

Confidential

2021/2022

Universidade de Lisboa

Faculdade de Farmácia

Effect of tableting-related parameters on the manufacture of oral solid dosage forms containing biologicals

Rúben Martins Fraga

Dissertation supervised by Prof. Dr. João F. Pinto and Prof. Dr. Amrit Paudel

Master in Pharmaceutical Engineering

Confidential

2021/2022

“The greatest enemy of knowledge is not ignorance; it is the illusion of knowledge.”

(Stephen Hawking)

Abstract

Tablets have been the most popular dosage form in the pharmaceutical market in the last century due to their ease of manufacturing and patient compliance. The interest in oral administration of biologicals, particularly enzymes, is recently growing. Proteins are exposed to different stresses during the production of tablets containing biologics, which may critically impact their biological function and catalytic activity. In this way, saccharides have been used in the formulation as excipients to protect the protein from these adverse conditions. Likewise, this work aimed to study the in-process stability of biologics (during tableting) intended for oral delivery, in which bovine liver catalase was selected as a model protein, and dextran 40, D-mannitol, and trehalose dihydrate were chosen as potential stabilizing excipients. Tablets comprising different ratios of catalase and saccharide (10/90, 30/70 and 50/50) were prepared, and critical protein properties such as activity, the number of particles (due to protein aggregation) and structure (studied via catalase enzymatic assay, micro-flow imaging and attenuated total reflectance Fourier transform infrared spectroscopy, respectively) were evaluated before and after compression. A loss of activity, an increase in the number of particles, and changes in the structure of catalase were observed after compression. Also, after spray-drying the mentioned saccharides and catalase, a loss of activity after tableting was observed, in which the mixtures with mannitol and trehalose preserved the activity of the enzyme during spray-drying. The results were analysed by Principal Component Analysis to reveal a relationship between the formulation materials, process and tablet attributes. A correlation was found between the compression force, activity, and the number of particles, suggesting that the force negatively affects the mentioned properties. The investigation showed the negative effect of compression force on catalase, causing an increase in the number of particles, changes in the structure and a consequent loss of activity in the physical blends with saccharides and with their co-spray-drying, demonstrating that the use of these excipients was not effective to the stabilization of the model protein.

Keywords: biologicals, catalase, saccharides, spray-drying, stability, tableting.

Resumo

Nos últimos séculos, os comprimidos têm sido a forma de dosagem mais popular no mercado farmacêutico, devido à fácil produção e adesão dos pacientes. O interesse em administração oral de produtos biológicos, particularmente enzimas como a catalase, tem crescido recentemente. O estudo desta enzima tem se demonstrado de elevado interesse devido ao seu fácil isolamento dos tecidos e devido às diversas áreas de aplicação. Durante a produção de comprimidos de produtos biológicos, proteínas são expostas a diferentes stresses (mecânicos e termais) que podem ter um impacto crítico na sua função biológica e atividade catalítica, devido ao efeito dos mesmos na estrutura da proteína (formação de agregados e alteração da estrutura secundária). Portanto, durante a produção de comprimidos contendo produtos biológicos, processos como a secagem (p.e., secagem por atomização) ou a compressão poderão afetar negativamente o produto biológico, levando a uma perda da sua eficácia. Desta forma, os sacarídeos têm sido utilizados em formulações como excipientes de forma a proteger a proteína destes efeitos adversos. Existem várias teorias que podem explicar a estabilização de proteínas com uso de sacarídeos, assim como a teoria da vitrificação e a teoria de substituição de moléculas de água. O dextrano, o manitol e a trealose são exemplos de sacarídeos estabilizadores utilizados em formulações, descritos na literatura.

Assim, este trabalho teve como principal hipótese a demonstração do efeito de compressão na atividade de produtos biológicos e tem como objetivos o estudo da estabilidade em processo de produtos biológicos para administração oral, particularmente o entendimento da estabilidade enzimática durante a compressão, a identificação de excipientes estabilizadores, neste caso sacarídeos, que permitam a produção de produtos biológicos e a identificação dos limites em que a atividade enzimática é afetada devido a forças de compressão.

Para este fim, catalase de fígado de bovino foi selecionada como proteína modelo e o dextrano 40, D-manitol e a trealose di-hidratada foram escolhidos como potenciais excipientes estabilizadores. Para esta investigação, comprimidos com diferentes rácios de catalase e sacarídeos (10/90, 30/70 e 50/50) e com diferentes forças de compressão (0,5, 1 e 2 T) foram produzidos, em que alguns comprimidos foram produzidos apenas com uma mistura física e em outros casos a mistura de catalase e do sacarídeo foi seca por atomização deforma a formar uma co-partícula. As propriedades críticas da proteína (em mistura e em comprimido) foram analisadas, em que a atividade biológica, o aumento do número de partículas e a estrutura secundária foram estudados através do ensaio enzimático da catalase, imagem de microfluxo e espectroscopia de reflexão total atenuada no infravermelho com transformada de Fourier, respetivamente. Estas propriedades foram avaliadas antes e após a compressão das misturas incluindo ou não secagem por atomização. Adicionalmente, de forma a estudar as

alterações estruturais das misturas após a secagem por atomização, foi realizada microscopia eletrónica de varredura e dispersão de raios-X de pequeno e amplo ângulo. Para complementar este estudo, foi feita uma Análise do Componente Principal (com as variáveis quantitativas – atividade biológica e número de partículas no intervalo de 25≤x≤50 μm), com o objetivo de observar a possível existência de uma relação entre a forca de compressão e as alterações na atividade biológica, número de partículas e sacarídeos utilizados. Por fim, a análise estatística de Bonferroni foi também utilizada para observar as diferenças entre as diferentes atividades biológicas e número de partículas entre as diferentes misturas com o mesmo rácio.

Após a análise das propriedades referidas foi observada uma diminuição da atividade biológica em todas as misturas após a compressão. Nas misturas e comprimidos apenas com catalase verificou-se o efeito da compressão com a diminuição da atividade e o aumento de número de partículas, onde não foram observadas alterações na intensidade dos picos característicos da Amida II. Nas misturas físicas (em que não foi realizada a secagem por atomização) com dextrano, observou-se estabilidade entre as diferentes forças usadas para o rácio 30/70, mostrando-se o rácio mais estável entre todas as misturas consideradas. Geralmente, nas restantes misturas (manitol e trealose), ocorreu uma diminuição gradual da atividade biológica com o aumento gradual da força utilizada, sugerindo uma relação inversamente proporcional entre a força utilizada e a atividade da catalase. Complementando esta diminuição de atividade, o número de partículas aumentou após a compressão (provavelmente devido à agregação) e alterações na estrutura secundária da proteína foram observadas. A Análise do Componente Principal, confirmou a relação entre a força de compressão e a diminuição da atividade e o aumento do número de partículas, mostrando forte correlação na matriz de correlação e, por último, demonstrou que não existe relação entre o sacarídeo utilizado e estas propriedades. Pela mesma anállise foi demonstrado que no caso de número de partículas o intervalo mais significante foi o de 25≤x≤50μm (em todas as misturas), em que foi encontrada uma correlação mais forte com atividade e força de compressão, em comparação com os outros intervalos. No caso da estrutura secundária, as alterações são mais visíveis na zona da Amida II (onde existem diferentes intensidades de acordo com a mistura e força usada) e na zona característica das ligações O-H, o que poderá significar possíveis alterações de ligações entre a catalase e o sacarídeo.

No caso das misturas em que foi utilizada a secagem por atomização, foi novamente observada a diminuição da atividade biológica, aumento do número de partículas e alterações de estrutura após o processo. Para estas misturas, o dextrano mostrou-se desestabilizador da proteína, sendo que a atividade biológica foi inferior em relação a da mistura física. No caso do manitol a atividade foi ligeiramente inferior e, no caso da trealose a atividade foi igual

à da mistura física. Assim, apenas existiu estabilização com o sacarídeo trealose durante a secagem por atomização. Adicionalmente, o número de partículas aumentou consideravelmente em relação ao número de partículas dos comprimidos com misturas sem secagem por atomização e existiram visíveis alterações na estrutura das misturas. Além das alterações na estrutura secundaria da proteína (semelhantes às referidas anteriormente), ocorreu uma alteração da estrutura cristalina do manitol para uma mistura de estruturas cristalina e amorfa e no caso da trealose ocorreu uma transição de estrutura cristalina para amorfa. Todas as partículas possuem uma superfície com aspeto irregular, contendo covas. Estas alterações de estrutura poderão ter relação direta com a estabilização da proteína. A Análise do Componente Principal foi semelhante à da com as misturas que não foram secas por atomização, observando-se disposição semelhante das amostras nos gráficos e pequenas alterações na matriz de correlação. Desta forma, foi confirmado que a secagem por atomização tem efeito reduzido nas propriedades da proteína, particularmente na atividade biológica.

Concluindo, foi observada uma relação entre a força de compressão, atividade biológica e número de partículas, sugerindo que a força de compressão afeta negativamente as propriedades mencionadas. Especificamente, a força de compressão, provoca mudanças estruturais que podem levar a agregação e por sua vez a uma perda de atividade biológica nas misturas físicas e nas mistura secas por atomização. A utilização de sacarídeos com o objetivo de estabilizar a catalase não se mostrou eficaz durante a compressão das misturas. Esta conclusão contraria a literatura que comprovam poder estabilizador destes sacarídeos durante a aplicação de stresses que afetam a estabilidade da proteína. A teoria hipotetizada foi desta forma confirmada com a observação do efeito negativo da força de compressão na estabilidade da proteína modelo.

Palavras-Chave: catalase, compressão, estabilidade, produtos biológicos, sacarídeos, secagem por atomização.

Acknowledgments

This thesis and the last five years of my life were marked by countless challenges and moments which I shared with several people… and this is my tentative to say thank you.

First of all, I want to thank Prof. Dr. João F. Pinto for giving me the opportunity to do the thesis abroad and for all the help and support over the last months. I would also like to thank Prof. Dr. Amrit Paudel for the support, help, and discussions since October.

For the outstanding work, motivation, patience, help, availability, support, and friendship, I owe my deepest gratitude to my direct supervisors, Dr. Joana Pinto and Dr. Michela Beretta. All the work over the last months would not be possible without your effort.

To the Research Center Pharmaceutical Engineering GmbH (Graz, Austria) for providing the facilities, equipment, materials and human resources to accomplish the experimental work.

To all the people I worked with at RCPE during this period, particularly the Material Science lab team and the Pilot Plant team, thank you for your patience in explaining everything and helping me with the tasks. Thank you to Valon, Aygün, Ozzy, and Patrick for the friendship and good moments.

To the friends I met in Graz that made it easier to be away from home, specifically Gean, Matilde, Andrea, Valentina, Nadine, Alessio, and Anna, I want to express my gratitude for being with me at all the get-togethers and parties. Also, a thank you to everybody I met here who, one way or another helped me in this challenge.

To my friends from Portugal, who have always supported me during the last five years. Particularly to my bestie Leonor for all the precious advice, patience, and the best friendship I could ask for. I would also like to thank Gonçalo, Eduardo, Marina, Maria, and Rondo for everything. To my group of friends from my hometown, Isidro, André, Besteiro, Robalo and Eduardo, that have been with me for many years. Finally, to all my friends who have been with me for the last five years and are an essential part of my life.

I want to express my gratitude to my family. Thanks to my grandparents for all the love and care since I remember that helped to make me what I am today. Thanks to my aunt and uncle, Sandra and Quim, because since I went to Lisbon to start my studies, they were like my second parents that helped me with everything and took care of me as a second child, and for that, I will never be able to show my gratitude in the way that you deserve. To my cousin André, that was as a brother, for all the moments we passed in the last five years (and before) which amused me in several moments.

Last but not least, thanks to my sister Íris for all the love, kindness, and friendship. You are the reason that makes me want to improve every day as a person and give the best of me to you. You are my light. Finally, thank my mum and dad for all their sacrifices since I remember, which allowed me to follow my dreams. If I reach this moment, it is because of you two. I hope that one day I can be half of what you are. I could not ask anything better than you two. Mom, dad, and little sister, I love you.

From the bottom of my heart, thank you all. You are the best.

Abbreviations

API - Active pharmaceutical ingredient

ATR-FTIR - Attenuated total reflectance Fourier transform infrared spectroscopy

BLC - Bovine liver catalase

CAT - Catalase

Cpd I - Compound I

DEX - Dextran

ECD - Equivalent circular diameter

MAN - Mannitol

NADPH - Nicotinamide adenine dinucleotide phosphate

OSD - Oral solid dosage form

PC1 - Principal component 1

PC2 - Principal component 2

PCA - Principal component analysis

Q^2 - Predictive ability

R^2 - Model fit

SD - Spray-drying

SEM - Scanning electron microscopy

STD - Standard deviation

SWAXS - Small- or wide-angle X-ray scattering

T_g - Glass transition temperature

TRH - Trehalose

UV/Vis - Ultraviolet-visible spectroscopy

WAXS - Wide-angle X-ray scattering

Table of Contents

Abstract V
Resumo VII
Acknowledgments XI
Abbreviations XIII
Table of Contents XV
List of Figures XIX
List of Tables XXIII
List of Equations XXIII
1. Introduction 1
1.1 Oral Solid Dosage Forms 1
1.2 Small Molecule Drugs and Biologics 1
1.3 Catalase 3
1.3.1 Historical Overview 3
1.3.2 Catalase-Related Diseases and Therapeutic Role 4
1.3.3 Mechanism of Action 5
1.3.4 Bovine Liver Catalase 6
1.4 In-Process Stability of Proteins 7
1.4.1 Protein Aggregation 8
1.5 Production of Tablets Containing Biologics 10
1.5.1 Primary Manufacture 11
1.5.2 Drying of Biologics 11
1.5.2.1 Spray-Drying 12
1.5.3 Tableting of Biologics 14
1.5.3.1 Compression 14
1.5.4 Coating 17
1.6 Mechanisms supporting the stabilization of biologics by saccharides 18
1.6.1 Background on saccharide stabilization 18
1.6.1.1 Vitrification Theory 18

1.6.1.2 Water Replacement Theory....19
1.6.2 Stabilizing Saccharides....20
1.6.2.1 Dextran....20
1.6.2.2 Mannitol....21
1.6.2.3 Trehalose....21
1.7 Hypothesis, Objectives and Structure of the Thesis....23
1.7.1 Hypothesis....23
1.7.2 Objectives....23
1.7.3 Structure of the Thesis....23
2. Materials and Methods....25
2.1 Materials....25
2.1.1 Model protein and saccharides....25
2.1.2 Other Materials....25
2.2 Methods....26
2.2.1 Preparation of blends....26
2.2.2 Spray-drying....26
2.2.3 Tableting....27
2.2.4 Preparation of solutions....29
2.3 Characterization methods....30
2.3.1 Catalase Activity Assay....30
2.3.2 Micro-Flow Imaging....31
2.3.3 Attenuated Total Reflection Fourier Transform Infrared Spectroscopy....31
2.3.4 Small/Wide-angle X-ray Scattering....32
2.3.5 Scanning Electron Microscopy....33
2.4 Statistical Analysis....33
2.4.1 Principal Component Analysis....33
2.4.2 Bonferroni Correction....34
3. Results and Discussion....35
3.1 Impact of Tabletting on Catalase Activity....35
3.1.1 Tablets with Catalase....35

3.1.2 Tablets with Catalase and Dextran 36
3.1.3 Tablets with Catalase and Mannitol 41
3.1.4 Tablets with Catalase and Trehalose 44
3.2 Impact of Tabletting on the Number of Particles 48
3.2.1 Tablets with Catalase 48
3.2.2 Tablets with Catalase and Dextran 51
3.2.3 Tablets with Catalase and Mannitol 54
3.2.4 Tablets with Catalase and Trehalose 57
3.3 Impact of Tabletting on Catalase Structure 60
3.3.1 Tablets with Catalase 60
3.3.2 Tablets with Catalase and Dextran 62
3.3.3 Tablets with Catalase and Mannitol 66
3.3.4 Tablets with Catalase and Trehalose 69
3.4 Principal Component Analysis 73
3.4.1 Principal Component Analysis of Non-spray-dried Mixtures 73
3.4.2 Principal Component Analysis of Spray-dried Mixtures 78
4. Conclusion 83
5. Future Work 85
6. Bibliography 87
7. Annexes 101
Annex A – Biological Activity Characterization Graphs: UV/Vis 101
Annex A.1 - Absorbance of non-spray-dried CAT mixtures in function of time 101
Annex A.2 – Absorbance of spray-dried CAT mixtures in function of time 102
Annex A.3 – Absorbance of non-spray-dried DEX mixtures in function of time 103
Annex A.4 – Absorbance of spray-dried DEX mixtures in function of time 104
Annex A.5 – Absorbance of non-spray-dried MAN mixtures in function of time 105
Annex A.6 - Absorbance of spray-dried MAN mixtures in function of time 106
Annex A.7 - Absorbance of non-spray-dried TRH mixtures in function of time 107
Annex A.8 - Absorbance of spray-dried TRH tablets in function of time 108
Annex B – Structural Characterization Graphs: ATR-FTIR 109

Annex B.1 – Infrared Absorbance Intensity in function of the wavenumber of raw DEX.....109
Annex B.2 – Infrared Absorbance Intensity in function of the wavenumber of raw MAN 109
Annex B.3 - Infrared Absorbance Intensity in function of the wavenumber of raw TRH.....110
Annex C – Structural Characterization Graphs: SWAXS 111
Annex C.1 – Intensity (counts) in function of 2θ (°) of raw MAN.....111
Annex C.2 - Intensity (counts) in function of 2θ (°) of raw TRH. 112
Annex C.3 - Intensity (counts) in function of 2θ (°) of spray-dried CAT and MAN co-particles. 113
Annex C.4 - Intensity (counts) in function of 2θ (°) of spray-dried CAT and TRH co-particles. 113
Annex D – Structural Characterization Graphs: SEM 115
Annex D.1 – SEM images of the CAT and DEX after Spray-drying.....115
Annex D.2 - SEM images of the CAT and MAN after Spray-drying.....116
Annex D.3 - SEM images of the CAT and TRH after Spray-drying. 117
Annex E – Multivariate analysis: PCA 118
Annex E.1 – Score Plot of the non-spray-dried mixtures, colored according to the saccharide used in the formulation. 118
Annex E.2 - Loading plot of the spray-dried mixtures.....119
Annex E.3 - Correlation matrix of only the spray-dried mixtures.....120
Annex E.4 - Loading Plot of non-spray-dried and spray-dried mixtures.....121

List of Figures

Figure 1 - Timeline of discoveries of catalase. 3
Figure 2 - A: Catalase structure; B: Heme group of catalase with a Fe^{III} in the center. 7
Figure 3 - Major aggregation pathways of proteins. A: Aggregate; N: Native; I: Intermediate; D: Denatured; X1 and X2: Reacted Chemically; P: Precipitated; U: Unfolding intermediates and unfolded states; PS: Protein self-association; CL: Chemical linkages; CD: Chemical degradation. 9
Figure 4 - Schematic representation of protein aggregation. 10
Figure 5 - Process flow during the production of tablets containing biologics. The coating step can be considered optional as it depends on the intended use of the final tablet. 11
Figure 6 - Major phases of spray-drying. The process starts with atomization (I); is followed by the droplet to particle conversion (II); and is finished by particle collection (III). 12
Figure 7 - Steps of compression during tableting. The die is filled with the powder (A). The compression initiates with the movement of the upper punch (B). The maximum compression force is given by (C). The decompression occurs in (D), and the final product is given by (E). 16
Figure 8 - Possible deformations during compression (lamination and capping). 16
Figure 9 - Chemical structure of dextran. 20
Figure 10 - Chemical structure of mannitol. 21
Figure 11 - Chemical structure of trehalose. 22
Figure 12 - Enzymatic activity of non-spray-dried and spray-dried CAT mixtures, as a blend and after compression and respective Bonferroni statistical analysis. Legend: A – Non-spray-dried blend and tablets; B – Spray-dried co-particle and tablets; C – Bonferroni statistical analysis. 36
Figure 13 - **Enzymatic activity of non-spray-dried and spray-dried DEX mixtures, as a blend and co-particle before and after compression.** Legend: A – 10/90 ratio; B – 30/70 ratio; C – 50/50 ratio; D – 30/70 spray-dried ratio. 38
Figure 14 - Bonferroni statistical analysis of the activity of the non-spray-dried and spray-dried DEX mixtures as a blend and after compression. Legend: A – Non-spray-dried tablets with different ratios; B – Non-spray-dried and spray-dried blend, co-particle and tablets with 30/70 ratio. 40
Figure 15 - Enzymatic activity of non-spray-dried and spray-dried MAN mixtures, as a blend and co-particle before and after compression. Legend: A – 10/90 ratio; B – 30/70 ratio; C – 50/50 ratio; D – 30/70 spray-dried ratio. 42
Figure 16 - Bonferroni statistical analysis of the activity of the non-spray-dried and spray-dried MAN mixtures as a blend and after compression. Legend: A – Non-spray-

dried tablets with different ratios; B – Non-spray-dried and spray-dried blend, co-particle and tablets with 30/70 ratio.....43
Figure 17 - Enzymatic activity of non-spray-dried and spray-dried TRH mixtures, as a blend and co-particle before and after compression. Legend: A – 10/90 ratio; B – 30/70 ratio; C – 50/50 ratio; D – 30/70 spray-dried ratio. 46
Figure 18 - Bonferroni statistical analysis of the activity of the non-spray-dried and spray-dried TRH mixtures as a blend and after compression. Legend: A – Non-spray-dried tablets with different ratios; B – Non-spray-dried and spray-dried blend, co-particle and tablets with 30/70 ratio.....47
Figure 19 – Number of non-spray-dried and spray-dried particles of the CAT blend, co-particle and tablets. Legend: A – Non-spray-dried CAT mixtures; B – Spray-dried CAT mixtures. 49
Figure 20 - Bonferroni statistical analysis of the number of particles in the 25≤x≤50 µm range, of CAT mixtures, as a blend, co-particle and after compression. Legend: A – Non-spray-dried CAT mixtures; B – Spray-dried CAT mixtures. 50
Figure 21 - Number of non-spray-dried and spray-dried particles of the DEX blend, co-particle and tablets. Legend: A – Non-spray-dried DEX mixtures; B – Spray-dried DEX mixtures. 52
Figure 22 - Bonferroni statistical analysis of the number of particles in the 25≤x≤50 µm range, of spray-dried DEX mixtures, as a blend, co-particle and after compression. Legend: A – Non-spray-dried DEX mixtures; B – Spray-dried DEX mixtures. 53
Figure 23 - Number of non-spray-dried and spray-dried particles of the MAN blend, co-particle and tablets. Legend: A – Non-spray-dried MAN mixtures; B – Spray-dried MAN mixtures. 55
Figure 24 - Bonferroni statistical analysis of the number of particles in the 25≤x≤50 µm range, of spray-dried MAN mixtures, as a blend, co-particle and after compression. Legend: A – Non-spray-dried MAN mixtures; B – Spray-dried MAN mixtures. 56
Figure 25 - Number of non-spray-dried and spray-dried particles of the TRH blend, co-particle and tablets. Legend: A – Non-spray-dried TRH mixtures; B – Spray-dried TRH mixtures. 58
Figure 26 - Bonferroni statistical analysis of the number of particles in the 25≤x≤50 µm range, of spray-dried TRH mixtures, as a blend, co-particle and after compression. Legend: A – Non-spray-dried TRH mixtures; B – Spray-dried TRH mixtures. 59
Figure 27 - ATR-FTIR spectrums (600-3700 cm^{-1}) of CAT as a blend, co-particle before and after compression. Legend: A – Non-spray-dried CAT blend (raw material); B – Non-spray-dried CAT tablets (after compression); C – spray-dried co-particle and tablets of CAT,.....62

Figure 28 - ATR-FTIR spectrum (600-3700 cm^{-1}) of DEX mixtures as a blend. 63
Figure 29 - ATR-FTIR spectrums (600-3700 cm^{-1}) non-spray-dried and spray-dried DEX mixtures, as a blend, co-particle and after compression. Legend: A – 10/90 ratio; B – 30/70 ratio; C – 50/50 ratio; D – 30/70 spray-dried ratio. 65
Figure 30 - ATR-FTIR spectrum (600-3700 cm^{-1}) of MAN mixtures as a blend......66
Figure 31 - ATR-FTIR spectrums (600-3700 cm^{-1}) non-spray-dried and spray-dried MAN mixtures, as a blend, co-particle and after compression. Legend: A – 10/90 ratio; B – 30/70 ratio; C – 50/50 ratio; D – 30/70 spray-dried ratio. 69
Figure 32 - ATR-FTIR spectrum (600-3700 cm^{-1}) of TRH mixtures as a blend. 70
Figure 33 - ATR-FTIR spectrums (600-3700 cm^{-1}) non-spray-dried and spray-dried TRH mixtures, as a blend, co-particle and after compression. Legend: A – 10/90 ratio; B – 30/70 ratio; C – 50/50 ratio; D – 30/70 spray-dried ratio. 72
Figure 34 - Loading Plot of the PCA of the non-spray-dried mixtures......75
Figure 35 - Score Plot of the PCA of the non-spray-dried mixtures (Colored according to the force used in the formulation)......76
Figure 36 - Score Plot of the PCA only of the spray-dried mixtures (Colored according to the force used in the formulation)......80
Figure 37 - Score Plot of the PCA of all the mixtures (Colored according to the force used in the formulation)......81

List of Tables

Table 1 - Comparison between the size of small molecule drugs, aspirin, and biologics, Human Growth Hormone, and Immunoglobulin G.....2
Table 2 - Disorders associated with catalase deficiency......4
Table 3 - Catalase and saccharides used in the experimental work......25
Table 4 – Other materials used in the experimental work......25
Table 5 - Mixtures considered for drying (spray-drying)......26
Table 6 - Mixtures of CAT and saccharides......28
Table 7 - Correlation matrix of PCA of all the non-spray-dried mixtures......77
Table 8 - Correlation matrix of PCA of all the mixtures.....82

List of Equations

Equation 1 - Decomposition of hydrogen peroxide to water and oxygen, catalyzed by catalase.....5
Equation 2 - Catalase's oxidation to Compound I.....5
Equation 3 – Reaction of Compound I with water.....5
Equation 4 – Equation for the calculation of CAT relative activity.....30

1. Introduction

1.1 Oral Solid Dosage Forms

The need for convenient dosage forms dates back to the early beginnings of medicine (Wilkinson, 1971). Since the 19th century, oral solid dosage forms (OSDs) have been the most popular dosage forms in the pharmaceutical market, mainly due to the easy and simple administration, which has led to high patient compliance and the high cost-effectiveness related to its manufacturing process (Almukainzi et al., 2014; Sefidani Forough et al., 2018).

An OSD consists of a final drug product - tablet, capsule, soft gel, sachet, pill, among others – that, by being ingested through the mouth and dissolved in the gastrointestinal tract, is delivered to the body through bloodstream absorption. Tablets are among the most common OSDs and are constituted by an active pharmaceutical ingredient (API) and other powder ingredients, known as excipients (CBR, 2022).

Tablets can differ in mass, hardness, size, shape, thickness, dissolution, and disintegration characteristics. Depending on their intended use, different types of tablets exist, such as compressed tablets, coated tablets, effervescent tablets, enteric-coated tablets, chewable tablets, and buccal and sublingual tablets, besides others (Ubhe & Gedam, 2020).

1.2 Small Molecule Drugs and Biologics

The attempt to treat diseases led to the continuous discovery and development of new compounds. Generally, these therapeutic entities can be divided into two main groups: small chemical molecules and biologics (or biologicals). The main difference between these two is related to their molecular mass and respective manufacturing process (Makurvet, 2021; Ngo & Garneau-Tsodikova, 2018).

Small molecule drugs are produced by chemical synthesis. As the name indicates, this drug category is smaller than biologics, with a range between 0.1 and 1 kDa and a simple chemical structure. Examples of small molecules are aspirin, procaine, and felbamate, among others (Makurvet, 2021).

In contrast, biologics are derived from biological processes, such as fermentation (Makurvet, 2021; Tusé et al., 2014). Biologics are complex molecules, with a size usually higher than 1 kDa, formed by carbohydrates, cells, nucleic acids, proteins, or a complex comprised of these substances. Examples of biologics include vaccines, hormones, recombinant therapeutic

proteins, insulin, and monoclonal antibodies, among others (Makurvet, 2021). Table 1 compares the size between both small molecule drugs and biologics:

Table 1 - Comparison between the size of small molecule drugs, aspirin, and biologics, Human Growth Hormone *(Adapted from Simon, 2014),* ***and Immunoglobulin G*** *(Adapted from Pasieka, 2016).*

Small Molecule Drug	**Biologics**	
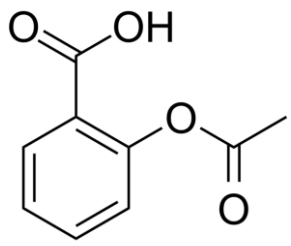	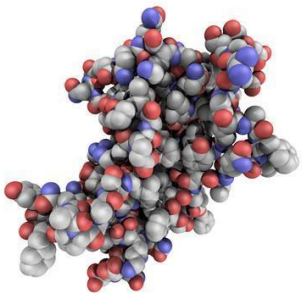	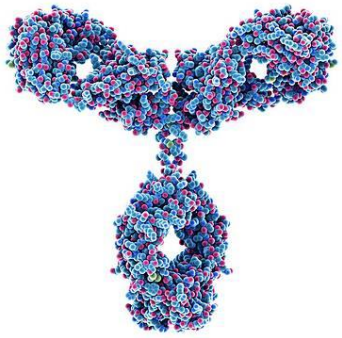
Aspirin	Human Growth Hormone	Immunoglobulin G
21 atoms	~3000 atoms	~35000 atoms

Contrary to small molecule drugs that can easily resist the stresses subjected during the manufacturing process, biologics are more sensitive to instabilities during handling. More specifically, biologics are sensitive to changes in pH, temperature, ionic strength, and chemical and mechanical stimuli. Variations in these factors can cause several forms of degradation, such as hydrolysis, aggregation, denaturation, oxidation, and isomerization. To avoid or decrease the rate of degradation, several control methods are generally employed: (I) transport and cold chain storage; (II) use of compatible buffers and excipients during formulation; (III) freeze and spray-drying in the production of OSD (Chauhan et al., 2020). Furthermore, the complex structure of biopharmaceuticals makes the clinical effects hard to predict due to the difficulty in characterizing their structure (Makurvet, 2021).

These drawbacks are overcome by the potential of biopharmaceuticals to afford higher pharmacodynamics specificity and therapeutic efficacy. As a result, the research and development of new biological products are rapidly growing. In 2016, around 50 % of the new chemical entities approved by the Food and Drug Administration were biologics. In addition, a growth of 9.5 % per year is expected in the biologics market (Chauhan et al., 2020).

The oral administration of biologics, particularly enzymes, usually targets treating inflammatory diseases, such as exocrine pancreatic insufficiency or enzyme intolerance. According to their

intended delivery site, different approaches must be considered during the tablet formulation and production (e.g., gastric-resistant coating) (Alothman et al., 2021; Makurvet, 2021; New, 2020).

In the present investigation, bovine liver catalase (BLC) was chosen as a model enzyme to explore the tableting processability of biologics for replacement enzymatic therapies through oral delivery.

1.3 Catalase

1.3.1 Historical Overview

The first report of catalase (CAT) can be traced back to the 19th century when hydrogen peroxide (H_2O_2) was discovered and suspected to induce tissue degradation in organisms. Since that discovery, several important findings have been reported, such as the detection of the iron atom in catalase's active center and the identification of compound I (Cpd I), among others. The timeline shown in Figure 1 represents the main discoveries related to CAT (Glorieux & Calderon, 2017):

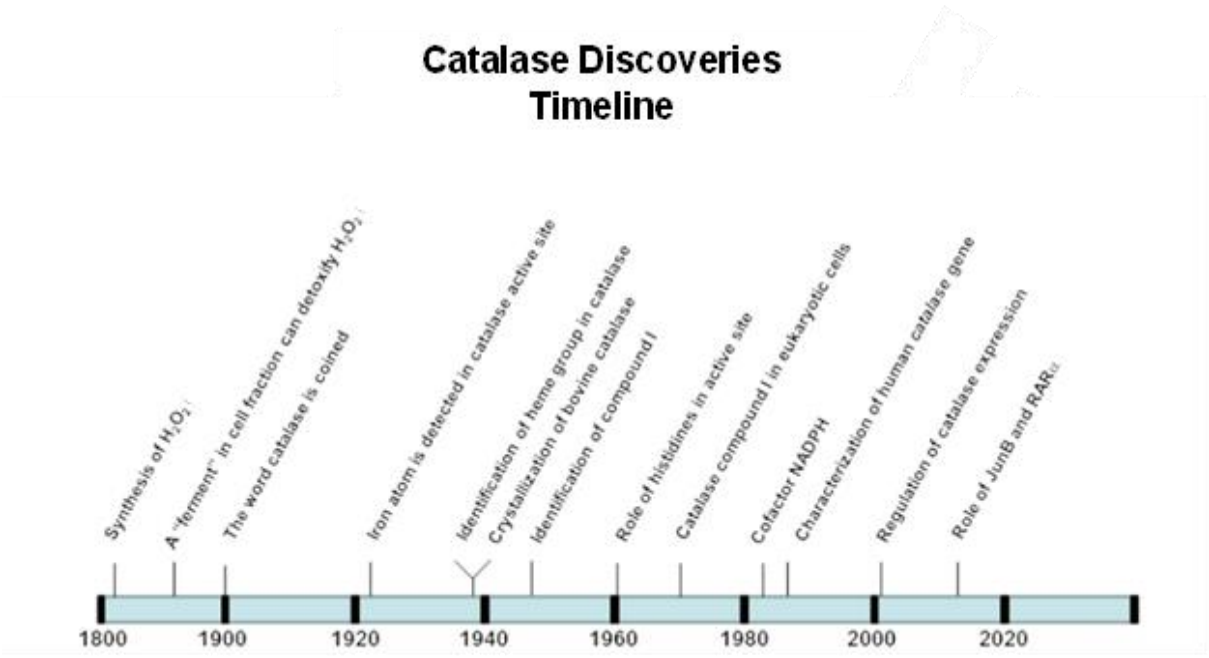

Figure 1 - Timeline of discoveries of catalase. *Adapted from Glorieux & Calderon, 2017.*

Catalases (EC 1.11.1.6 - Oxidoreductase) are divided into three distinct groups: (I) typical or true catalases; (II) catalase-peroxidase; and (III) manganese catalases. Both typical catalase and catalase-peroxidase groups contain a heme group in their active center, while the

manganese group catalase has a manganese group in the active center. The typical catalase group is the largest group, which is present in almost all aerobic organisms (Glorieux & Calderon, 2017; Sepasi Tehrani & Moosavi-Movahedi, 2018; Yuzugullu Karakus, 2020). The CAT structure has been studied extensively due to its easy isolation from tissues and interest in several applications, e.g., food and textile processing (Liu & Kokare, 2017) and pharmaceutical drugs (Nandi et al., 2019).

1.3.2 Catalase-Related Diseases and Therapeutic Role

Many diseases are related to catalase deficiency or malfunctioning, such as neurological and metabolic disorders, among others (Table 2). These disorders are associated with genetic variations in the CAT gene and its promoter region, which can cause a loss of activity and low levels of CAT (Ahn, 2006; Nandi et al., 2019).

Table 2 - Disorders associated with catalase deficiency.

Neurological	Alzheimer's and Parkinson's disease; Bipolar disorders.
Metabolic	Type I and II diabetes; Hypertension; Osteoporosis.
Other	Cancer; Anemia; Acatalasemia.

Since CAT has an essential role in decomposing H_2O_2 into innocuous products (Equations 1, 2, and 3 in Section 1.3.3), it is used to treat several oxidative stress-related disorders. The main challenge is the delivery of the enzyme to the correct site and within the right quantities (Nandi et al., 2019). In this way, several techniques to deliver CAT to the organism have been used, such as poly(lactic-co-glycolic acid) nanoparticles (Nandi et al., 2019), hydrogels, 3D printing products (Chauhan et al., 2020), and tablets (Alothman et al., 2021). During the development, production, and delivery of biologic drug formulations, new drawbacks arise, such as the effect of shear stress in CAT (Bekard et al., 2011; Charm & Wong, 1981).

1.3.3 Mechanism of Action

CAT degrades the hydrogen peroxide into water and oxygen and protects the cell against oxidative stress as a natural antioxidant. With this function, catalase plays an essential role in preventing apoptosis, inflammation, mutagenesis, and stimulation of a broad spectrum of tumors. As represented by the following equation, CAT transforms two moles of hydrogen peroxide into two moles of water and one mole of oxygen (Equation 1) (Alfonso-Prieto et al., 2009). Under optimal conditions, each subunit of CAT can decompose up to 2 x 10^5 moles of H_2O_2, making it one of the enzymes with the highest turnover rates known (Alothman et al., 2021). These high turnover rates can indicate the existence of both inlet and outlet paths to avoid interference of incoming hydrogen peroxide and exhausting oxygen during the decomposition of H_2O_2 (Goyal & Basak, 2010).

$$2\,H_2O_2 \rightarrow 2\,H_2O + O_2 \qquad \textit{(Equation 1)}$$

The degradation reaction of hydrogen peroxide (Equation 1) is divided into two steps (Glorieux & Calderon, 2017):

(I) The first step involves catalase's oxidation to a hypervalent iron intermediate, denominated as Cpd I. During this stage, the heme protein is oxidized by one hydrogen peroxide molecule, forming an oxoferryl porphyrin cation radical, Cpd I: Equation 2.

$$Enz\,(Porf\text{-}Fe^{III}) + H_2O_2 \rightarrow Cpd\ I\,(Porf^{\bullet+}\text{-}Fe^{IV}{=}O) + H_2O \qquad \textit{(Equation 2)}$$

(II) Once the Cpd I is formed, it quickly reacts with one molecule of H_2O_2, and a molecule of O_2 and H_2O is generated in a two-electron redox process: Equation 3.

$$Cpd\ I\,(Porf^{\bullet+}\text{-}Fe^{IV}{=}O) + H_2O_2 \rightarrow Enz\,(Porf\text{-}Fe^{III}) + H_2O + O_2 \qquad \textit{(Equation 3)}$$

The substitution of Equation 2 into Equation 3 results in Equation 1.

The heme group of catalase plays an essential role during the reactions since Fe^{III} bounded at the center of the porphyrin ring can be oxidized to Fe^{IV} or ferryl species. This reaction can be improved by the presence of an iron ligand in the heme group, such as tyrosine (Goyal & Basak, 2010).

CAT is an important nicotinamide adenine dinucleotide phosphate (NADPH) binding protein. The role of NADPH on CAT structure is not well understood, however, three theories were proposed. The first theory consists of NADPH decreasing the susceptibility of CAT, so when there are low concentrations of hydrogen peroxide, the enzyme is inactivated. The second theory is more focused on BLC and considers that NADPH is a remnant of a system that plays the role of an intermediary. Finally, samples of purified bovine liver and human catalase were found to bind and release NADPH, indicating that CAT can act as a regulatory protein, releasing $NADP^+$ to the cellular media when the cell is under peroxidative stress (Goyal & Basak, 2010).

Regarding inhibition, the reaction of oxidation by H_2O_2 does not directly affect the active site of CAT, however, it can lead to conformational changes through the oxidation of amino acid residues (necessary during catalysis). In addition, binding cyanide blocks access to the heme group to other iron ligands. Furthermore, exogenous nitric oxide can inhibit CAT activity, even though this effect is reversible (Goyal & Basak, 2010).

1.3.4 Bovine Liver Catalase

Bovine liver catalase belongs to the group of typical CAT and is a ubiquitous tetrameric enzyme constituted by four identical subunits of 60 kDa (Figure 2 – A). Each subunit contains a heme group (Figure 2 – B) and an NADPH in its active center (Lennarz & Lane, 2013; Nandi et al., 2019; RCSB-PDB, 2022; Scibior & Czeczot, 2006).

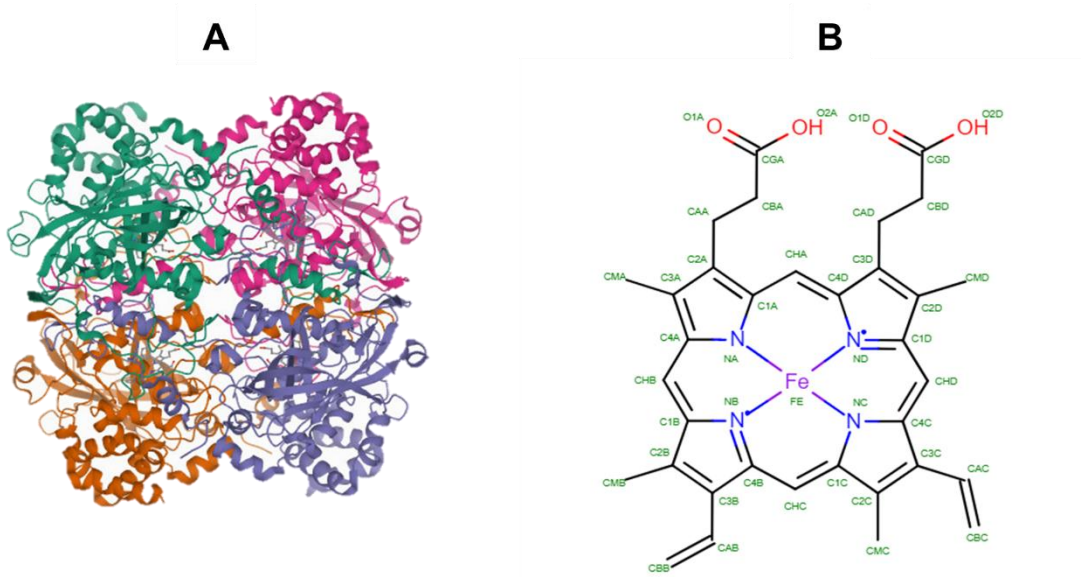

Figure 2 - A: Catalase structure; B: Heme group of catalase with a Fe^{III} in the center. *The green letters in Figure B represent the designation of the carbon. Adapted from "RCSB-PDB", 2022.*

BLC's secondary structure is comprised of 26% of α-helix and 12% of β-sheets (Dunford, 1982; Zeeshan et al., 2019). Zeeshan et al., investigated the impact of secondary structure changes and thermal stress when CAT was in the solid and aqueous solution. A correlation between the changes in the secondary structure and the loss of biological activity for both aqueous solution and solid protein was found. The biological activity was entirely lost in the aqueous solution state, and a minor loss of activity was observed in the solid state (Zeeshan et al., 2019). The results of this study indicate a correlation between the secondary structure of CAT and its biological activity. Furthermore, Wurster & Ternik reported a negative influence of compression pressure on catalase biological activity (Wurster & Ternik, 1995).

1.4 In-Process Stability of Proteins

Proteins are exposed to different environments and conditions during bioprocessing. These physicochemical environments have a critical significance in the protein structure and function due to the low energy threshold between the denatured and native state (Bekard et al., 2011). These alterations in the protein conformation can result in changes in biological function or catalytic activity (Bekard et al., 2011; Zeeshan et al., 2019) and protein aggregation (Chiti & Dobson, 2006; Dobson, 2003).

Protein degradation can be classified into physical or chemical degradation. Physical degradation mechanisms such as denaturation and non-covalent degradation are the most

common and consist of unfolding the protein's three-dimensional structure. In the native state, the hydrophobic parts of the protein are generally folded inward. When perturbations that can lead to the unfolding or denaturation occur, the hydrophobic groups are exposed to the outside of the three-dimensional protein's structure and can cause adsorption or non-covalent aggregation. Usually, this type of degradation occurs in the liquid state, however, it can also happen during the solid state. In turn, chemical degradation mechanisms are covalent aggregation, oxidation, deamidation, and Maillard browning. The last three referred mechanisms depend on the moisture content (Mensink et al., 2017).

Structural perturbations of proteins can result from different pH, temperature, ionic strength, and the presence of denaturants or organic solvents. Furthermore, these structural perturbations can also result from the exposition of hydrodynamic shear forces of mixing, shaking, vortexing, and flow through conduits (Bekard et al., 2011; Emami et al., 2018; Mensink et al., 2017; Rohs et al., 1999).

Interest in the degradation induced by shear stress is growing since it is a common consequence during bioprocessing. In this case, the handling of the biotherapeutics or the different steps during the bioprocessing, such as centrifugation or pumping, have critical importance in the protein structure (Bekard et al., 2011). Furthermore, these perturbations can also occur during the tableting of biologics due to the exposure to shear, thermal and mechanical stress (Wei et al., 2019).

1.4.1 Protein Aggregation

Due to the increase in the number of biologics in the pharmaceutical market, protein aggregation has become an essential focus of study. The extent of aggregation depends on several factors, such as the intrinsic (protein structure) and extrinsic (processing conditions, physicochemical environment, among others) (Wang et al., 2010).

The aggregates can be formed through different mechanisms, which can be divided into: (I) unfolding intermediates and unfolded states - U; (II) chemical linkage – CL - or protein self-association - PS; and (III) chemical degradation - CD. Figure 3 represents the major aggregation pathways (Wang et al., 2010):

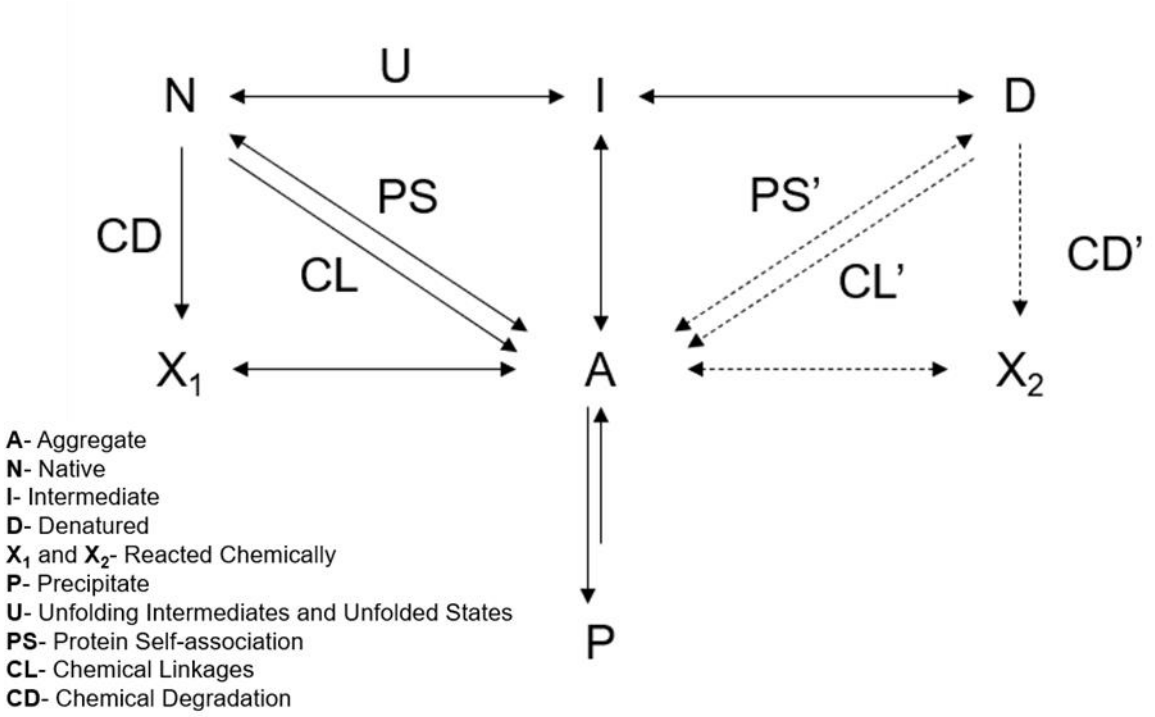

Figure 3 - Major aggregation pathways of proteins. *A: Aggregate; N: Native; I: Intermediate; D: Denatured; X1 and X2: Reacted Chemically; P: Precipitated; U: Unfolding intermediates and unfolded states; PS: Protein self-association; CL: Chemical linkages; CD: Chemical degradation. Adapted from Wang et al., 2010.*

On the one hand, some pathways are reversible (Figure 3), meaning that some proteins could disaggregate in equilibrium or conditions that revert the aggregation (different pH, and temperature, besides others). On the other hand, pathways such as the CD, CL, CD', CL', and the paths between A and P are not reversible (Wang et al., 2010). In the solid state, chemical covalent aggregation is a more predominant route of aggregation rather than physical non-covalent aggregation. In the solid state, chemical aggregation is accelerated by exposure to atmospheric water or residual moisture and, in most cases, is linked to a thiol-disulfide interchange (Mensink et al., 2017).

Aggregates can range in: (I) size, from visible particles to dimers; (II) linking, with non-covalent or covalent linkages; (III) structure, with ordered or disordered structure; (IV) solubility; and (V) reversibility (Ratanji et al., 2013). When the size of the aggregates increase, sedimentation may occur (Mensink et al., 2017).

Figure 4 is a schematic representation of protein aggregation, considering the aggregate's size and structure (Ratanji et al., 2013). Stresses derived from bioprocessing can trigger protein aggregation. The aggregation starts with the association of two or more protein molecules. This association results in the formation of oligomers, which in turn, can form subvisible particles. These subvisible particles can be amorphous or linear (crystalline) and can form visible particles:

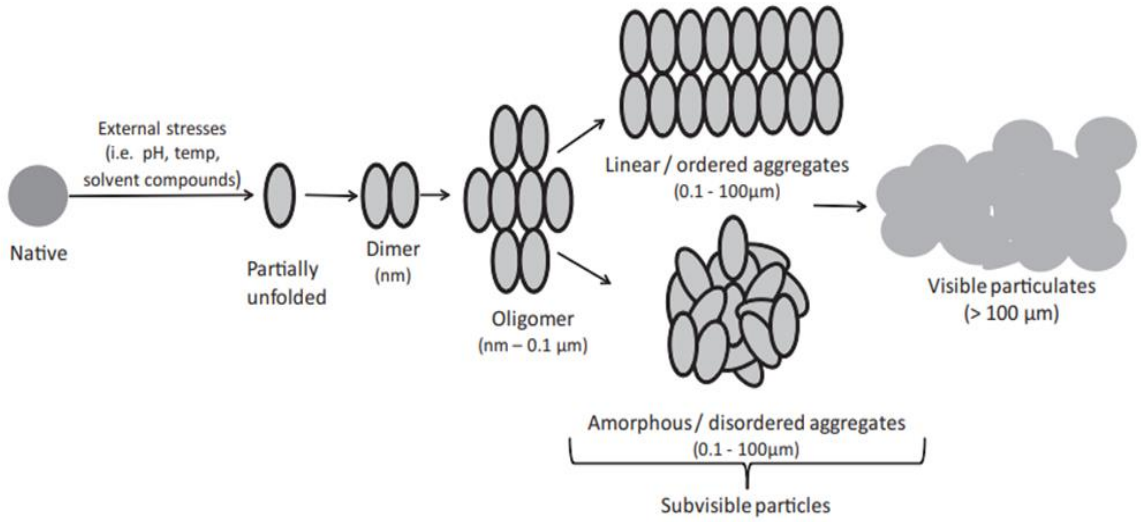

Figure 4 - Schematic representation of protein aggregation. *Adapted from Ratanji et al., 2013.*

In Figure 4, it is possible to observe that the aggregates can range in size sharply and have a linear or crystalline structure (ordered aggregates) or an amorphous structure (disordered aggregates). As mentioned before (Section 1.4), the aggregation will affect proteins' biological function or catalytic activity (Bekard et al., 2011; Chiti & Dobson, 2006; Dobson, 2003; Zeeshan et al., 2019). Thus, it is crucial to understand how aggregation occurs during processing and develop strategies to mitigate it.

1.5 Production of Tablets Containing Biologics

During the production of tablets containing biologics, three critical steps must be considered: (I) drying of biologics; (II) compression of biologics into tablets; (III) enteric coating of tablets (depending on the application) (Klukkert et al., 2015). An overview of the process flow related to the production of tablets containing biologics is represented in the following scheme (Figure 5):

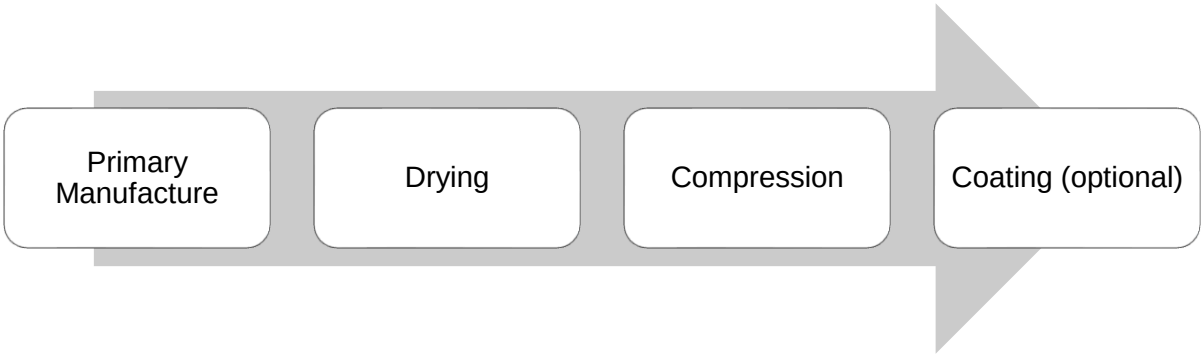

Figure 5 - Process flow during the production of tablets containing biologics. *The coating step can be considered optional as it depends on the intended use of the final tablet.*

All these steps significantly contribute to the successful development of tablets containing biologics (Wei et al., 2019), as stress-inducing factors depend on the process parameters and can lead to detrimental structural alterations of biomolecules. Thus, careful consideration of the impact of process parameters on the biologic characteristics is needed during product development (Klukkert et al., 2015).

1.5.1 Primary Manufacture

The development of biological drug products is a central pillar of the pharmaceutical and biotechnology industries. To optimize biotherapeutics' potential, protein engineering technologies developed biologics with improved specificity, potency, stability, solubility, and pharmacokinetics (Zhu et al., 2017). The production process of proteins includes processes such as fermentation (Balbás & Lorence, 2004).

This step has an important role in the final protein´s characteristics which will, in turn, impact its processing behaviour (e.g., during tableting). For example, the susceptibility to aggregate is an intrinsic characteristic that changes in proteins and will affect bioprocessing (Wang et al., 2010).

1.5.2 Drying of Biologics

The easy degradation of proteins during manufacturing and storage led to strategies to improve protein stability. Thus, drying strategies are frequently used to process and dehydrate biologics to produce solid state protein formulations with enhanced stability. These strategies include (I) spray-drying; (II) freeze-drying; (III) spray freeze drying; (IV) supercritical fluid

drying; (V) vacuum drying; and (VI) foam drying. From the mentioned techniques, freeze-drying and spray-drying are currently employed to obtain commercial solid dosage forms of biologics (Emami et al., 2018).

1.5.2.1 Spray-Drying

Spray-drying (SD) takes advantage of a gaseous hot drying medium to produce dried particles from the transformation of fluid material. Due to the increasing demand for SD of particles with complex characteristics, SD is in continuous development and improvement. Advantages such as rapidity and the continuous and single-step nature of the process make SD a versatile and reliable technique often preferred over other methods such as emulsion or solvent evaporation (Santos et al., 2018).

It is possible to describe this process in three phases: (I) atomization; (II) droplet-to-particle conversion; and (III) particle collection. During SD, a solid containing a fluid is pumped through an atomizer, in which the liquid feed is broken up into a spray of fine droplets. After that, the fine droplets come into contact with a hot gas stream, and dry particles are formed. Lastly, the dried particles are separated from the drying gas and collected (Santos et al., 2018). A schematic representation of the three major phases of SD is shown in Figure 6:

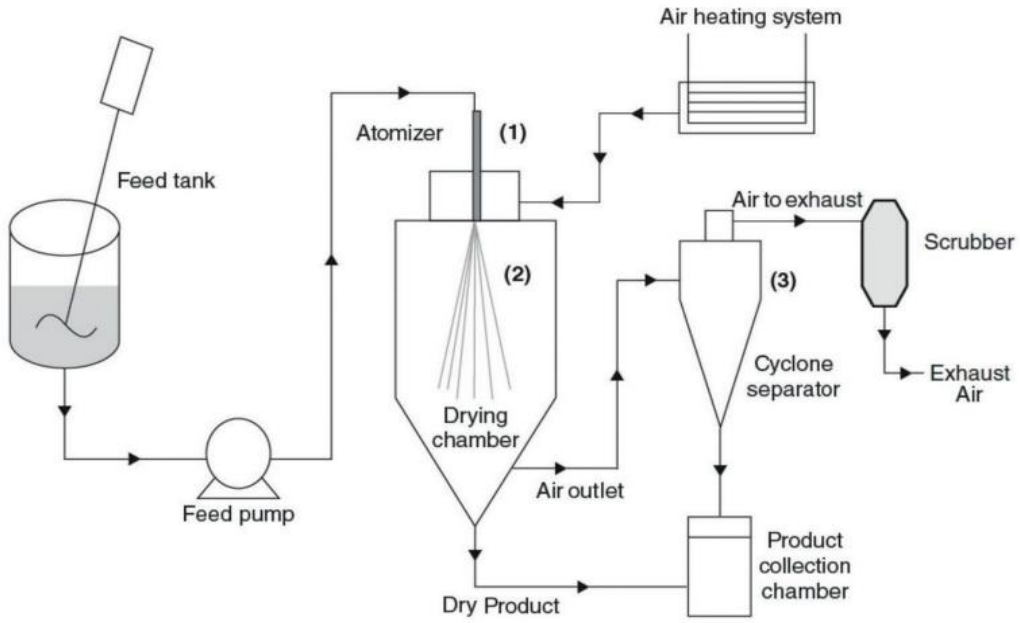

Figure 6 - Major phases of spray-drying. *The process starts with atomization (I); is followed by the droplet to particle conversion (II); and is finished by particle collection (III). Adapted from Santos et al., 2018.*

The SD processing parameters significantly impact the efficiency of the process and the characteristics of the dried particles. Some examples are given below (Santos et al., 2018):

(I) Atomization Pressure: The pressure involved during the atomization step has a critical role in determining the droplet size, i.e., an increase in pressure causes a decrease in the droplet size;

(II) Feed Flow Rate: When the atomization pressure is constant, an increase in the feed flow rate will cause the formation of larger droplets. During the atomization process of higher feeding volumes, the nozzle has the same energy to spend, so the droplet fissions will decrease, which reduces its size.

(III) Inlet Temperature: The inlet temperature relates to the drying gas temperature. Higher inlet temperatures allow higher solvent evaporation rates as a consequence of the thermal charge of the drying gas (i.e., more efficient heat and mass transfer). However, better drying performances are not achieved by only increasing the inlet temperature since the wet-bulb temperature of the surrounding air is also influenced by it. An example of this effect is the increase in the inlet temperature, which can lead to a rise in the wet-bulb temperature, which in its turn destroys the dried product (Baysan et al., 2019). In the case of heat-sensitive molecules, thermal degradation of the dried product can be prevented by lower surrounding air wet-bulb temperatures by decreasing inlet temperatures;

(IV) Drying Gas Flow Rate: This parameter refers to the volume of the drying gas pumped to the drying chamber. An increase in the flow rate increases the particle movements in the chamber, leading to a minimization of the air-droplet interaction time, which causes an incomplete removal of particle moisture. Also, better efficiency of the cyclone separation can be reached by increasing the drying gas flow rate. Thus, it is necessary to use a drying gas flow rate able to completely remove the particle moisture, as well as to have an efficient cyclone separation.

As described, the process parameters have a critical role in determining the quality of the final product. Thus, the process parameters must be selected according to the targeted final particle attributes.

Due to the characteristics of the SD technology mentioned above, it is possible to dry heat-sensitive materials, such as proteins, without a negative influence on their biological activity. However, due to the high sensitivity of biopharmaceuticals to stresses, it is necessary to precisely define the process space where stability is guaranteed (Pinto et al., 2021; Santos et al., 2018).

To prevent an eventual loss of activity of the biologic, the steps involved in the SD process need to be understood, optimized, and controlled. The biologic's stability can differ depending on the process equipment, processing conditions, and the used materials (protein formulation and excipients). Regarding the equipment, the nozzle type, cyclone design, and the spray-dryer are considered related factors affecting the quality of the dried biopharmaceutical. For the used materials, the type of protein, class of excipient, and selected media has been shown to critically affect the quality of bio-powders (Pinto et al., 2021).

All in all, the drying may critically impact downstream processes (e.g., tableting) and the final product characteristics. For example, the drying (e.g., the temperature and the particle size effect) can cause the formation of aggregates and in turn, the aggregation affects the tabletability of the material. Also, the porosity, bulk and tapped density are dependent on the process parameters and influence the final product. Moreover, the SD technique used will affect the necessary compression force used to produce the tablet (Hegedűs & Pintye-Hódi, 2007).

1.5.3 Tableting of Biologics

Tableting of biologics is relatively new, but it is considered one of the most critical unit operations for the potential degradation of the protein by thermal, mechanical, and shear stresses (Wei et al., 2019).

Previous studies exposed and assessed different formulation and production strategies for developing tableted oral biotherapeutics (Alothman et al., 2021; Chauhan et al., 2020; Makurvet, 2021; New, 2020). For instance, the tableting of biologics has been demonstrated to promote protein aggregation (Thipparaboina et al., 2016). Also, the resulting heat from compression showed to be able to generate hot spots in the tablet, leading to the protein's denaturation (Brader et al., 2015). In addition, Busignies et al. showed a bioactivity loss in small interfering ribonucleic acid lipoplexes of 40% after tablet compression (Busignies et al., 2020). So, even though there is a significant interest in the oral delivery of biologics through tablets, the understanding of the effect of tableting on proteins is still lacking (Wei et al., 2019).

1.5.3.1 Compression

Powder compression is a fast, economical process with high production capacity in which a powder is placed in a die and compressed by punches to form a compact (Fonteyne et al., 2011). Typically, during manufacturing, rotary presses are used, however, for a more in-depth

analysis, especially in the early phases of development, single punch presses are used (Zimmermann et al., 2018). The single-punch press uses only a single station of tooling with one upper and one bottom punch and a die. In this equipment, only the upper punch does force during the compression step. The rotary press has multiple tooling stations, in which the punches move between the compression rolls to form the tablets. In this press, both punches move to make the tablet. The objective of this press is to have a higher production volume of tablets contrasting to the single punch press that is used more often in the earlier stages of tablet development ("A Guide to Tablet Presses - Fette America", 2022).

In the pharmaceutical industry, compression is considered one of the main unit operations because it determines critical quality attributes of the final product (tablet), such as tensile strength, porosity, friability, weight uniformity, content uniformity, hardness, and thickness. In addition, these factors have an impact on drug disintegration, dissolution, and in turn, bioavailability (Nagar et al., 2010). Thus, the critical quality attributes of the final product can be affected by critical material attributes and critical process parameters employed during the compression step.

Compression properties can change according to the powder particle size distribution, particle shape, hygroscopicity, crystallinity, polymorphism, etc. Also, critical process parameters such as the turret speed, pre-compression force, main compression force, paddle speed, filling depth, and punch penetration depth influence the critical quality attributes of the final product. Furthermore, depending on the punch design, it is possible to obtain tablets of different sizes and shapes (Nagar et al., 2010).

During compression, the increase in force leads to a reduction of the bulk powder volume, resulting in an initial rearrangement of the powder particles. As the force continues to increase, new bonds are established between the powder particles, and a compact is obtained (Patel et al., 2006).

The different steps of compression are represented in Figure 7. Firstly, the die is filled with powder (A). After that, the upper punch is lowered and, upon contact, applies a certain force on the powder, leading to particle rearrangement and initial compression (pre-compression step) (B). In (C), the maximum compression force is achieved. Finally, decompression occurs, and the tablet is ejected by an upward movement of the bottom punch (D). The final tablet is represented by (E) (Sanchez-Castillo et al., 2003).

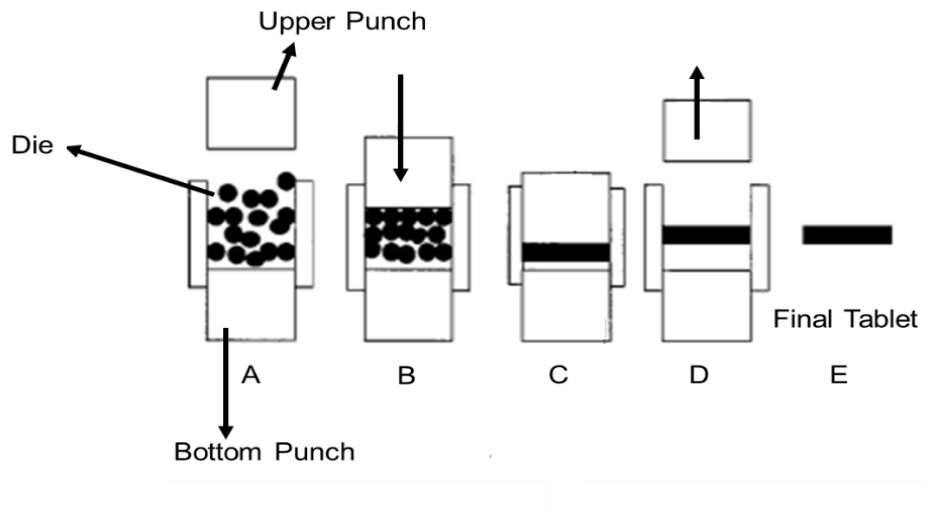

Figure 7 - Steps of compression during tableting. *The die is filled with the powder (A). The compression initiates with the movement of the upper punch (B). The maximum compression force is given by (C). The decompression occurs in (D), and the final product is given by (E). Adapted from Sanchez-Castillo et al., 2003.*

During compression, three types of deformation can occur: (I) elastic deformation, which is a reversible deformation; (II) plastic deformation, which is an irreversible deformation, that occurs when the elastic limit of the material is exceeded; and (III) fracture (Bogda, 2013). The main problems during tableting are associated with the occurrence of tablet defects, mainly by lamination and capping (Figure 8), however, chipping, sticking, and mottling can also occur (Albert et al., 2017). These problems represent a breakdown in the integrity of the tablet when the upper punch is withdrawn from the die (Sanchez-Castillo et al., 2003).

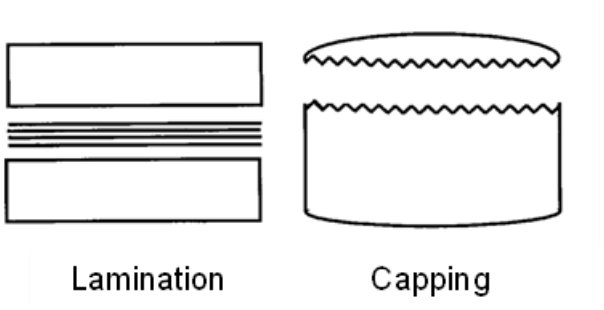

Figure 8 - Possible deformations during compression (lamination and capping). *Adapted from Sanchez-Castillo et al., 2003.*

Lamination consists of tablet decomposition in layers, usually at the center, while in capping, the cap of the tablet breaks off. Both lamination and capping can result from air entrapment, high internal stresses, insufficient dwell time, non-uniform distribution of the powder in the die, and excessive turret speed (Mazel et al., 2015; Sanchez-Castillo et al., 2003).

A significant concern in the compression of proteins is the formation of aggregates due to the reduction of intermolecular distances. As mentioned before (Section 1.4), aggregation and changes in the biologic can result in a loss of bioactivity detrimental to the product performance (Klukkert et al., 2015; Thipparaboina et al., 2016; Wei et al., 2019). Besides the formation of aggregates, the heat generated by compression must be considered. For thermosensitive proteins, heat can lead to denaturation and activity loss (Brader et al., 2015). One example of factors that might affect protein stability (aggregation and consequent loss of activity) is the humidity and moisture content (depending on the hygroscopicity of the protein) during tableting. In fact, the humidity can induce morphology changes, punch sticking, powder caking and tablet lamination, which cause manufacturability issues and affect the final tablet quality. Moreover, the particle size may also affect some proteins' secondary structure and tabletability (Wei et al., 2019) and the tablet´s tensile strength or weight due to alterations in the bulk density (Shah, 2017).

Overall, studies regarding the effect of compression in proteins seem to show that this operation negatively influences the stability of this type of biologics due to changes in their structure (denaturation and aggregation) and, consequential, loss of activity.

1.5.4 Coating

The coating process consists of the application of a dry outer layer of coating material on the surface of a dosage form (Porter, 2021). A coating solution is applied to the tablets typically in a coating pan (or fluidized bed, among others), and consequently, the tablet's surface gets covered with the coating film. After, the film dries and forms a non-sticky dry surface. Some critical parameters are involved in this technique, such as the droplet size, spray pattern, and nozzle spacing, besides other non-related spray parameters (Basu et al., 2013).

The objective of the process is to confer characteristics such as (I) the facilitation of the product identification; (II) protection of the API from the environment, improving the stability and bioavailability; (III) addition of active coating (with API); and (IV) modification of the drug release of the dosage form. The coating of tablets can be done with different techniques in which there are four main techniques for coating, such as (I) film coating; (II) sugar coating; (III) compression coating; and (IV) microencapsulation (Chen et al., 2017; Porter, 2021).

This process is optional during the production of tablets since it depends on the application of the tablet (Klukkert et al., 2015). The coating solution and the used coating technique must be chosen according to the type of tablet (i.e., when coating tablets comprising biologics, the

coating solution or the technique might have a negative effect on the structure and activity of the biologic).

1.6 Mechanisms supporting the stabilization of biologics by saccharides

The production of protein pharmaceuticals has the major challenge of preserving the protein's stability during formulation, production, packaging, shipping, and long-term storage. Thus, proteins are usually formulated with additives to maintain their native structure and biological activity to avoid chemical and physical degradation. Carbohydrates are among the most well-used additives employed to preserve proteins' stability (Lee et al., 2006; Mensink et al., 2017).

1.6.1 Background on saccharide stabilization

Over several decades, the mechanisms by which saccharides stabilize proteins have been discussed in the literature. In recent years, new theories on protein-sugar miscibility, molecular flexibility, and global and local mobility of the protein have appeared as a refinement of the vitrification and water replacement theories (Grasmeijer et al., 2013; Mensink et al., 2017; Ubbink, 2016).

1.6.1.1 Vitrification Theory

The vitrification theory postulates that degradation is slowed down through the immobilization of the protein in an amorphous and rigid glassy sugar matrix since some degradation mechanisms, such as unfolding, require molecular mobility. So, the immobilization of proteins in a rigid glassy sugar matrix might prevent the protein from unfolding or aggregating and from a consequent loss of activity due to the lack of molecular mobility. In this way, it is possible to describe the stabilization process through vitrification from a kinetic perspective. The capability of the different saccharides to stabilize sensitive APIs, such as proteins, through vitrification will depend upon the miscibility of the components and glass transition temperature (Mensink et al., 2017). For instance, the level of molecular dispersion of protein in excipients matrices will determine the stability of the biologic and its resistance to denaturation or changes in the tertiary structure (Ubbink, 2016). The presence of water also has an essential role in

vitrification, as this solvent can reduce the T_g of sugar glasses (Grasmeijer et al., 2013; Mensink et al., 2017).

However, this theory has seen modifications in the last few years. The vitrification theory is based on arresting global molecular mobility (α relaxation). However, recent studies have reported that specific groups' local mobility (β relaxation) can, in certain cases, be a better predictive theory than global mobility. For instance, it has been proposed that physical and chemical degradation are correlated with global and local mobility, respectively. For physical degradation, mobility must occur at a larger scale, whereas in the case of chemical degradation, the mobility of specific groups is more critical. Nonetheless, global mobility could also affect chemical degradation since different routes of chemical degradation need the mobility of different lengths (Grasmeijer et al., 2013; Mensink et al., 2017; Ubbink, 2016).

1.6.1.2 Water Replacement Theory

The water replacement theory hypothesizes that hydrogen bonds are formed between the sugar and protein hydroxyl groups during drying. Likewise, the hydrogen bonds between the protein and water are replaced, and the native conformation of the biomolecule is kept (Golovina et al., 2009; Grasmeijer et al., 2013; Mensink et al., 2017).

Similarly to the vitrification theory, the water replacement theory also suffered refinements during the last years. The comparative study of saccharides' capacity to replace water showed that smaller oligosaccharides with flexible backbones are better stabilizers of proteins after a drying process (lyophilization) than their more rigid and larger counterparts (polysaccharides). This phenomenon can result from the steric impediment produced by the interaction between protein and smaller saccharides, leading to tighter packing that reduces the free volume and improves the stabilization of the biomolecule (Grasmeijer et al., 2013; Mensink et al., 2017).

It is well known that the interactions between saccharides and proteins are essential for protein stabilization. Besides the replacement of hydrogen bonds, the interaction between sugar and protein can also occur via the aromatic protein residues and the C-H groups of the sugar. These interactions established via the aromatic residues of the protein and C-H groups of the sugar are denominated as CH-π interactions and have an essential role in protein-ligand binding but a moderate role in stabilization (Asensio et al., 2012; Mensink et al., 2017).

Also, the molecular crowding effect can justify protein stabilization by sugars. This effect consists of substituting the water surrounding the protein with macromolecular entities, such as (Köhn & Kovermann, 2019; Sasahara et al., 2003).

As no single theory mentioned can fully describe the stabilization of proteins by saccharides, it is necessary to relate the stabilizing capacity of saccharides to degradation pathways and stress conditions in order to choose the most suitable stabilization mechanism for a specific case (Mensink et al., 2017).

1.6.2 Stabilizing Saccharides

An extensive range of saccharides has been used in the study of protein stabilization. Saccharides as trehalose (Olsson et al., 2020), sucrose, fructose, glucose (Ajito et al., 2018; Olsson et al., 2020), dextran (Sasahara et al., 2003), and mannitol (Izutsu et al., 1994) have been reported to be capable of stabilizing proteins. In this work, were selected three different sugar classes to be tested. The polysaccharide dextran (DEX), the sugar alcohol mannitol (MAN), and the disaccharide trehalose (TRH).

1.6.2.1 Dextran

DEX is an amorphous polysaccharide synthesized by lactic acid bacteria from sucrose (Figure 9). Two forms of dextran are available, dextran 40 and dextran 70, named according to the average molecular weight of the polysaccharides used in the preparation (Sajna et al., 2015).

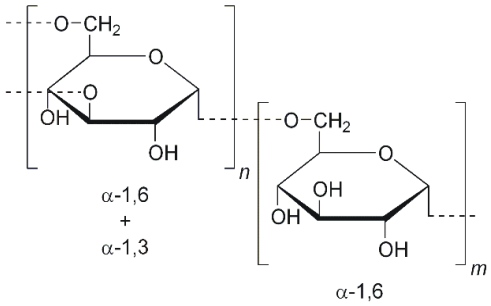

Figure 9 - Chemical structure of dextran.

DEX is one of the most preferred polysaccharides as a protein stabilizer (Pinto et al., 2021). For instance, Sasahara et al. studied the use of DEX on conformation and protein stability using thermal stress to unfold hen egg-white lysozyme and dextran induced conformation change of cytochrome c. The stabilization effect of DEX was confirmed by the macromolecular crowding effect since there was a substantial increase in volume occupancy and a decrease in the quantity of water (Sasahara et al., 2003).

1.6.2.2 Mannitol

MAN is a sugar alcohol, isomer of sorbitol, with a low molecular weight (Figure 10). It is found in marine algae and trees and is commercially sold as a crystalline powder (Shawkat et al., 2012). It is a sugar of increasing interest as a pharmaceutical excipient, particularly in solid dosage forms (Kaialy et al., 2016). MAN exists in an amorphous form, hemihydrate form, and anhydrous form. From the anhydrous form, α, β, and δ polymorphs were identified which, from the δ form results from the hemihydrate form (Yoshinari et al., 2002; Nunes et al., 2004). Among the mentioned polymorphic forms, the form β is the most stable one (Penha et al., 2021).

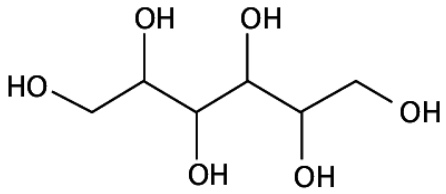

Figure 10 - Chemical structure of mannitol.

Izutsu et al. reported the use of MAN to stabilize L-lactate dehydrogenase, β-galactosidase, and L-asparaginase. The authors showed that amorphous MAN could protect both enzymes, however, with a crystallization of the sugar, the stabilization decreased on freeze-drying. Furthermore, the use of fully crystallized MAN did not stabilize L-lactate dehydrogenase. This study showed the importance of keeping the sugar's amorphous structure during freeze-drying (Izutsu et al., 1994).

1.6.2.3 Trehalose

TRH is a disaccharide formed by two molecules of glucose (Figure 11). It is a non-reducing sugar and can be found in fungi, yeast, plants, and bacteria. In plants, it has a protective function against abiotic stresses (Rasool et al., 2019). TRH has two crystalline forms (anhydrous and dihydrate) and an amorphous form (α-D-glucopyranosyl-α-D-glucopyranoside). The anhydrous form comprises three different forms, such as α, β and γ (Jain & Roy, 2008; Sussich et al., 1998). TRH is one of the most preferred disaccharides in protein stabilization (Pinto et al., 2021).

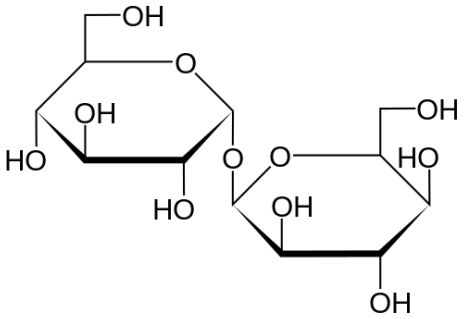

Figure 11 - Chemical structure of trehalose.

It is well known that TRH is a superior protector of biological materials against desiccation and dehydration and was shown that is a very effective stabilizer during lyophilization. It is expected that TRH works as a stabilizer of several proteins due to its effect on the structure and properties of solvent water, contrary to other sugars and polyols. Kaushik & Bhat demonstrated that the surface tension effect has a critical role in stabilization, and in addition, the interactions of the side chain of the protein with trehalose also contribute to the stabilization (Kaushik & Bhat, 2003).

1.7 Hypothesis, Objectives and Structure of the Thesis

1.7.1 Hypothesis

The stability of catalase and other biologicals is affected by shear stresses during tableting.

1.7.2 Objectives

The study aims to investigate the in-process tableting stability of biologics intended for oral delivery. Catalase was selected as a model protein, for enzyme replacement therapy, given its sensitivity to processing conditions. Therefore, the objectives of this study are:

(I) Understanding of the effect of tableting on the stability of enzymatic replacement therapies;

(II) Establishment of methodologies able to quantify and discriminate the effect of processing on the aggregation and activity of tablets containing enzymes;

(III) Identification of optimal excipients enabling the manufacturing and optimal protection of tableted enzymes;

(IV) Identification of the thresholds beyond which enzymatic activity is lost due to the shear and compression forces.

1.7.3 Structure of the Thesis

The Thesis starts with the characterization of the raw CAT serving as a reference to identify changes in the biologic upon compression (biological activity, number of particles and structural changes). After, different mixtures comprising CAT and different saccharide types were prepared and subjected to the same characterization, allowing the evaluation of the saccharides' suitability to preserve the CAT activity after compression. The correlations between the process parameter and the CAT properties were assessed via PCA and based on the developed PCA, the mixtures (at fixed CAT loading) for subsequent SD study were selected. The chosen mixtures were then spray-dried and tableted and the produced tablets were characterized. In addition, the surface morphology and polymorphism were studied in the spray-dried mixtures. Finally, another PCA was done to visualize the changes in the correlations between the variables when adding the spray-drying step.

2. Materials and Methods

2.1 Materials

2.1.1 Model protein and saccharides

The model protein chosen was CAT (from the bovine liver) since it is known to have stability problems during processing. Excipients were added to the formulation in order to investigate its benefits on CAT's structure. For CAT, it was assumed that each mg of CAT has 3500 units (3500 units/mg). The catalase and saccharides used in the experimental work are summarized in Table 3.

Table 3 - Catalase and saccharides used in the experimental work.

Material	Material Grade	Brand	CAS
CAT	Catalase from bovine liver *(2000-5000 units/mg)*	BOC Sciences (United States of America)	9001-05-2
DEX	Dextran 40 *(≥98%)*	Pharmacosmos (Denmark)	5510 0040 1006
MAN	Parteck® M 200 *(≥98%)*	Merck (Germany)	69-65-8
TRH	Trehalose Dihydrate *(≥99%)*	Merck (Germany)	6138-23-4

CAT – Catalase; DEX – Dextran; MAN – Mannitol; TRH - Trehalose

2.1.2 Other Materials

Other materials used in the experimental work are listed in Table 4. The potassium dihydrogen phosphate and potassium phosphate dibasic trihydrate were used to prepare a phosphate buffer solution (50 mM Potassium Phosphate Buffer, pH 7.0 at 25 °C). The hydrogen peroxide 30 % (w/w) was diluted to produce a solution with a concentration of 0.036 % (w/w).

Table 4 – Other materials used in the experimental work.

Material Grade	Brand	CAS
Potassium Dihydrogen Phosphate (*for analysis*)	Merck (Germany)	7778-77-0
Potassium Phosphate Dibasic Trihydrate *(≥99%)*	Sigma-Aldrich (United States of America)	16788-57-1
Hydrogen Peroxide 30% *(for analysis)*	Sigma-Aldrich (United States of America)	7722-84-1

2.2 Methods

2.2.1 Preparation of blends

The blends of materials were prepared by accurately weighing the amount of CAT (m_{CAT}) to an eppendorf; using a Mettler Toledo XP205 balance (Germany). Then, the amount of sugar (m_{sugar}) was weighted to another eppendorf, and the weighted materials were added to the same eppendorf. The mixture was mixed using the vortex until the blend looked visually homogeneous (approximately 15 seconds). The blends were stored at -20 °C until their use.

2.2.2 Spray-drying

Four mixtures (Table 5) were spray-dried in this step. To that end, the materials in all mixtures were weighed and placed in a 50 mL plastic tube, where they were then blended using a vortex. After blending, 5 mL of deionized water was added to the plastic tubes, and the mixtures blended again until their visual dissolution. The solutions were kept on ice until the start of the SD.

Table 5 - Mixtures considered for drying (spray-drying).

Formulation	m_{CAT} (mg)	m_{sugar} (g)	Ratio CAT/sugar
CAT	500	-	100/0
CAT + DEX	500	1.16	30/70
CAT + MAN	500	1.16	30/70
CAT + TRH	500	1.16	30/70

The SD process was performed with the Mini Spray Dryer B-290 (Büchi, Switzerland), using a two-fluid nozzle with an orifice size of 1.4 mm. The inlet temperature was set to 110 °C, the airflow to 34 mm (in this equipment, the airflow is determined by a sphere´s height that determines the airflow), the pump rate to 20 %, the aspirator rate to 100 % yielding, and an outlet temperature of 61 °C. The dried particles were collected into a flask and then scrapped into a plastic tube. The plastic tubes were stored at -20 ºC in individual aluminium bags. Silica was placed between the bags until further characterization (i.e., biological activity, number of particles and secondary structure).

2.2.3 Tableting

Tableting was performed in a manual hydraulic tablet press MP250 from Maassen (Germany) fit with flat face round standard Euro D punches with an 8 mm diameter. 100 mg of powder were compressed at forces of 0.5, 1, and 2 tons (corresponding to 76.62, 153.23, and 229.84 MPa) and a dwell time of 3 s. Tablets were collected in a plastic bag and stored, in a freezer, at -20 ºC in an aluminium bag. Silica was added between the bags.

The powders and respective blends used, as well as the final tablet formulation, are summarized and labelled in Table 6.

Table 6 - Mixtures of CAT and saccharides.

Form	Saccharides	m_{CAT} (mg)	m_{sugar} (mg)	Ratio	Force (T)	Spray-drying	Designation
Powder	-	100	0	100/0	0	No	CAT 0T
Tablet	-	100	0	100/0	0.5	No	CAT 0.5T
Tablet	-	100	0	100/0	1	No	CAT 1T
Tablet	-	100	0	100/0	2	No	CAT 2T
Powder	-	100	0	100/0	0	Yes	CAT SD 0T
Tablet	-	100	0	100/0	0.5	Yes	CAT SD 0.5T
Tablet	-	100	0	100/0	1	Yes	CAT SD 1T
Tablet	-	100	0	100/0	2	Yes	CAT SD 2T
Blend	DEX	10	90	10/90	0	No	DEX 10/90 0T
Blend	DEX	30	70	30/70	0	No	DEX 30/70 0T
Blend	DEX	50	50	50/50	0	No	DEX 50/50 0T
Tablet	DEX	10	90	10/90	0.5	No	DEX 10/90 0.5T
Tablet	DEX	30	70	30/70	0.5	No	DEX 30/70 0.5T
Tablet	DEX	50	50	50/50	0.5	No	DEX 50/50 0.5T
Tablet	DEX	10	90	10/90	1	No	DEX 10/90 1T
Tablet	DEX	30	70	30/70	1	No	DEX 30/70 1T
Tablet	DEX	50	50	50/50	1	No	DEX 50/50 1T
Tablet	DEX	10	90	10/90	2	No	DEX 10/90 2T
Tablet	DEX	30	70	30/70	2	No	DEX 30/70 2T
Tablet	DEX	50	50	50/50	2	No	DEX 50/50 2T
Powder	DEX	30	70	30/70	0	Yes	DEX SD 30/70 0T
Tablet	DEX	30	70	30/70	0.5	Yes	DEX SD 30/70 0.5T
Tablet	DEX	30	70	30/70	1	Yes	DEX SD 30/70 1T
Tablet	DEX	30	70	30/70	2	Yes	DEX SD 30/70 2T
Blend	MAN	10	90	10/90	0	No	MAN 10/90 0T
Blend	MAN	30	70	30/70	0	No	MAN 30/70 0T
Blend	MAN	50	50	50/50	0	No	MAN 50/50 0T
Tablet	MAN	10	90	10/90	0.5	No	MAN 10/90 0.5T
Tablet	MAN	30	70	30/70	0.5	No	MAN 30/70 0.5T
Tablet	MAN	50	50	50/50	0.5	No	MAN 50/50 0.5T
Tablet	MAN	10	90	10/90	1	No	MAN 10/90 1T
Tablet	MAN	30	70	30/70	1	No	MAN 30/70 1T
Tablet	MAN	50	50	50/50	1	No	MAN 50/50 1T
Tablet	MAN	10	90	10/90	2	No	MAN 10/90 2T
Tablet	MAN	30	70	30/70	2	No	MAN 30/70 2T
Tablet	MAN	50	50	50/50	2	No	MAN 50/50 2T
Powder	MAN	30	70	30/70	0	Yes	MAN SD 30/70 0T
Tablet	MAN	30	70	30/70	0.5	Yes	MAN SD 30/70 0.5T
Tablet	MAN	30	70	30/70	1	Yes	MAN SD 30/70 1T
Tablet	MAN	30	70	30/70	2	Yes	MAN SD 30/70 2T
Blend	TRH	10	90	10/90	0	No	TRH 1090 0T
Blend	TRH	30	70	30/70	0	No	TRH 30/70 0T
Blend	TRH	50	50	50/50	0	No	TRH 50/50 0T
Tablet	TRH	10	90	10/90	0.5	No	TRH 10/90 0.5T
Tablet	TRH	30	70	30/70	0.5	No	TRH 30/70 0.5T
Tablet	TRH	50	50	50/50	0.5	No	TRH 50/50 0.5T
Tablet	TRH	10	90	10/90	1	No	TRH 10/90 1T
Tablet	TRH	30	70	30/70	1	No	TRH 30/70 1T
Tablet	TRH	50	50	50/50	1	No	TRH 50/50 1T
Tablet	TRH	10	90	10/90	2	No	TRH 10/90 2T
Tablet	TRH	30	70	30/70	2	No	TRH 30/70 2T
Tablet	TRH	50	50	50/50	2	No	TRH 50/50 2T
Powder	TRH	30	70	30/70	0	Yes	TRH SD 30/70 0T
Tablet	TRH	30	70	30/70	0.5	Yes	TRH SD 30/70 0.5T
Tablet	TRH	30	70	30/70	1	Yes	TRH SD 30/70 1T
Tablet	TRH	30	70	30/70	2	Yes	TRH SD 30/70 2T

2.2.4 Preparation of solutions

Catalase (CAT) solution

During the preparation of the CAT solutions, catalase from bovine liver (2000-5000 units/mg) from BOC Sciences (USA) was used and stored at -20 ºC. For the preparation of the stock solution, 10 mg of CAT were weighted in the analytical scale Mettler Toledo XP205 to an eppendorf. Then, 1 mL of filtrated cold phosphate buffer (50 mM Potassium Phosphate Buffer, pH= 7.0 at 25 °C) was added to the eppendorf and mixed using a vortex. The concentration of all CAT solutions was 10 mg/mL. It was assumed that each milligram of CAT had 3500 units/mg.

Immediately before the CAT enzymatic assay, the stock solution was diluted to approximately 100 units/mL in cold phosphate buffer. During the enzymatic assay, the solution was kept on ice. This step was performed for all the solutions.

Blends and powders

For the preparation of the non-spray-dried blends, the blends were prepared according to Section 2.2.1. After, was added 10 mL of filtrated cold phosphate buffer (50 mM Potassium Phosphate Buffer, pH= 7.0 at 25 °C) and mixed using the vortex until the blend dissolved.

In the case of the spray-dried powders, 100 mg of the powder were weighted, using a Mettler Toledo XP205, into a 50 mL plastic tube and 10 mL of filtrated cold phosphate buffer (50 mM Potassium Phosphate Buffer, pH= 7.0 at 25 °C) were added. Then, the sample was mixed using a vortex until being dissolved. The final concentration of the solution was 10 mg/mL.

Tablets

Firstly, the tablets were weighted to confirm if the weight was the same before the tableting. Then, according to the actual weight of the tablet, filtrated cold phosphate buffer (50 mM Potassium Phosphate Buffer, pH= 7.0 at 25 °C) was added to have a final concentration of 10 mg/mL of CAT. To facilitate the dissolution of the tablet, it was broken using a spatula. The volume of the added phosphate buffer varied since the tablet's weight was different in every formulation. Finally, the mixture was blended until dissolved.

2.3 Characterization methods

2.3.1 Catalase Activity Assay

The enzymatic assay used to evaluate the activity of CAT is described by Equation 1 in Section 1.3.3. According to the equation, one unit of catalase transforms 1.0 µmol of H_2O_2 into its by-products. At 25°C, pH 7.0, the transformation described in Equation 1 takes 60 s, in which the concentration of H_2O_2 decreases from 10.3 mM to 9.2 mM. Likewise, the rate of transformation of H_2O_2 into its by-products was followed by observing the rate of decrease of the absorbance at 240 nm (Abs240). This was done via ultraviolet-visible spectroscopy (UV/Vis spectroscopy) ("Enzymatic Assay of Catalase (EC 1.11.1.6)", 2022).

The UV-Vis spectroscopy is an analytical technique that is used to determine the absorption or transmission of UV (200 nm ≤ λ ≤ 400 nm) or visible light (400 nm ≤ λ ≤ 700 nm) of a sample in comparison with a blank sample or a reference, at different wavelengths. Both absorption and transmission are in a segment of the ultraviolet spectrum and the adjacent visible areas in the spectrum of electromagnetic radiation (Tom, 2021).

To characterize the CAT activity, immediately before the enzymatic activity assay, the solutions prepared according to Section 2.2.4 were diluted to approximately 100 units/mL CAT using cold phosphate buffer and kept on ice until usage. 2.90 mL of hydrogen peroxide 0.036 % (w/w) were pipetted to a quartz cell, and the substrate temperature was equilibrated to 25 ºC. When the temperature reached equilibrium, 0.10 mL of the CAT solution (~100 units of catalase/ mL) were added to the quartz cell (light path = 1 cm), which was immediately mixed by inversion of the cuvette and inserted into the UV/Vis spectrophotometer UV-2700 from Shimadzu (Japan). The instrument was blanked with the phosphate buffer.

The decrease of the absorbance (Abs_{240}) was monitored by taking one reading per second for 180 s. The analysis was performed in triplicates ("Enzymatic Assay of Catalase (EC 1.11.1.6)", 2022). Based on the UV/Vis results, the relative activity of CAT was calculated according to the following equation:

$$\textit{Relative Activity (\%)} = \frac{Abs_{180s}\ \textit{sample} - Abs_{0s}\ \textit{sample}}{Abs_{180s}\ \textit{baseline} - Abs_{0s}\ \textit{baseline}} \times 100 \qquad \textit{(Equation 4)}$$

Where the Abs_{180s} is the value of absorbance of the sample and baseline after 180 s and Abs_{0s} is the absorbance of the sample and baseline at 0 s. For the CAT alone, the baseline considered was the non-tableted raw enzyme material, while for the sugar mixtures with the

enzyme, the non-tableted blends of this with the CAT at the relevant ratio were considered. To this end, it was considered that the Abs_{180s} is the activity of CAT to the respective formulation.

2.3.2 Micro-Flow Imaging

Micro-Flow Imaging (MFI) is a powerful tool in the biopharmaceutical industry used to visualize, quantify, and characterize aggregates and undesirable particles in therapeutic samples. In the MFI, the fluid sample passes the optic through a flow cell, where microscopic images are automatically captured by a camera (Marvin et al., 2019; van Beers et al., 2017).

This technique can report several parameters, such as the equivalent circular diameter (ECD), concentration, particle area, perimeter, circularity, and aspect ratio, among others. The particle size is given by the ECD, which represents the diameter of a circle that has the same surface area as the particle (van Beers et al., 2017; "Area, ECD, and Intensity: Micro-Flow Imaging", 2022).

For the MFI, the solutions were prepared according to Section 2.2.4 and diluted in filtrated cold phosphate buffer (to decrease the number of particles in the solution, the phosphate buffer was filtrated using a 0.22 µm nylon syringe filter) to a final concentration of 1 mg/mL.

For the MFI measurements was used the micro flow imaging microscope MFI 5100 from ProteinSimple (United States of America). Firstly, the illumination was optimized using the filtrated phosphate buffer. Thereafter, a sample of 0.50 mL was dispensed, and from this, 0.264 mL was analysed. The system was cleaned with deionized water and filtrated phosphate buffer between measurements.

The data was processed with the MFI View Analysis Suite, where edge and stuck particles were removed, and only particles with an ECD larger than 5 µm were considered.

2.3.3 Attenuated Total Reflection Fourier Transform Infrared Spectroscopy

Attenuated Total Reflection Fourier Transform Infrared Spectroscopy (ATR-FTIR) is a spectroscopic technique that has been shown to be one of the most accessible analytical techniques used in the characterization of the secondary structure of proteins. In fact, this technique provides data that allows a fast characterization based on the characteristic

absorbance of molecular vibrations of the sample (Kazarian & Chan, 2006; Kazarian & Chan, 2013; Tatulian, 2012; Cruz-Angeles et al., 2015).

The ATR-FTIR is based on the phenomenon of the attenuation effect of light. This occurs when the light is internally reflected at an interface between a material with a high refractive index - internal reflection element - and a material that has a low refractive index to absorb IR - sample.

The ATR-FTIR does not require sample preparation. Therefore, the samples were in the solid state and were directly placed on the crystal for analysis. The measurements were executed with the solid state samples. The analysis was carried out with the Vertex 70, from Bruker (United States of America). The solid samples were placed in the ATR accessory, and to increase the area of contact between the sample and the crystal, a pressure applicator with a torque knob was used.

The spectra were acquired in triplicates, using 128 scans with a resolution of 4 cm^{-1} and 64 scans of background at 20 ºC. During the acquisition, the wavenumber range selected was from 400 to 4000 cm^{-1}.

All of the FTIR data was treated according to the following steps: (I) Asymmetric least squares smoothing baseline mode, with a smoothing factor of eight and ten iterations, from 600 to 3700 cm^{-1}; (II) Normalization (0-1); and (III) Savitzky-Golay smoothing with a second-order polynomial. The spectrum was cut from 1900 to 2700 cm^{-1} for easy visualization.

2.3.4 Small/Wide-angle X-ray Scattering

Small- and wide-angle X-ray scattering (SWAXS) is an X-ray-scattering method triggered by processes such as photon absorption or ligand-binding, which has the potential to detect a wide range of structural transitions. This technique has several applications, such as molecular docking or structure determination (Chen & Hub, 2015). The SWAXS measurements aimed to determine the polymorphic form of the saccharides after the SD.

The SWAXS measurements were performed with S3 Micro from Hecus (Austria) at 25°C. Each sample was rotating and was measured as a singlet using a potency of 50 kV+1mA, an exposition time of 600 s, and a hold time of 100 s. In this experimental work, only wide-angle X-ray scattering (WAXS) was used to study the structure of the materials.

2.3.5 Scanning Electron Microscopy

Scanning electron microscopy (SEM) is a technique in which a scanning microscope scans a surface with a beam of electrons, providing information on crystalline structure, chemical composition, or surface topography (Vernon-Parry, 2000).

The surface morphology of the spray-dried materials was performed using an electron microscopy equipment (JEOL-JSM-S200LV, JOEL, Massachusetts, USA), equipped with a secondary electron detector. Prior to analysis, particles were gold coated in a sputtering chamber (JEOL JFC-1200, JOEL, Massachusetts, USA). The samples were scanned at a voltage of 25 kV, and the photographs were taken at four magnifications, 500x, 1000x, 1500x, and 2000x.

2.4 Statistical Analysis

2.4.1 Principal Component Analysis

Principal Component Analysis (PCA) is a multivariate technique that consists of a dimensionality reduction of the information contained in a dataset while preserving its variability. The PCA is the base of a multivariate analysis that allows an uncovering of the correlations between observations and variables and between variables. The model's objective is to summarize the information of the dataset in indices called Principal Components (Jolliffe & Cadima, 2016; Mishra et al., 2017). The PCA was performed using SIMCA (Umetrics®, Sweden), version 17.0.0.24543.

In the PCA, 18 variables were considered: (I) CAT loading; (II) force; (III) Abs_{180s} (activity); and (IV) number of particles from the ranges of 5≤x≤10, 10≤x≤25, 25≤x≤50, 50≤x≤75, 75≤x≤100, 100≤x≤300, and 300≤x≤MAX µm, as well as the respective standard deviation (STD). Only quantitative variables were used. The variables that did not have a normal distribution were transformed using the logarithmic function, which led to improved performance. The model fit (R^2) and the predictive ability (Q^2) were considered.

2.4.2 Bonferroni Correction

The Bonferroni Correction is an often-used method to adjust probability values during multiple statistical tests. The method is widely used to perform a comparison between different groups at baseline or to study the relationship between variables, as pretended in this experimental work. This method assumes that if the probability is equal to or less than 0.05, a significant difference in correlation will be observed (Armstrong, 2014).

The statistical analysis was conducted with OriginPro® 2022b (Originlab®, United States of America), version 9.9.5.167. In this analysis, one or more lower-case letters are attributed to a variable to be compared between them.

3. Results and Discussion

3.1 Impact of Tabletting on Catalase Activity

3.1.1 Tablets with Catalase

A decrease in the CAT activity after compression (Error band graph in Annex A.1) was observed (Figure 12 - A), with the highest decrease occurring for the highest compression force applied. Compression force induces shear and thermal stresses on materials leading to a change in the structure of the protein with subsequent loss of activity (Bekard et al., 2011; Chiti & Dobson, 2006; Dobson, 2003; Wei et al., 2019; Wurster & Ternik, 1995; Zeeshan et al., 2019).

The enzymatic activity assay of the spray-dried materials showed a sharp decrease in relative activity compared to the respective baseline and the non-spray-dried CAT tablets (Figure 12 - B). The formulation CAT SD 0.5T showed higher relative activity than the non-tableted co-particle, however, there is a high STD associated with it, suggesting that the activity might not be so different (Error band graph in Annex A.2). The loss of biological activity after SD is well described in the literature. Studies have shown a significant loss of activity of CAT after SD due to processing conditions (Grasmeijer et al., 2019; Haque et al., 2015; Schaefer & Lee, 2015). This loss of activity is critical as it will detrimentally impact the quality of the final product.

The change in the relative activity of the enzyme with the application of force was confirmed by the Bonferroni statistical analysis (Figure 12 - C).

In the non-spray-dried mixtures, a similarity is observed between the relative activity of the different mixtures (lower-case letter: b). Similar activity also occurs in the spray-dried mixtures (lower-case letter: d), but with a slightly higher activity to CAT SD 0.5T (lower-case letter: c). However, this might be due to sampling and heterogeneous distribution of the unstable CAT in the SD samples.

Overall, a decrease in the activity is observed after the tableting of all the mixtures (with and without SD) compared with the CAT 0T. The spray-dried mixtures have a lower activity than the non-spray-dried mixtures, showing the effect of the SD on CAT. CAT SD 0.5T has a higher activity than the other spray-dried mixtures, however, the reproducibility of such results needs to be assessed. Thus, a negative effect on the activity is observed after the tableting, which is more evident after SD.

Concluding, a negative effect on the activity is observed when catalase is dried and tableted.

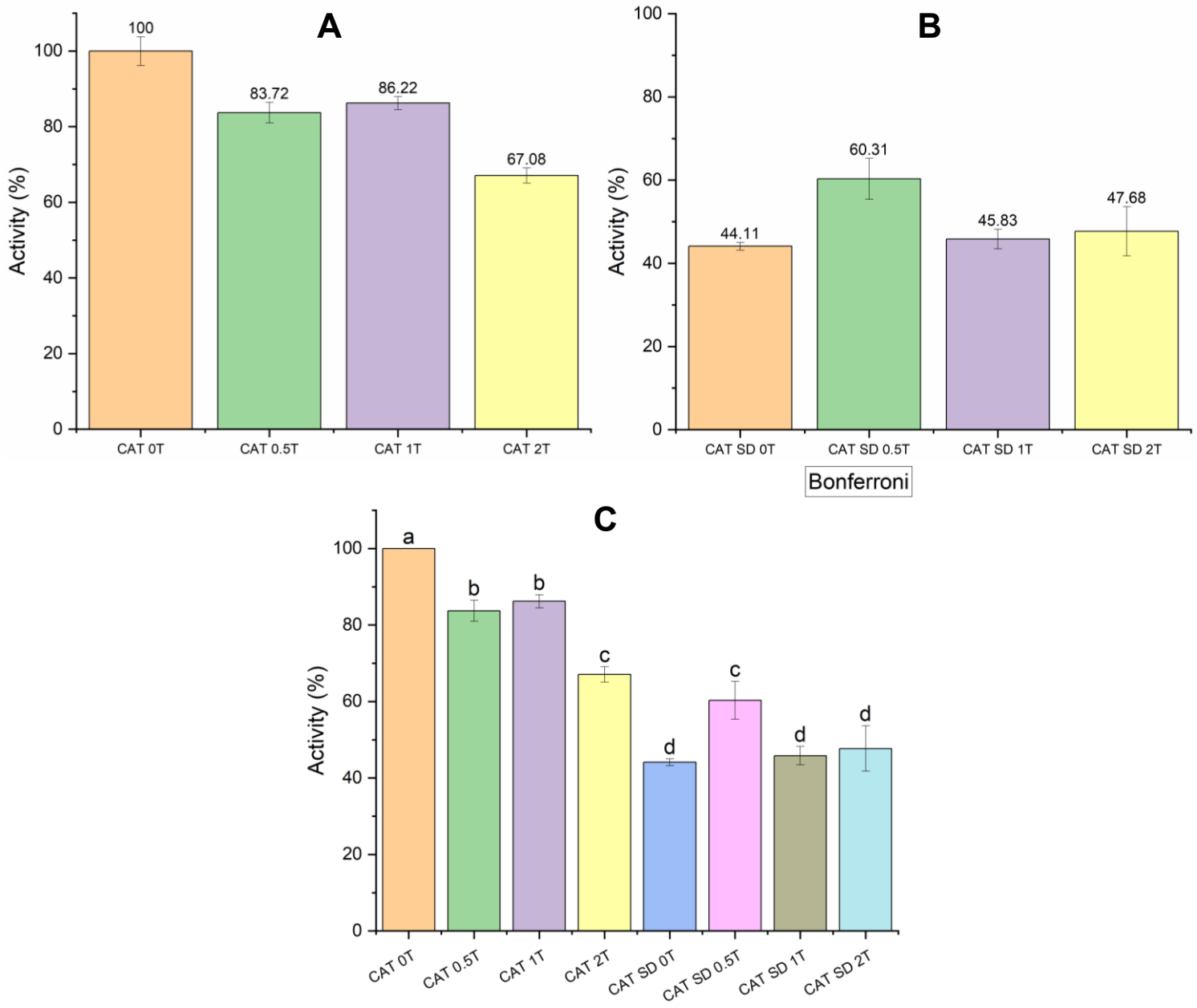

Figure 12 - Enzymatic activity of non-spray-dried and spray-dried CAT mixtures, as a blend and after compression and respective Bonferroni statistical analysis. *Legend: A – Non-spray-dried blend and tablets; B – Spray-dried co-particle and tablets; C – Bonferroni statistical analysis.*

3.1.2 Tablets with Catalase and Dextran

Figure 13 – A, B and C show that in the presence of DEX, a loss of CAT activity occurs when the blends are compressed (error band graphs are represented in Annex A.3). This loss was more significant than the one that occurred in the tablets with 100 mg of non-spray-dried CAT alone. Between the tablets, the activity ranges from approximately 60 to 70 %. Both the ratio

of 10/90 and 50/50 have the highest activity in the tablet with 1 T, while in the ratio of 30/70, the activity remains higher and constant for both the three forces applied. This could be an indication that the 30/70 ratio is more adequate to have some stabilizing interactions between excipient and protein and maintain the activity at higher compression forces (at 2 T, higher activity is observed for the DEX-CAT tablets than for CAT alone). In this case, mechanical stabilization may be at work. As DEX is a plastic material, it can be that during tableting, it deforms without breaking and, thus, mechanically protects CAT (Tye et al., 2005). Also, to DEX 10/90 and DEX 50/50, the force of 1 T shows the highest activity between tablets, that can be due to a non-linear trend between the loss of activity and the applied force. The contact area between the materials to 1 T can be larger, or bonding between the sugar and excipient might be occurring, and when the force is increasing, these two beneficial effects are lost because of other mechanisms that are occurring (e.g., fragmentation). At 0.5 T, the force is too low to have the same level of plastic deformation that is occurring with 1 T (Antikainen & Yliruusi, 2003; Rostiashvili & Vilgis, 2014; Skelbæk-Pedersen et al., 2019).

However, DEX is not stabilizing CAT when the blends are compared with the tablets, in which occurs a loss of around 30 % of activity in every ratio. This lack of stabilization, from the blends to the tablets, could be due to the hygroscopicity of DEX, as this promotes the adsorption of water molecules into the system, leading to destabilization of the protein in the solid state (Xie et al., 2011).

Additionally, it was interesting to observe that no synergy exists between the un-stabilizing effect of DEX and higher compression forces, as no discernible further detrimental impact in the enzymatic activity was observed as higher forces were applied (since the activity remains similar or it is higher to the force of 1 T).

The mixtures with spray-dried DEX showed a sharp decrease in their relative activity (Figure 13 - D). Moreover, a pattern of the activity change is visible, in which the activity decreases with the increase of the applied force (Error band graph in Annex A.4). These results suggest that the presence of DEX in a co-particle with CAT affects the protein's activity negatively since the relative activity of CAT in the DEX mixtures is lower than in the tablets with 100 mg of CAT.

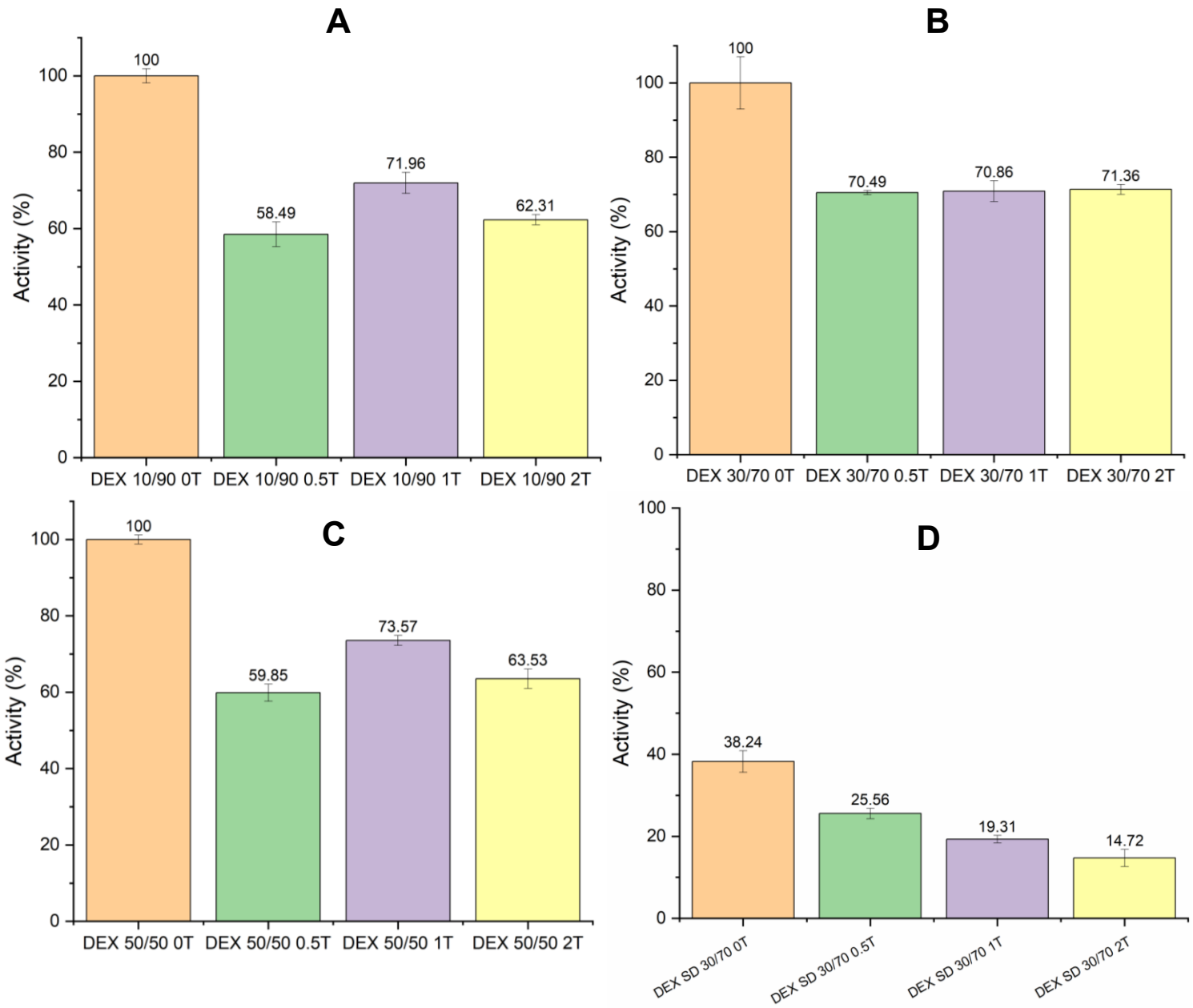

Figure 13 - ***Enzymatic activity of non-spray-dried and spray-dried DEX mixtures, as a blend and co-particle before and after compression.*** *Legend: A – 10/90 ratio; B – 30/70 ratio; C – 50/50 ratio; D – 30/70 spray-dried ratio.*

In the PCA, further discussed in Chapter 3.4.1, general correlations were observed between the Abs_{180s} (activity) as a function of compression force. Likewise, the Bonferroni statistical analysis was performed on this variable (Abs_{180s}) for a more in-depth comparison.

From the statistical analysis of the UV/Vis results (Figure 14 - A), it is possible to observe some similarities between the variables of the same ratios (e.g., DEX 30/70) and, in some cases, between mixtures of different ratios (lower-case letter: b). The mentioned ratio seems to be the

most stable one after compression due to no changes observed in the correspondent lower-case letter.

The activity of the non-spray-dried mixtures decreases after the tableting (not showing stabilization) but is rather constant among the three forces applied (showing stabilization). The tablets with the spray-dried materials have a sharp decrease compared with the non-spray-dried mixtures, and in addition, a trend of decrease in activity is visible with the increase of the force) (Figure 14 -B).

In the case of the non-spray-dried mixtures, it seems that DEX stabilizes CAT when different compression forces are applied, but this is not the same for the spray-dried tablets. In this case, an increasingly decrease in activity occurred after tableting from 0.5 to 2 T. Studies regarding the protection of proteins with DEX showed that DEX was not capable to protect the dried protein due to the inability to form hydrogen bonds with the dried protein (Allison et al., 1999), which explains the inability of the polysaccharide to protect the enzyme after SD. However, considering the results from the compression of the blends, it is suggested that during tableting, the stabilization provided by DEX is mechanical and not chemical. As explained before, due to its amorphous nature, DEX will behave as a plastic material, deforming without breaking and, thus, mechanically protecting CAT.

However, this positive effect is not seen in the spray-dried powders. A potential explanation might be that compression can induce amorphous-amorphous phase separation, affecting the miscibility of the composition and then compromising the stabilization or due to the heterogeneity of the spray-dried particles that can cause more separation of particles than the physical blends (more homogeneous). This phenomenon could be confirmed using Raman mapping (Ayenew et al., 2012). The decrease of activity after the SD suggests that although DEX protects CAT mechanically (within the different forces applied) during the tableting of the lyophilized enzyme, this is not efficient in protecting the protein during desiccation.

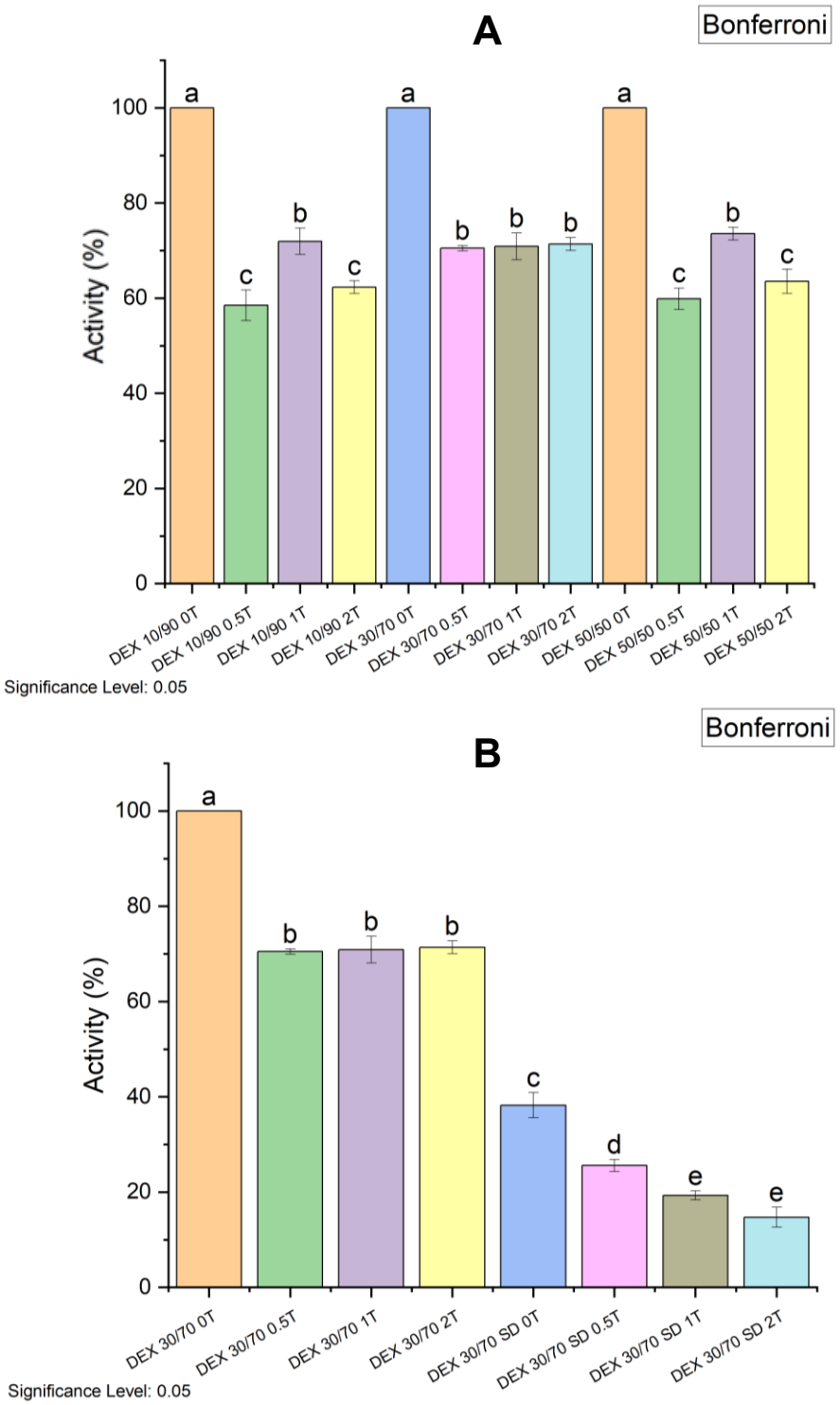

Figure 14 - Bonferroni statistical analysis of the activity of the non-spray-dried and spray-dried DEX mixtures as a blend and after compression. *Legend: A – Non-spray-dried tablets with different ratios; B – Non-spray-dried and spray-dried blend, co-particle and tablets with 30/70 ratio.*

3.1.3 Tablets with Catalase and Mannitol

The MAN tablets had a similar pattern as the DEX tablets (Figure 15 – A, B and C). A decrease in activity occurs with the application of force, with ranges approximately between 25 to 50 % loss depending on the CAT loading and force used. The exception is MAN 10/90 0.5T (Figure 15 - A), which does not follow this behaviour and should be repeated for confirmation. The respective error band graphs are represented in Annex A.5.

The enzymatic assay showed a decrease of activity with the SD (activity of MAN SD 30/70 0T lower than MAN 30/70 0T) and, in addition, a decrease in the relative activity after tableting (Figure 15 - D). However, compared to the SD of CAT alone, MAN's presence seems to stabilize the protein during drying and led to a higher activity (88.32 % vs. 44.10 % for MAN-CAT SD co-particles and CAT SD, respectively). Additionally, it was interesting to observe that the formulation MAN SD 30/70 0.5T did not follow the same pattern as the other mixtures (Error band graph in Annex A.6) and should be repeated to confirm its reproducibility (a decrease of activity with the increase of the applied force occurs). This higher activity of MAN SD 30/70 1T can also be due to a non-linear compression profile due to structural changes after SD (see Section 3.3.3), as described in Section 3.1.2.

In the Bonferroni statistical analysis, a clear decrease in activity from the blends to the tablets is visible (Figure 16 - A). The change of activity follows a pattern in all the different ratios, in which the activity decreases with the increase of force. However, the formulation MAN 10/90 0.5T did not follow this behaviour (UV/Vis measurements should be repeated for this formulation to verify the reproducibility of these results). Moreover, by comparing the different mixtures with the same applied force, it is possible to see some similarities (characterized by the same lower-case letters).

In the spray-dried mixtures (Figure 16 - B), the activity decreases after the tableting as in the previous mixtures. The activity of the non-spray-dried tablets is rather stable, with only a slight decrease at the highest force used. MAN SD 30/70 0T has a slight decrease in activity compared with MAN 30/70 0T, probably due to the SD process, and MAN SD 30/70 0.5T had a sharp dropin activity, but the repeatability of the results obtained for this formulation should be verified. Without considering this potential outlier, the activities of the mixtures are slightly lower comparing the same forces (same class). Thus, the SD had a slight negative effect, shown by the small decrease of activity in the spray-dried mixtures. As mentioned before, this effect can be due to a mixture of different forms of MAN in which the presence of a crystalline and amorphous form affects the stabilizer capacity of MAN, caused by a lower T_g of MAN that causes the transition of the form (Chen et al., 2021).

Moreover, MAN is a brittle material, meaning that with compression, inter-molecular forces are established due to brittle fragmentation, however, this crystal fragmentation can lead to a negative impact on CAT (damaging the protein) and can explain the lower activity of CAT (Hagelstein et al., 2018; Koner et al., 2015). When the shear strength is higher than the breaking strength, a brittle fracture can occur (de Backere et al., 2022; Koner et al., 2015; Qiu et al., 2017). In the situation of the MAN mixtures, it seems that the crystalline form is less detrimental in affecting the stability of CAT than the co-particle of MAN since, in the second, more instability is observed in the activity of CAT due to the presence of a mixture of forms.

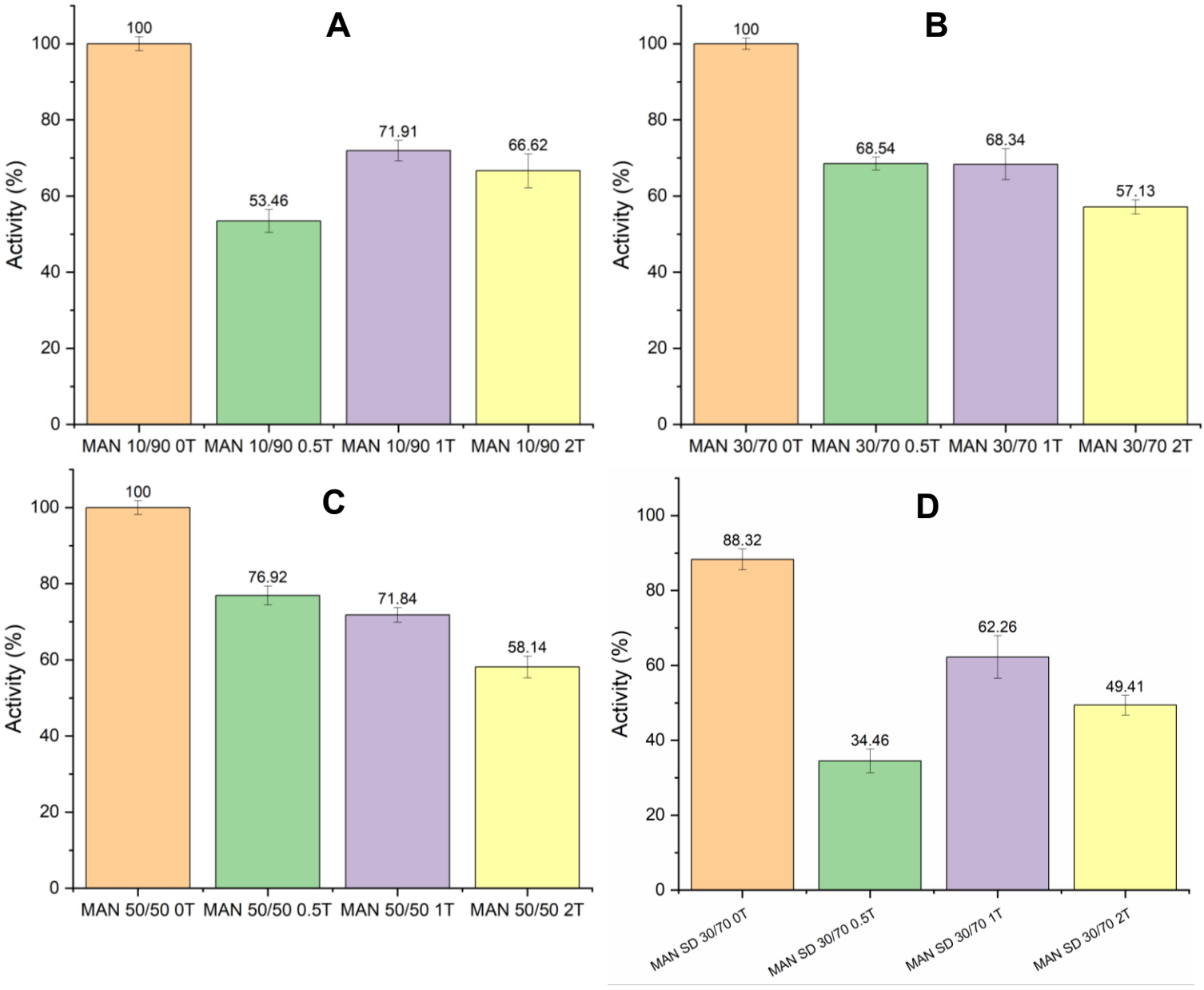

Figure 15 - Enzymatic activity of non-spray-dried and spray-dried MAN mixtures, as a blend and co-particle before and after compression. *Legend: A – 10/90 ratio; B – 30/70 ratio; C – 50/50 ratio; D – 30/70 spray-dried ratio.*

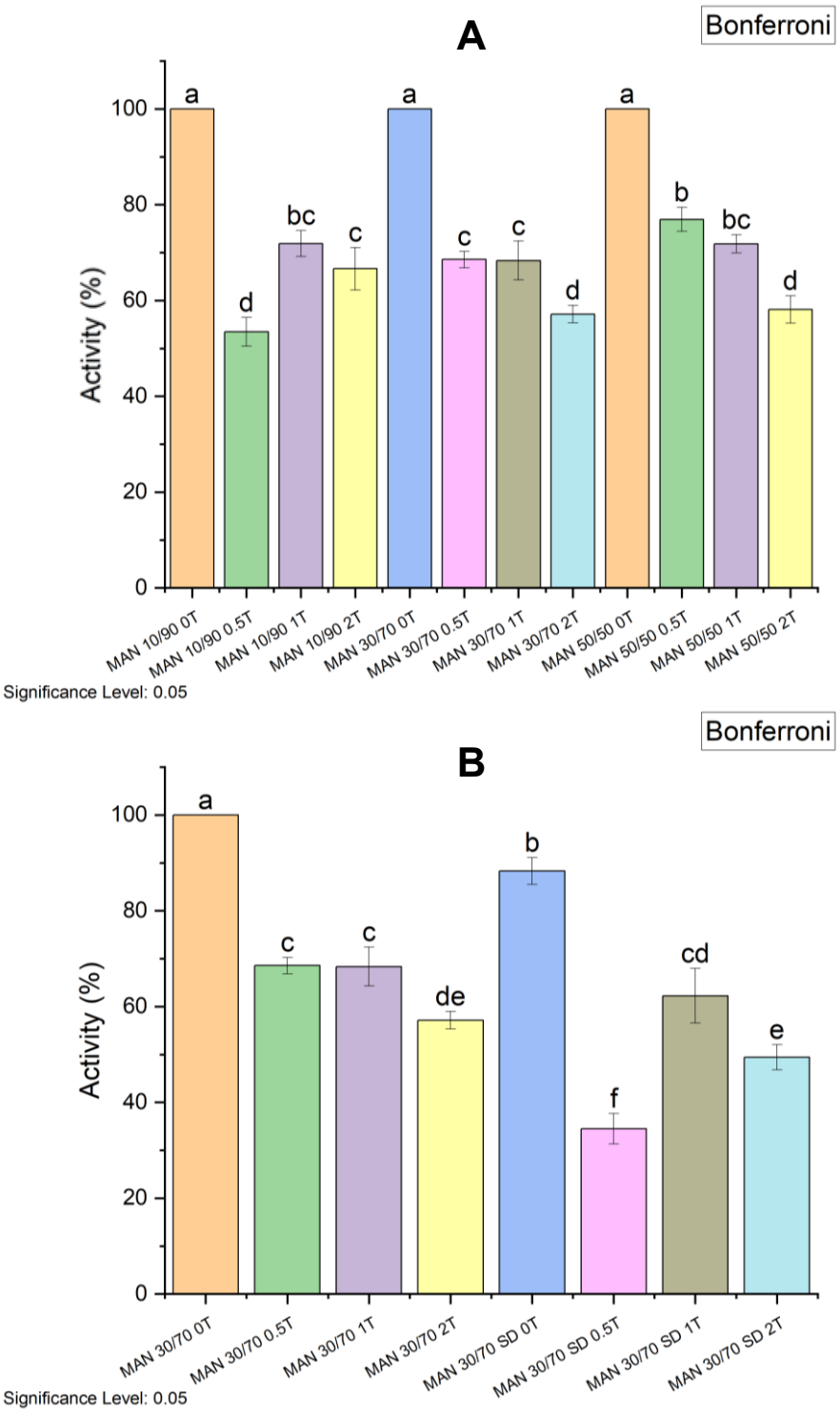

Figure 16 - Bonferroni statistical analysis of the activity of the non-spray-dried and spray-dried MAN mixtures as a blend and after compression. *Legend: A – Non-spray-dried tablets with different ratios; B – Non-spray-dried and spray-dried blend, co-particle and tablets with 30/70 ratio.*

3.1.4 Tablets with Catalase and Trehalose

The non-spray dried tablets with TRH lost activity with the application of force, similar to what has been observed for the tablets comprising the other saccharides (Figure 17 – A, B and C). However, a consistent pattern in the decrease of activity is visible with TRH in which, for all the ratios, the activity is gradually lower with increased forces, contrary to the other saccharides, a clear trend of the decrease in activity with the increase of force is visible. The CAT loading of 30 mg seems to be the most stable since the difference between 1 T and 2 T is similar. The respective error band graphs are represented in Annex A.7.

In the TRH spray-dried mixtures, a trend of the decrease in activity with the increase of the force applied is observed as in the non-pray-dried mixtures (Figure 17 - D). Focusing on the TRH SD 30/70 0T, it seems that TRH is stabilizing the protein since, after SD, the activity remains similar to the respective baseline, contrary to what was observed in the dry-state mixtures of TRH. After the tableting, a decrease of approximately 30 % of the activity is observed, in which the activity is inversely proportional to the applied force (Error band graph in Annex A.8). However, it is worth mentioning that compared to the CAT SD alone and in the presence of the other saccharides, the co-particles of TRH-CAT showed the highest activity after compression, further indicating a potential stabilizing effect of the sugar when drying and further processing the protein material.

Figure 18 - A confirms the clear pattern of a decrease in the enzyme's activity. Also, similarities in the activity between different ratios can mean that the ratio had little effect on the protection of the protein. Nonetheless, the 30/70 ratio showed more stability than the other ratios.

Moreover, with the spray-dried formulation, a decrease in activity after the tableting also occurs. To the forces of 1 and 2 T, the activity is similar, showing some stability with the increase of force (Figure 18 - B). TRH SD 30/70 0T had an activity higher than the non-spray-dried blend, however, the values are assumed as the same due to the associated error. From this comparison, the protective effect of TRH during the SD is visible. The spray-dried tablets showed similar activities as the non-spray-dried tablets (activity of the TRH and CAT: crystalline-amorphous) blend is similar to the activity of the TRH and CAT co-particle (amorphous-amorphous). Similar activities with and without SD confirm the stabilizing effect of TRH against the SD processing parameters. However, despite TRH stabilizing CAT, it is not viable to have one extra step to have a similar activity to the non-spray-dried CAT.

To the possible stabilization of CAT in the non-spray-dried tablets, mechanical stabilization is observed (between the different forces used during the tableting) since in the ATR-FTIR spectra are not visible significant changes after tableting, which could significate changes in

the interactions between the protein and the sugar that could mean chemical stabilization (see Section 3.3.4).

In addition, after the SD, there is a transition of TRH structure from crystalline to amorphous. In this case, the amorphous structure looks like a better stabilizer than the crystalline form since, after the SD process, the activity of CAT is similar. A similar activity after SD can be explained by the fact that TRH is a good protein stabilizer during dehydration and storage because it can replace the water molecules on the protein's surface and create hydrogen bonds with the protein (Liao et al., 2002). These changes are sustained by changes in the intensity of the O-H peak of sugar-alcohols around 3300 cm^{-1} after the SD (See Section 3.3.4).

Furthermore, TRH is a brittle material before SD because it has a crystalline structure, which can mean that during the tableting of the non-spray-dried materials, the protein is affected negatively by the brittle fragmentation of TRH and can explain the further decrease of activity identified during tableting when compared to the enzyme tableted alone (de Backere et al., 2022). After the SD, the structure transits to a more plastic material (amorphous structure). The amorphous structure is more suitable to form hydrogen bonds, and in addition, the plastic deformation during the tableting can increase the formation of particle-to-particle regions and increase protein stability (Chen et al., 2021; Jain, 1999). However, the results suggest that this stabilization is not occurring during the tableting. As explained before to DEX (Section 3.2.2), during the tableting amorphous-amorphous phase separation might occur due to the plastic deformation of the material, which might affect the stabilization of the protein (Ayenew et al., 2012).

Summarizing, it was observed that the amorphous structure of TRH can stabilize CAT during the SD due to the similar activity to the non-spray-dried tablets, but not during the tableting. Comparing the results, it is not an advantage to spray-dry CAT with TRH to increase the stability because without SD is possible to have the same activity with a cheaper and faster process.

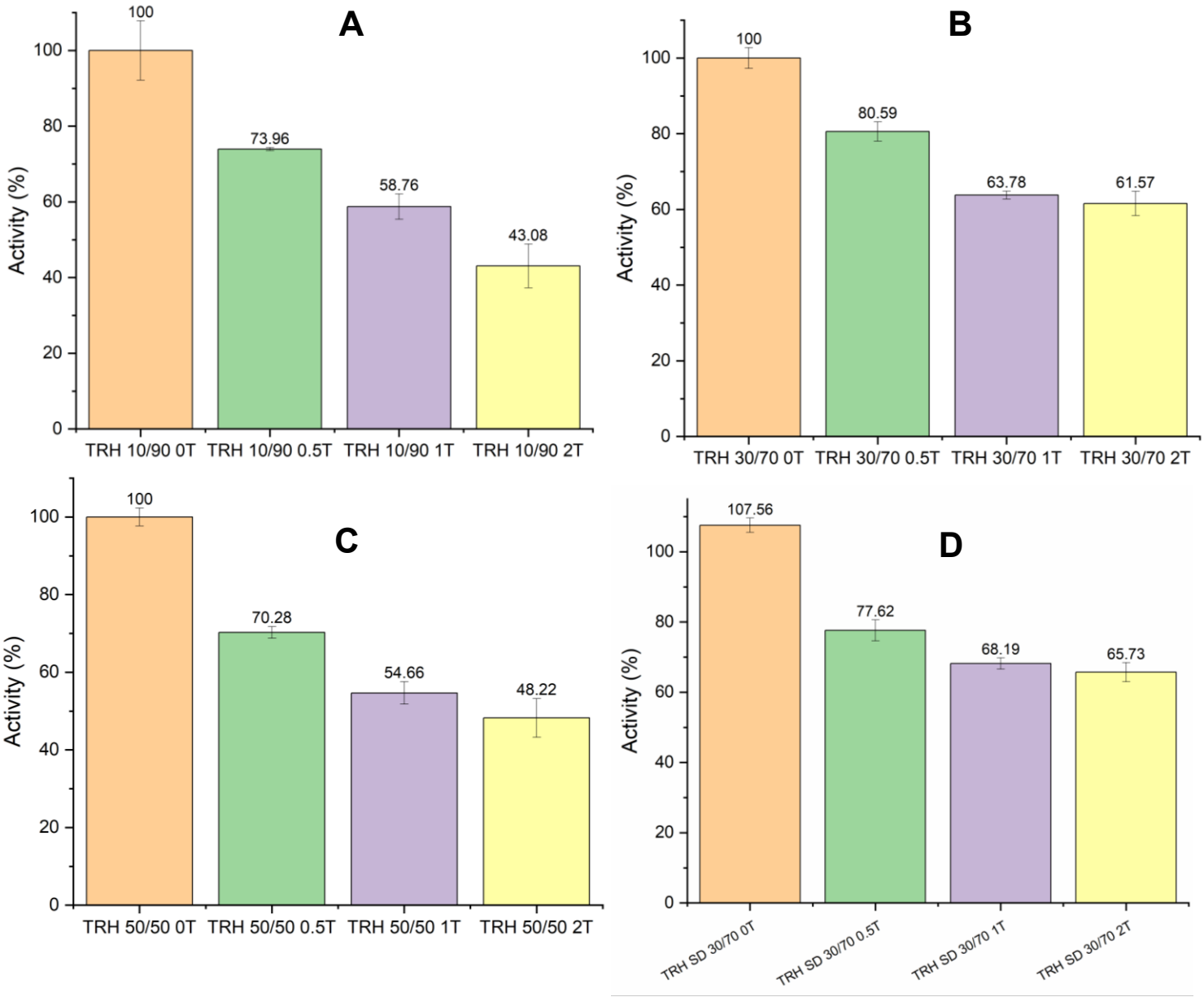

Figure 17 - Enzymatic activity of non-spray-dried and spray-dried TRH mixtures as a blend and co-particle before and after compression. *Legend: A – 10/90 ratio; B – 30/70 ratio; C – 50/50 ratio; D – 30/70 spray-dried ratio.*

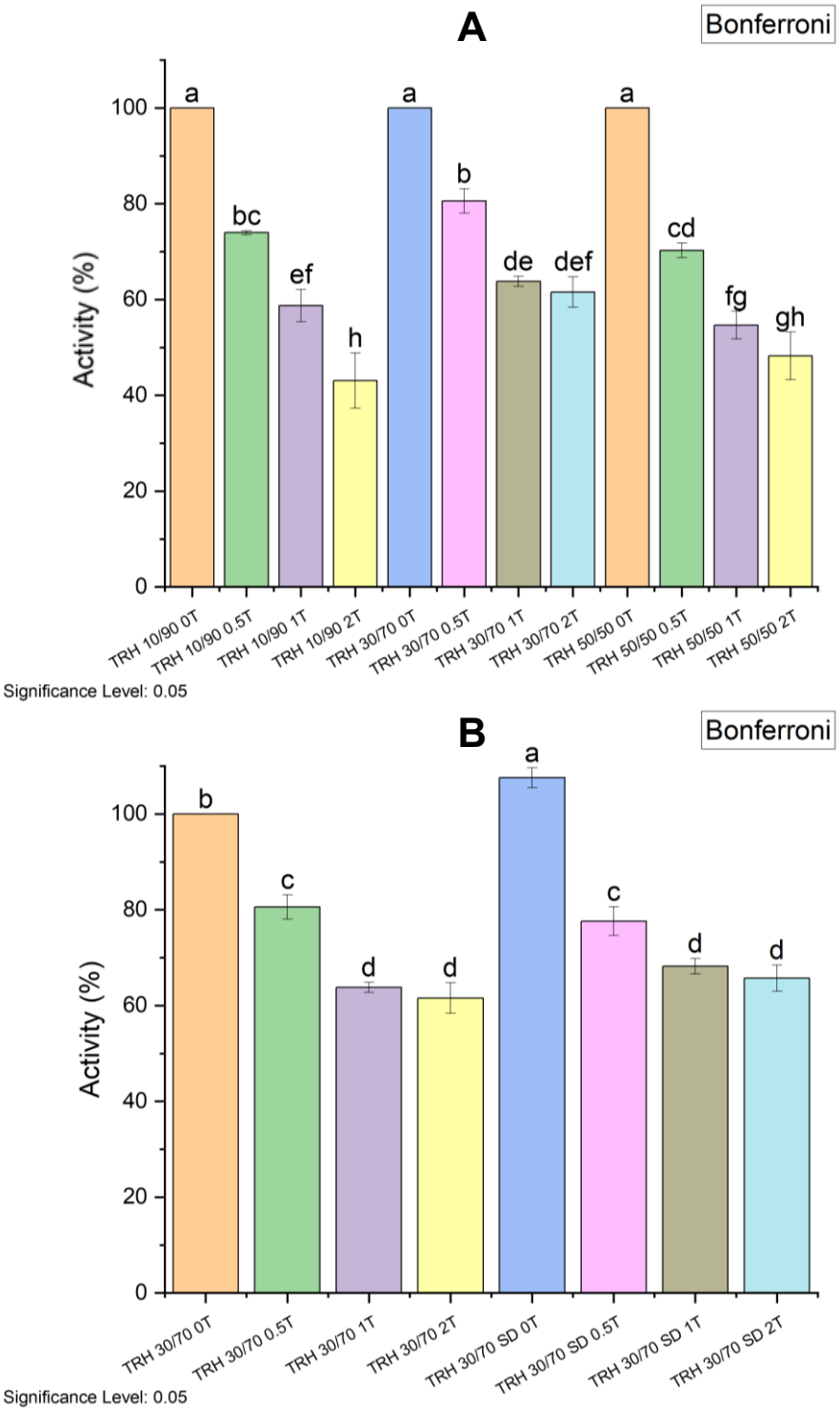

Figure 18 - Bonferroni statistical analysis of the activity of the non-spray-dried and spray-dried TRH mixtures as a blend and after compression. *Legend: A – Non-spray-dried tablets with different ratios; B – Non-spray-dried and spray-dried blend, co-particle and tablets with 30/70 ratio.*

3.2 Impact of Tabletting on the Number of Particles

3.2.1 Tablets with Catalase

The application of force also led to a significant increase in the number of particles. The number of particles increased from approximately 1300 (CAT 0T) to 20 000 - 35 000 (CAT 0.5T, CAT 1T, and CAT 2T). As it is possible to see in Figure 19 - A, the particles start to appear in higher numbers between the ECD ranges of 50≤x≤75 and 25≤x≤50 µm. These results seem to confirm that the loss of activity is due to the formation of aggregates (particularly evident in the increase of the ECD class 25≤x≤50 µm) due to the loss of CAT's conformational stability when subjected to shear and thermal stresses during compression (Chiti & Dobson, 2006; Dobson, 2003). In turn, for the 25≤x≤50 µm range, the number of particles increased for the two highest forces, 1 and 2 T. Moreover, the number of particles in the two highest forces was similar, in which both forces shared the same class (lower-case letter: a).

The MFI graph of the spray-dried mixtures (Figure 19 - B) shows a sharp difference between the highest forces (1 and 2 T) and the remaining ones. In the 25≤x≤50 µm class, the particles in the forces 0 T and 0.5 T are almost inexistent. However, overall, a higher number of particles was seen after SD. As an additional step is added to production, this can lead to an increase in particles due to contamination occurring during the process. This means that these particles might not necessarily be aggregates due to instability.

The correlation matrix of the PCA (Section 3.4.1) showed a correlation between the Abs_{180s} and the number of particles in the range 25≤x≤50 µm, indicating a relationship between the activity and the number of particles. Also, the high correlation between the force applied and both Abs_{180s} and the number of particles of the range 25≤x≤50 µm showed the impact of the force on these variables. Through the analysis, it is also possible to observe a higher correlation between this range and the Abs_{180s} compared with the other variables.

The Bonferroni statistical analysis was performed using the 25≤x≤50 µm range (Figure 20 – A and B). For the non-spray-dried mixtures is confirmed the difference in the number of particles with the increase of the force in which exists an approximate number of particles to the two highest forces (Figure 20 - A). Figure 20 - B (spray-dried mixtures) shows that in the 25≤x≤50 µm range of the MFI, exists a sharp difference between the first two mixtures and the last two.

The loss of activity seems to be in accordance with the increase of the number of particles with the application of force. However, when comparing the UV/Vis results with the MFI results, the pattern of change was different. While the activity of CAT decreased with the increase of force,

the number of particles had a maximum value of 1 T (Figure 20). Nevertheless, the increase in the number of particles can be related to the loss of activity, which can mean that the particles show the formation of aggregates that can lead to this effect (Bekard et al., 2011; Chiti & Dobson, 2006; Dobson 2003; Wei et al., 2019; Wurster & Ternik, 1995; Zeeshan et al., 2019).

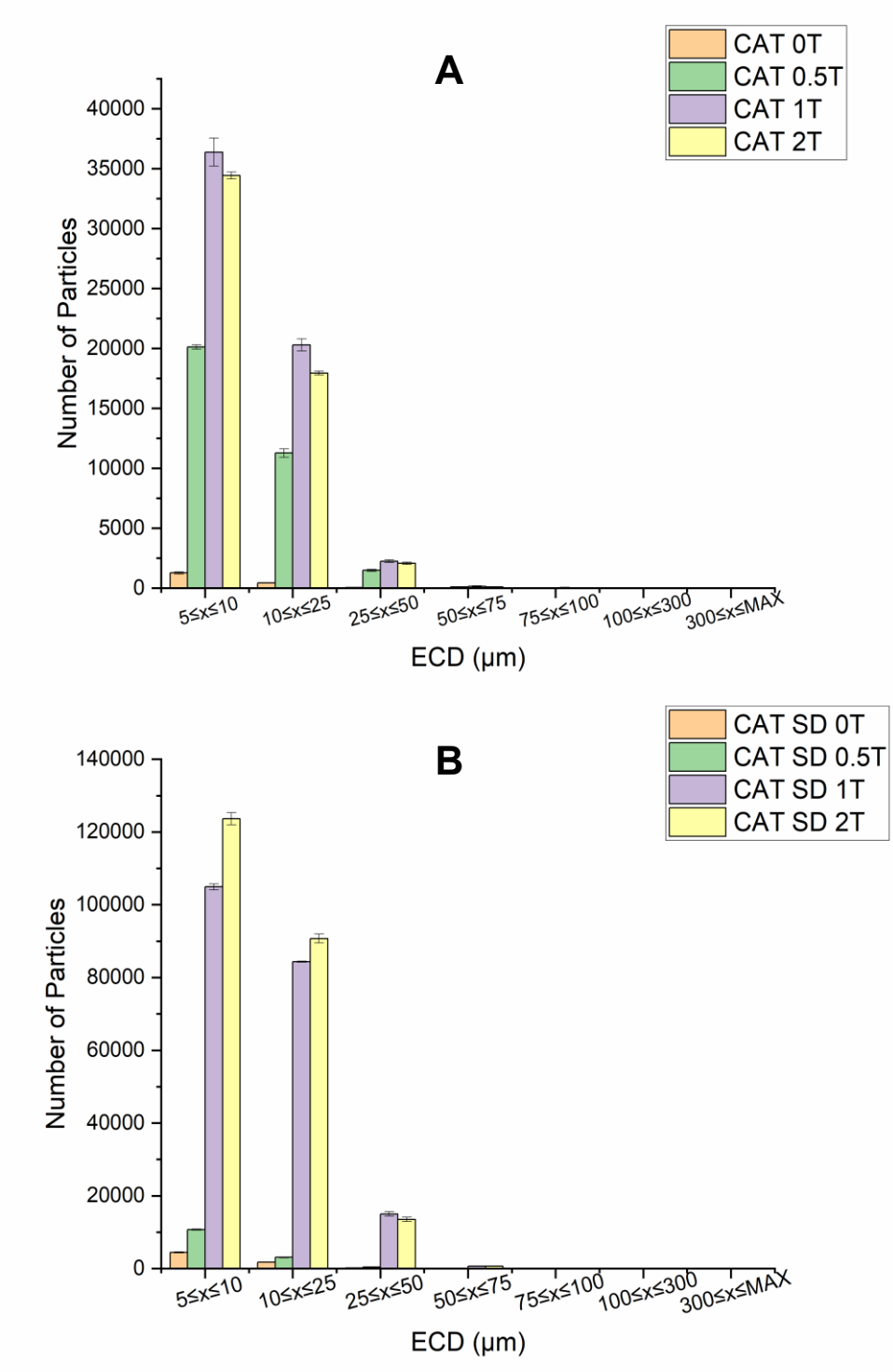

Figure 19 – Number of non-spray-dried and spray-dried particles of the CAT blend, co-particle and tablets.

Legend: A – Non-spray-dried CAT mixtures; B – Spray-dried CAT mixtures.

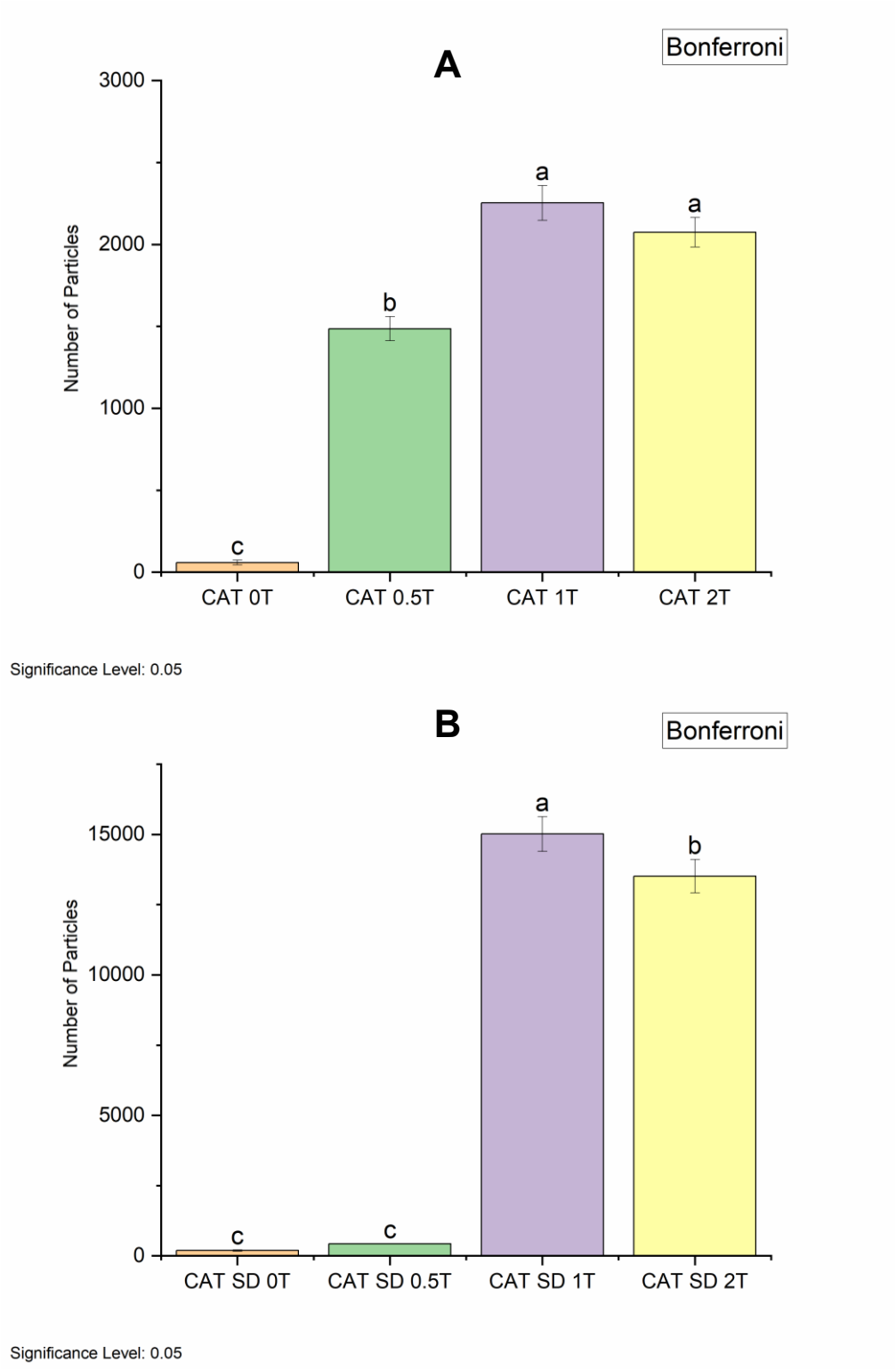

Figure 20 - Bonferroni statistical analysis of the number of particles in the 25≤x≤50 µm range, of CAT mixtures, as a blend, co-particle and after compression. *Legend: A – Non-spray-dried CAT mixtures; B – Spray-dried CAT mixtures.*

3.2.2 Tablets with Catalase and Dextran

In the DEX mixtures (Figure 21), the particles started to appear in larger numbers between the ECD ranges of 50≤x≤75 and 25≤x≤50 µm for both non-spray-dried and spray-dried mixtures. In the 25≤x≤50 µm class (Figure 21 - A), when compared with the DEX blends, the number of particles increased from between 100 and 800 particles to values between 2000 and 6000 particles in solution. Moreover, these mixtures have a higher number of particles than tablets with 100 mg of CAT. From the MFI graph of the spray-dried mixtures, a slight decrease in the number of particles compared with the non-spray-dried mixtures is observed (Figure 21 - B). As in previous mixtures, the number of particles in the force 1 T is higher than the number of particles with the highest force.

In the MFI, there is more variability in the results. Particularly for DEX 10/90, there is a significant difference in the number of particles. The mixtures with a ratio of 10/90 have more particles than the other ratios, and it is observed a smaller difference in the number of particles between different forces than in the remaining ratios. The sharp difference between the number of particles of the ratio of 10/90 and the other ratios might be due to one error during the measurement (i.e., dilution error). This can be supported by the fact that to the 10/90 ratio, the highest activity is observed in the highest number of particles.

Even if, in the PCA (Section 3.4), a correlation exists between the Abs_{180s} and the number of particles in the selected range, analysing both Bonferroni graphs, a similar pattern behaviour is not seen. For example, the DEX 10/90 mixtures have the most significant number of particles, however, they have similar activity to the DEX 50/50 mixtures, which have less than one-third of the number of particles.

From the visualization of the Bonferroni statistical analysis of the CAT's activity in the DEX spray-dried mixtures, it is possible to see the trend of decreasing activity with the increase of the applied force (Figure 13 - D and 22 - A). In the analysis, the increase in the number of particles from the spray-dried blend to the tablets is sharp, and the number of particles between tablets is similar (same lower-case letter: a). This seems to indicate that, as for CAT SD alone, the changes in the activity of the spray-dried CAT-DEX co-particles are not correlated to changes in the higher order structure (HOS) of the protein or if the increase of the number of agglomerates is not correlated to a further loss of activity (which plateau). The second theory was described in the literature in which the loss of activity decreases slower as the less activity CAT has, leading to a plateau (Mofidi Najjar et al., 2017). However, the DEX SD 30/70 0.5T should be repeated due to the high STD.

Contrary to Figure 22 - A, in Figure 22 – B is no visible trend of the increase in the number of particles. After SD, a decrease in the correlation between variables was observed, hence the PCA (Section 3.4.2) only sees a correlation between the blends and tablets and Abs_{180s}, which does not occur for the spray-dried mixtures. This suggests that the loss of activity is not correlated (or has little correlation) to the higher number of particles during this additional process step, which makes it difficult to detect properly some aggregates that might be present. The high number of particles can be due to further contamination during the added process step.

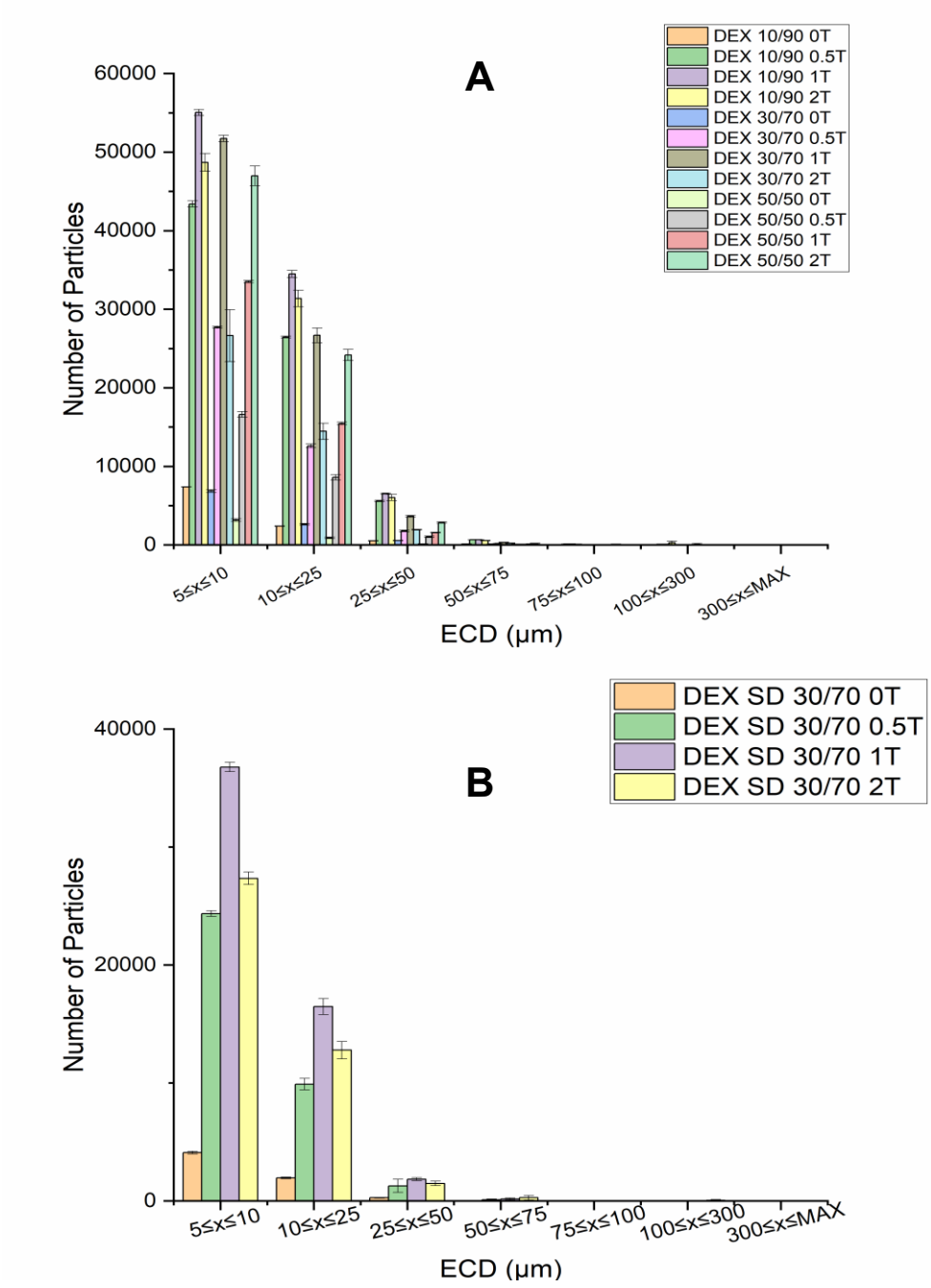

Figure 21 - Number of non-spray-dried and spray-dried particles of the DEX blend, co-particle and tablets.
Legend: A – Non-spray-dried DEX mixtures; B – Spray-dried DEX mixtures.

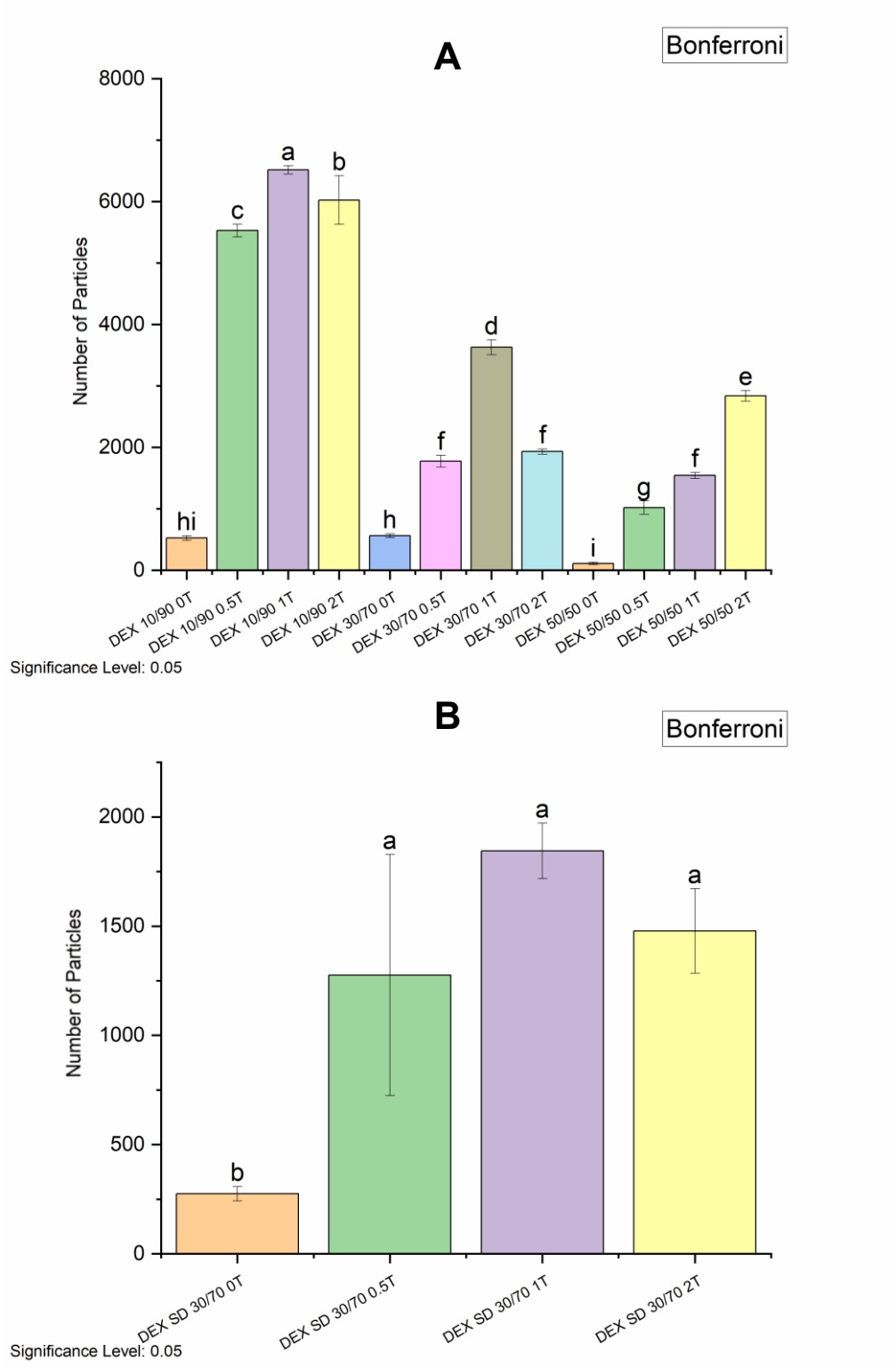

Figure 22 - Bonferroni statistical analysis of the number of particles in the 25≤x≤50 µm range, of spray-dried DEX mixtures, as a blend, co-particle and after compression. *Legend: A – Non-spray-dried DEX mixtures; B – Spray-dried DEX mixtures.*

3.2.3 Tablets with Catalase and Mannitol

In the non-spray-dried MAN mixtures, the increase of the number of particles in some mixtures with different ratios increased with the increase of force (Figure 23), particularly in the 25≤x≤50 µm range. Again, the particles started to appear in larger amounts between the ECD ranges of 50≤x≤75 and 25≤x≤50 µm (with and without SD). In the smaller range (5≤x≤10 µm), the variation of the number of particles is more random since it does not follow any pattern. Also, a sharp decrease in the number of particles from the tablets with 100 mg of CAT to the MAN mixtures was observed.

The number of particles in the spray-dried MAN mixtures increased compared to the non-spray-dried MAN mixtures, however, a decrease was observed in comparison with the spray-dried tablets with 100 mg of CAT (Figure 23 - B). In the first situation, the increase in the number of particles in relation to the non-spray-dried tablets is expected due to the extra steps of the SD. Furthermore, the number of particles becomes progressively higher with the increase of the applied force in all the ranges.

From the Bonferroni statistical analysis, it is confirmed that in the 25≤x≤50 µm range, particles increase occurs with the increase of applied force (Figure 24 - A). Generally, these results are in line with the trend observed in the UV/Vis results. So, this increase in the number of particles seems to be correlated to a loss of activity. The correlation in the PCA (Section 3.4.1) between the number of particles in this range and the Abs_{180s} further corroborates this result.

To this saccharide, the patterns of increase in the number of particles are equal to all the mixtures, in which the number of particles increases progressively with the increase of the applied force (Figure 24 – A and B). This might indicate that the increase of the force increases the stress applied to the protein, causing aggregation. Moreover, an error associated with the process might increase the number of particles by contamination.

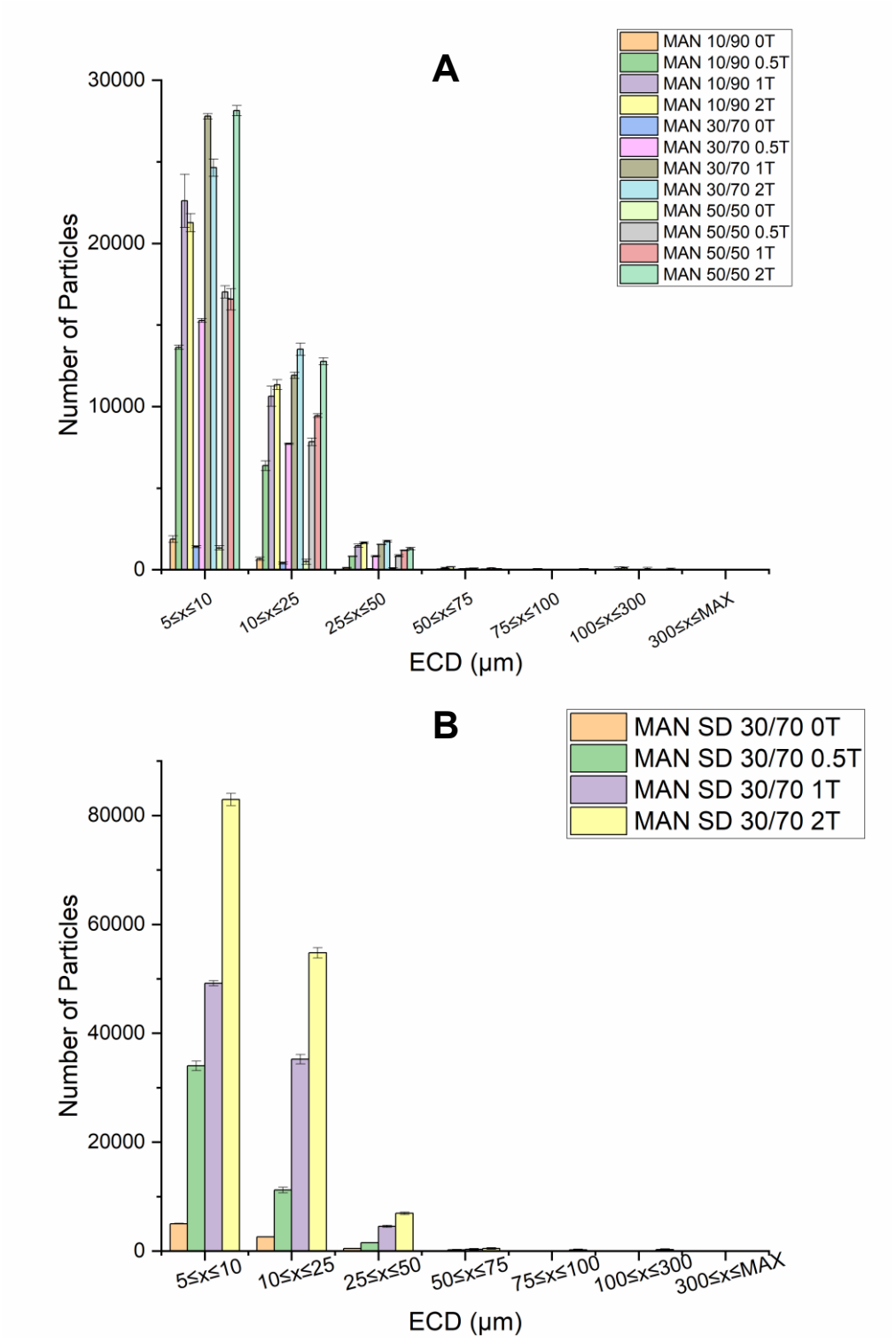

Figure 23 - Number of non-spray-dried and spray-dried particles of the MAN blend, co-particle and tablets.

Legend: A – Non-spray-dried MAN mixtures; B – Spray-dried MAN mixtures.

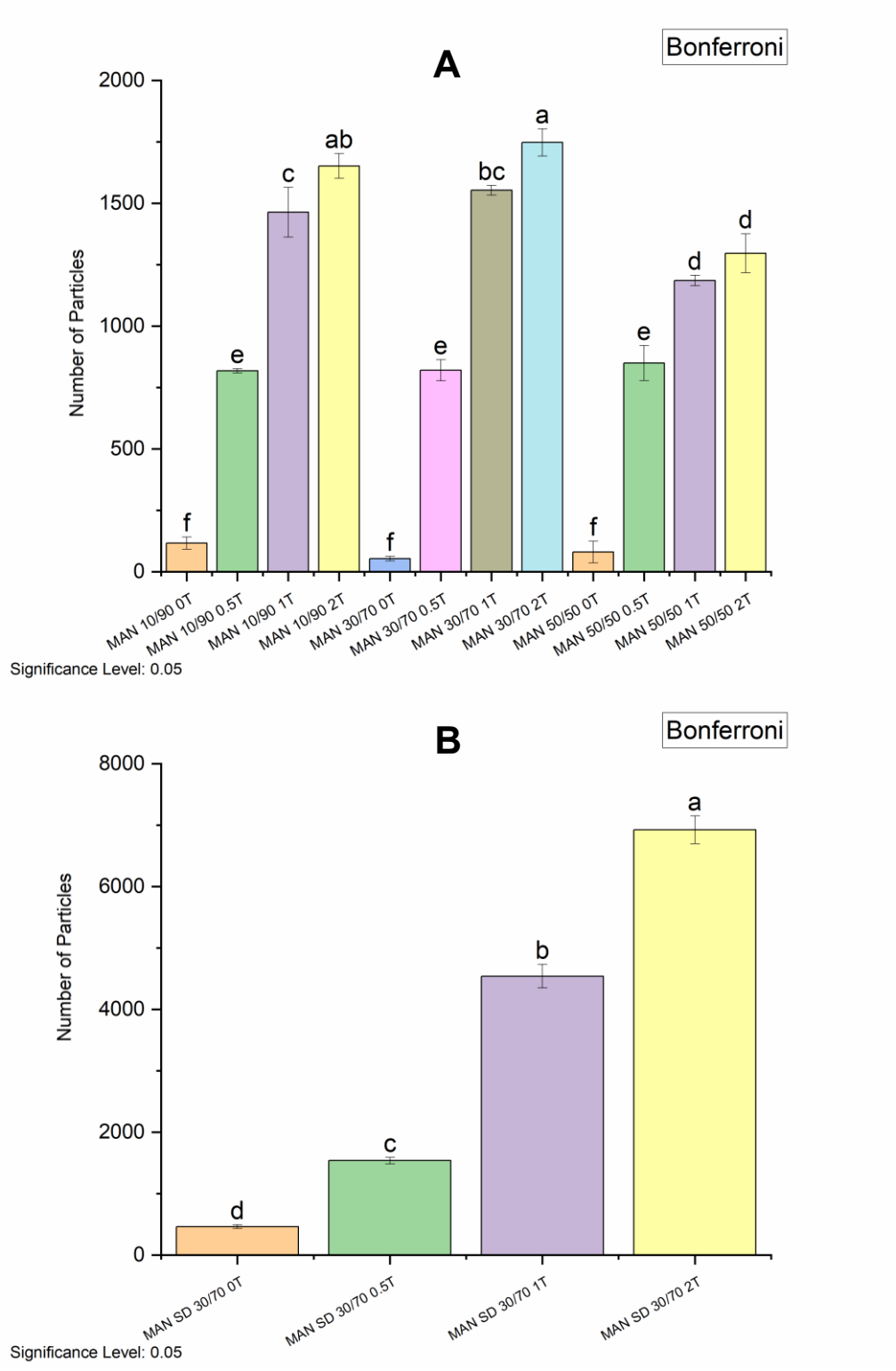

Figure 24 - Bonferroni statistical analysis of the number of particles in the 25≤x≤50 µm range, of spray-dried MAN mixtures, as a blend, co-particle and after compression. *Legend: A – Non-spray-dried MAN mixtures; B– Spray-dried MAN mixtures.*

3.2.4 Tablets with Catalase and Trehalose

In the three smaller size ranges, the number of particles in the TRH mixtures increased with the increase of the force applied (Figure 25 - A). As in the previous mixtures, the particles appeared from the range of 50≤x≤75 to 25≤x≤50 μm. Furthermore, the number of particles is smaller than the number of particles in tablets with 100 mg of CAT, showing protection of the CAT regarding the formation of aggregates.

The number of particles of spray-dried TRH mixtures was similar to the one of the non-spray-dried tablets (Figure 25 - B). To the TRH SD 30/70 2T, the increase was sharp compared with the force 1 T, and compared with the activity (Figure 17 - D), the difference in the activity is minimum, so it can be probably due to contamination of the sample the number of particles increased, so this formulation could be repeated to see the reproducibility of the result or if the increase of the number of agglomerates is not correlated to a further loss of activity (which plateau), as mentioned in the previous section.

Considering the mixtures with and without SD (Figure – 26), the number of particles increases with the increase of the applied force, which is confirmed by the Bonferroni statistical analysis for the 25≤x≤50 μm range. To this saccharide is observed the same behaviour as to MAN, which progressively increases with the increase of the applied force. The number of particles is lower to the spray-dried mixtures, with the exception of TRH SD 30/70 2T, which seems that was contaminated due to the sharp difference with the other mixtures (Figure 26 - B).

Simultaneously to the increase in the number of particles, it is observed a decrease in the activity of the TRH mixtures – an inverse trend – that corroborates the results between the different techniques and observations in the PCA (see Section 3.4). In addition, the fact that there is a correlation between the variables (observed in the PCA) might indicate that the loss of activity is correlated with the increase in the number of particles.

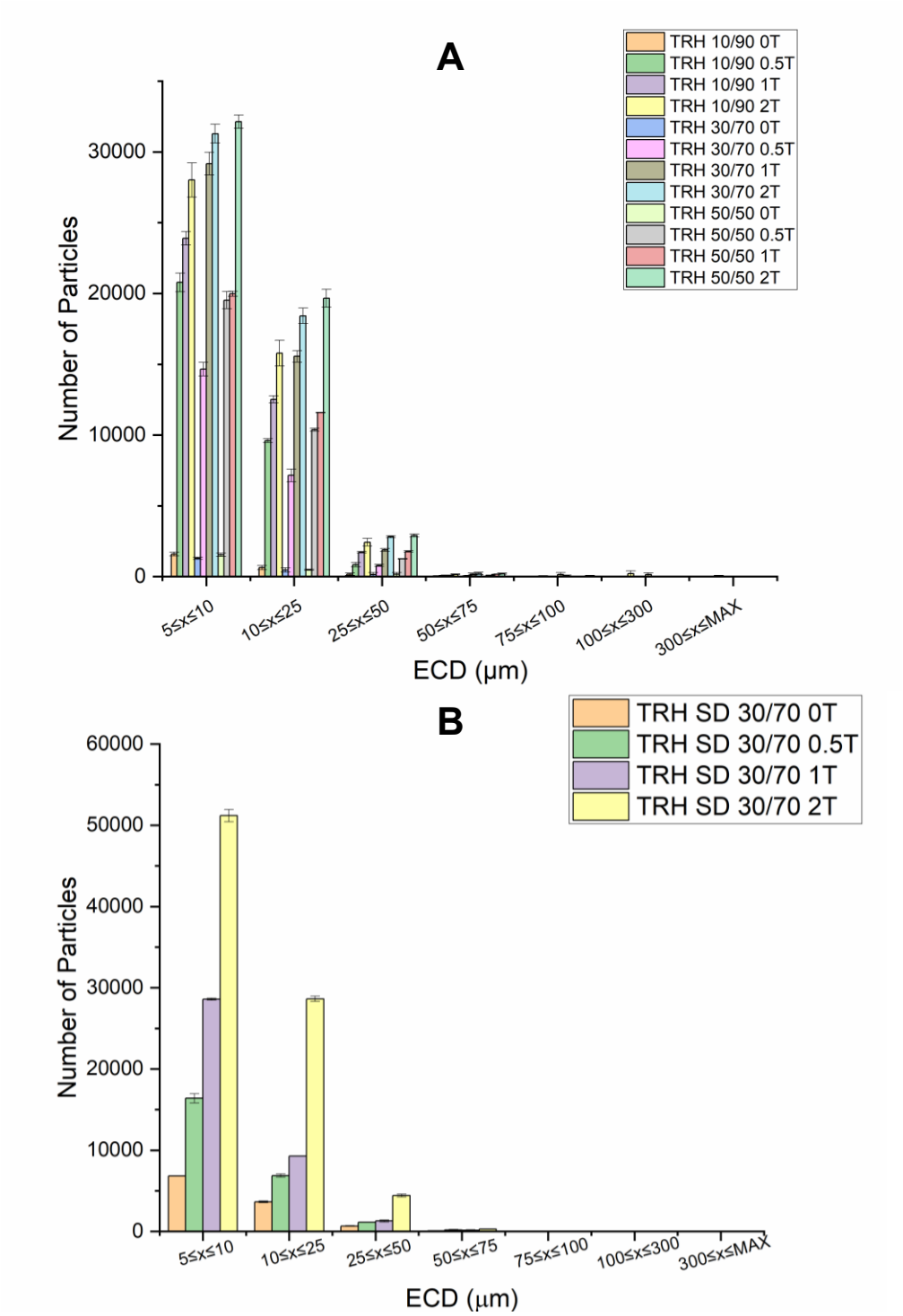

Figure 25 - Number of non-spray-dried and spray-dried particles of the TRH blend, co-particle and tablets.

Legend: A – Non-spray-dried TRH mixtures; B – Spray-dried TRH mixtures.

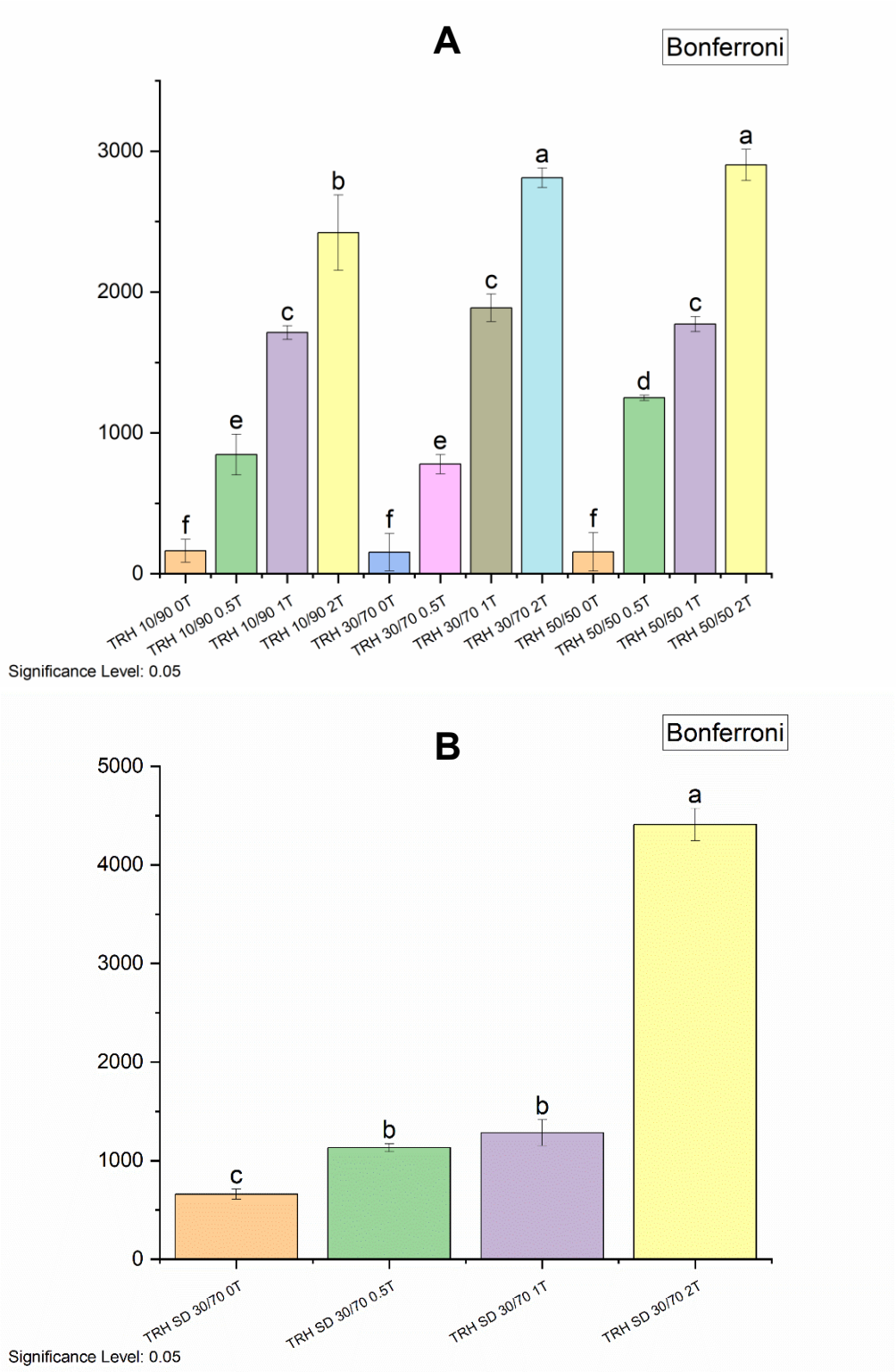

Figure 26 - Bonferroni statistical analysis of the number of particles in the 25≤x≤50 µm range, of spray-dried TRH mixtures, as a blend, co-particle and after compression. *Legend: A – Non-spray-dried TRH mixtures; B – Spray-dried TRH mixtures.*

3.3 Impact of Tabletting on Catalase Structure

3.3.1 Tablets with Catalase

The changes in CAT's structure were studied using ATR-FTIR. The secondary structure of proteins is mainly characterized by α-helix and β-sheet. Among the Amide groups identified in the FTIR spectrum, Amide I and Amide II have a particular interest in the study of proteins' secondary structure. Amide I is present in the region of 1600-1690 cm^{-1}, while Amide II is present in the region of 1575-1480 cm^{-1} and Amide III in the region of 1229-1301 cm^{-1} (Kokaly, 2001). In the spectrum of CAT 0T (Figure 27 - A), it was possible to observe some main peaks, such as Amide I (~1650 cm^{-1}), Amide II (~1550 cm^{-1}), and Amide A (~3300 cm^{-1}). The peak of Amide I is a result of the C=O stretching, N–H bending, or C–N stretching, while the Amide II can result from N–H bonding or C–N stretching, and finally, the Amide A can result from N-H stretching (Kokaly, 2001).

No significant changes in the peaks of Amide I and II in the CAT tablets were observed (Figure 27 - B). There was a slight decrease in the peak intensity between CAT 0.5T and the other tablets. A more visible change is observed in the Amide III region (1229-1301 cm^{-1}). In this region, the peaks of CAT 0T and CAT 2T overlap, suggesting no changes in the Amide III band up on the application of 2 T of force. On the contrary, a change in the peaks' intensity is observed for CAT 0.5T and CAT 1 T. Different peak intensity in the four samples is observed around 2900 cm^{-1} concerning C-H stretching. Furthermore, even though the peak is not visible in the region of Amide B (3100 cm^{-1}), a shift of the CAT 2T in comparison with the other mixtures was observed. Finally, in the Amide A band (3300 cm^{-1}), an increase in the intensity of the peak of CAT 2T was detected, which can indicate an increase in the strength of the N-H bond.

Overall, the main peaks used in the study of changes in the secondary structure of proteins (Amide I and II) were not affected, which can mean that the secondary structure of CAT was not affected by the application of force. Besides the changes in the peak intensity among the different forces applied, CAT 0T had similar behaviour to the CAT 2T (upper force limit), indicating that the forces of 0.5 and 1 T had a more significant impact on the spectra than the highest force used. The fact that the highest force did not affect the enzyme's structure in the same extension may be due to a refolding of the structure, which makes the structure back to the initial structure.

Although no changes were detected in the Amide I and II, some differences were seen between the spectra with the application of force, however it is less clear what structural changes these

indicate and how these are related to the loss of activity. Further investigations are needed, such as techniques such as nuclear magnetic resonance or circular dichroism, to study the secondary structure of the enzyme.

From the ATR-FTIR spectra of the spray-dried CAT tablets (Figure 27 - C), it is observed that the Amide I and II peaks are not changing (secondary structure), however, differences are visible in the intensity of the peaks between CAT 0T and the spray-dried mixtures. Although it is not certain where these changes occur in the structure, it might indicate some changes in the molecular structure, however, further investigation is needed. The difference in intensity in the peaks in the region of 2900 cm^{-1} (Amide B) and 1250 to 1400 cm^{-1} (Amide III) suggest that changes in the CAT structure are occurring with the application of force. In fact, CAT SD 0T has a lower intensity in the entire spectra (besides Amide I, II, and A) compared with CAT 0T, suggesting that the SD affected the structure of CAT (Grasmeijer et al., 2019; Haque et al., 2015).

The changes in the spectra can corroborate the relationship between the loss in activity and the increase in the number of particles (an increase in aggregation). Aggregation could have been originated due to changes in the secondary structure that are translated into activity loss.

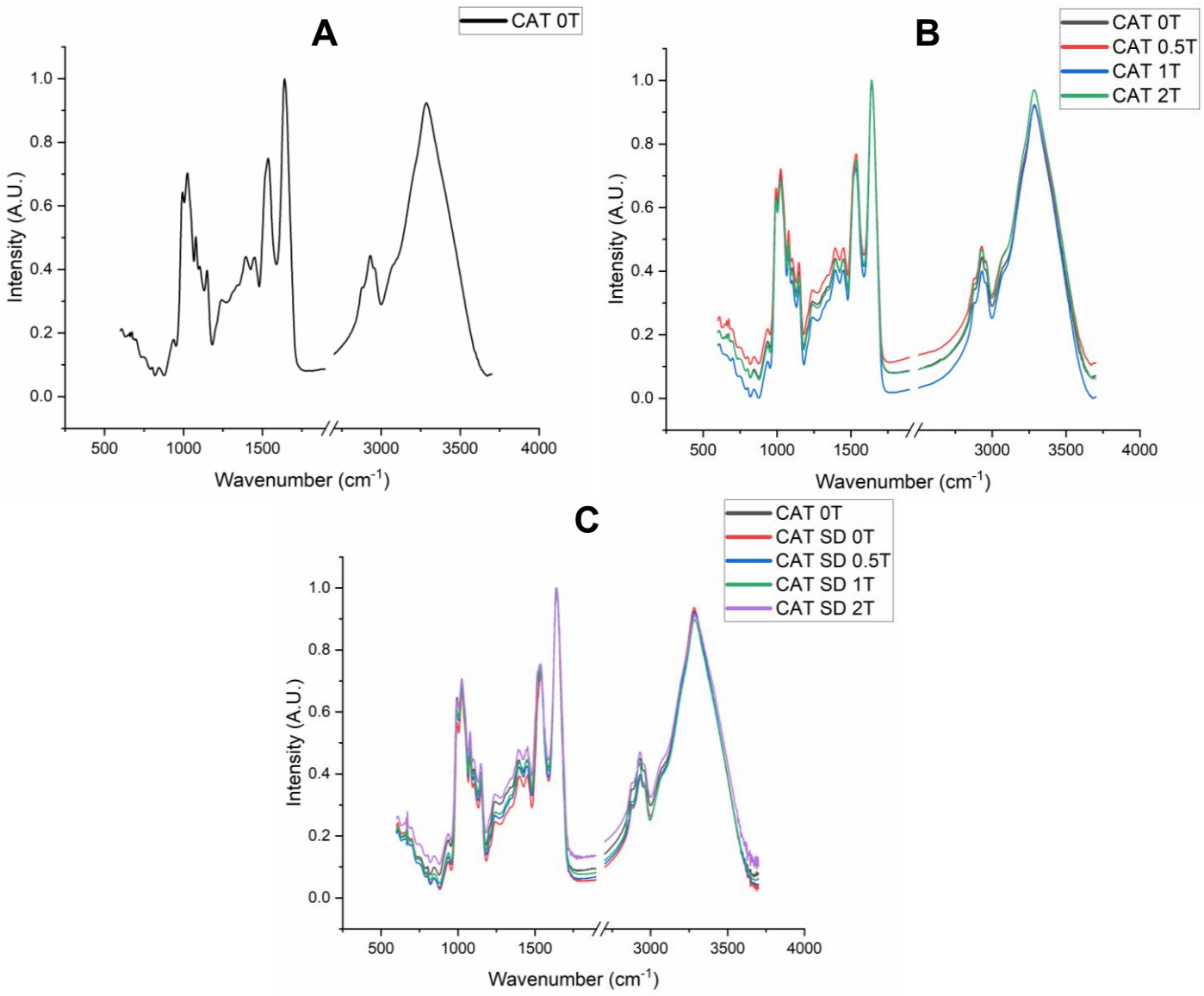

Figure 27 - ATR-FTIR spectrums (600-3700 cm^{-1}) of CAT as a blend, co-particle before and after compression. *Legend: A – Non-spray-dried CAT blend (raw material); B – Non-spray-dried CAT tablets (after compression); C – spray-dried co-particle and tablets of CAT.*

3.3.2 Tablets with Catalase and Dextran

To the ATR-FTIR technique, the spectra of the raw DEX blends with different ratios and tablets were collected and analysed (Figure 28). The DEX used was in the amorphous form (Annex B.1) since this is the only current form for this sugar. The spectrum of the blends with different ratios shows an increase in the intensity of the Amide peaks with the increase of the CAT loading.

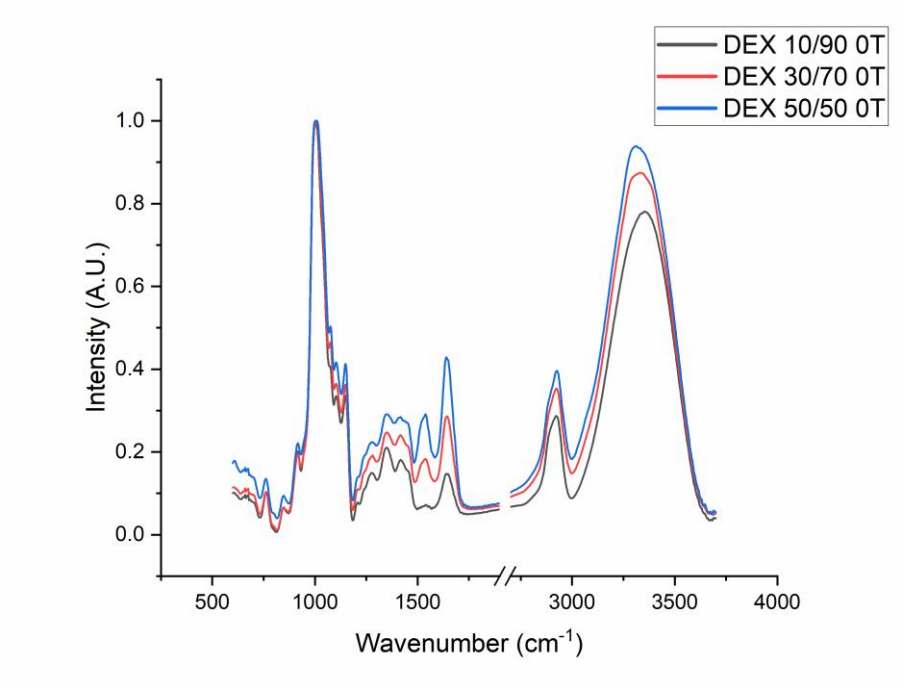

Figure 28 - ATR-FTIR spectrum (600-3700 cm^{-1}) of DEX mixtures as a blend.

The tablets were analyzed by CAT-sugar ratios (Figure 29 – A, B, C and D). As observed in the blends of CAT and saccharide, the intensity of the peaks of Amide I and II were dependent on the CAT loading (the larger the CAT quantity in the formulation, the more intense the secondary structure characteristic peaks are). Besides the different intensities of the peaks in almost all wavenumbers, there is a signal shift in the peaks of approximately 2900 and 3300 cm^{-1} of tablets compared with the blend. This phenomenon occurs for the three different CAT loadings. The type of shift can result from protein unfolding due to the exposition of thermal and mechanical stresses after compression (Yan et al., 2004). Furthermore, in Figure 29 – C, it is observed a different ratio of the peaks in the region of 1000 cm^{-1} which can indicate changes in the chain flexibility around the glycosidic bond (α 1-6) after compression (Siddiqui et al., 2014).

Moreover, the intensity of the peaks seems to change without following the same pattern, i.e., comparing the peaks between CAT loadings, it is observed that the changing pattern is not the same for all the forces between saccharides.

In conclusion, after the analysis, there are observable changes in the spectra. This suggests that the force used is affecting CAT's structure and might be causing an increase in the contact area and, thus, increasing the interactions, which can stabilize the ratio of 30/70 (Boonyaratanakornkit et al., 2002).

Differences between the spectra of the spray-dried mixtures are observed, particularly changes in the peaks' intensity (Figure 29 - D). These intensity changes are potentially

indicating some structural changes in sugar and protein. To the formulation with 0 and 2 T, the peak of Amide I almost disappears, and the intensity of the peak of Amide II becomes less intense. This can mean changes in the secondary structure which can, in turn, affect the activity of CAT in these mixtures. The intensity of the peak in the region of 3300 cm^{-1} can indicate that the tableting is affecting the O-H bonding (in the sugar) and the N-H stretching in the Amide A of CAT. Concluding, the changes between the spectra indicate that alterations in the structure of CAT are occurring.

The main differences between the non-spray-dried and spray-dried mixtures are the intensity of the Amides peaks, which can be related to the protein´s secondary structure. Simultaneously to the lowest intensity of Amide peaks, the spray-dried mixtures also have the lowest activity among all the mixtures. This corroborates the variation in activity because it suggests that alterations in the structure (e.g., interactions between bonds) can occur, and these changes could be the cause of the loss of activity.

Furthermore, from SEM analysis, it is possible to observe that the co-particles have a spherical dimpled and irregular shape (Annex D.1). Also, similar particles to the ones described by Ngono et al. (co-particles of protein and sugar) were obtained, indicating the presence of co-particles of enzyme and excipient (Ngono et al., 2019).

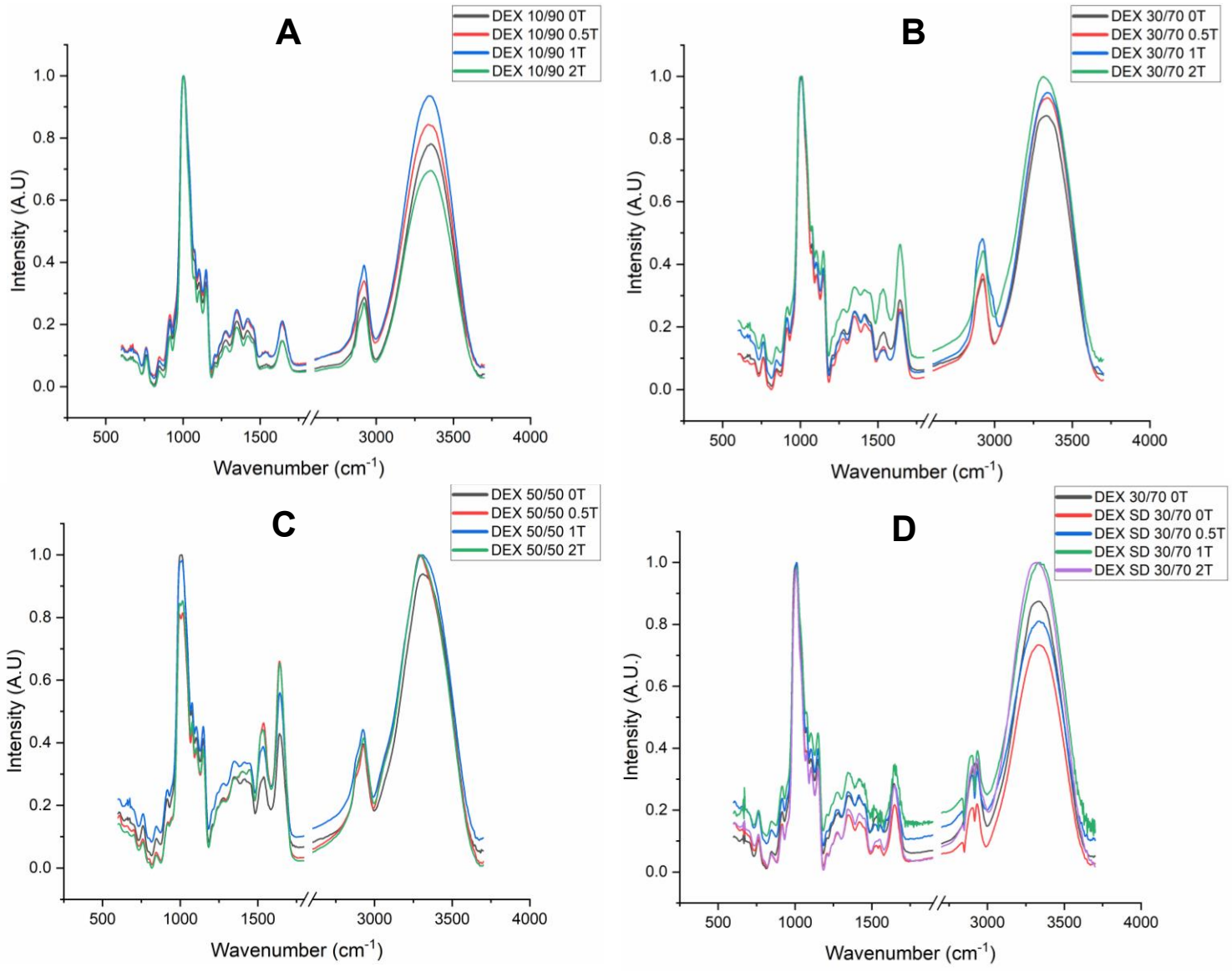

Figure 29 - ATR-FTIR spectrums (600-3700 cm^{-1}) non-spray-dried and spray-dried DEX mixtures, as a blend, co-particle and after compression. *Legend: A – 10/90 ratio; B – 30/70 ratio; C – 50/50 ratio; D – 30/70 spray-dried ratio.*

3.3.3 Tablets with Catalase and Mannitol

From ATR-FTIR spectra of the raw saccharide (Annex B.2 and C.1), it is possible to conclude that the raw MAN used is in the β form since, when compared with the literature is possible to observe characteristic peaks of this form (~1030 and 1130 cm^{-1}) and different peak intensity (Cares-Pacheco et al., 2014; Poornachary et al., 2013).

Figure 30 shows the spectra of the MAN blends with different ratios, showing an increase in the secondary structure characteristic peaks with the increase of CAT loading. With higher loadings of MAN, the peak in the region of 3400 cm^{-1} is more visible, probably because of the O-H bonding, since MAN is a sugar alcohol (Talari et al., 2016).

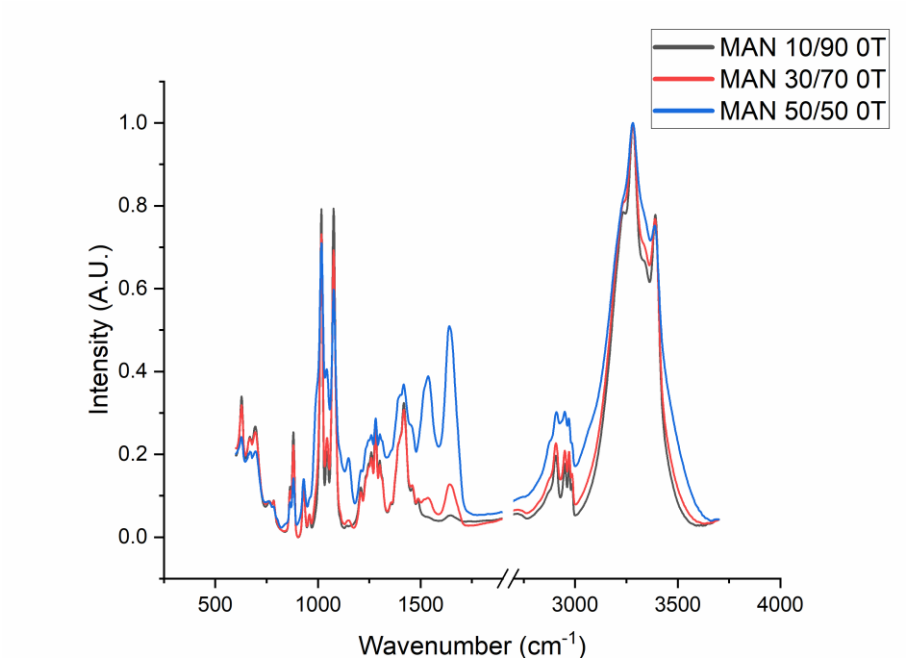

Figure 30 - ATR-FTIR spectrum (600-3700 cm^{-1}) of MAN mixtures as a blend.

Contrary to DEX spectra, in the case of MAN, the alterations in the spectra are not so clear (Figure 30 – A, B and C). To the ratio of 10/90, the spectra are completely overlapping, indicating that it was not possible to detect any potential changes in the protein structure. With the increase of the CAT loading, the characteristic peaks of CAT start to be visible (Amide I and II) and more intense. Contrary to the previous sugar, the Amide A peak was more hidden by the N-H stretching peak of MAN so that the excipient would mask any changes in this region. The consequences of the application of force are different between the ratio of 30/70 and 50/50. While in the ratio of 30/70, the intensity of the peaks increases with the increase of force, in the 50/50, the intensity decreases with the increase of force applied. This can indicate that different changes in the structure can occur. In the mixtures MAN, 50/50 is observed that

with the increase of applied force, the peak of the O-H bonding (characteristic of sugar alcohols) loses resolution and converges with the peak of the Amide A. Even though the polymorphism of MAN can change with different conditions (Su et al., 2017; Zhu & Yu, 2017), no changes were observed with ATR-FTIR.

The small changes in the structure of CAT can be because MAN effectively protects sugar against aggregation and prevents structure changes (Izutsu et al., 1994; Singh & Singh, 2003). This result is in accordance with the decrease in the number of particles in the MFI technique compared with 100 mg of CAT tablets. However, this does not seem to translate into a beneficial effect in preserving the protein's activity, as the relative activity of CAT in the tablets with MAN is lower than in the tablets with only CAT in the formulation. In this case, not even at higher compression forces, the sugar seems able to stabilize the protein because the activities are lower than the activities of the tablets with 100 mg of CAT at all compression forces used.

In Figure 31 - D, some differences are observed between the spectra of different spray-dried mixtures. The visible changes in the intensity of the peaks are visible in the Amide I and II region, which can indicate changes in the secondary structure of CAT. The same changes are observed in the Amide B region. Furthermore, the disappearance of the peaks in the region of 1100-1500 cm^{-1} and 2750-3000 cm^{-1} suggests that changes in the sugar's structure occurred after the SD. Before SD, the form of MAN was the β form, and after the SD seems that was a transition to the α form (existing a mixture of both forms, concluded by comparison of the characteristics peaks) and through the wide-angle X-ray scattering (WAXS) spectra of the spray-dried sample, a transition from the crystalline to the amorphous form is observed (Annex C.3) (Burger et al., 2000; Cares-Pacheco et al., 2014; Zellnitz et al., 2019).

Additionally, to confirm the ATR-FTIR spectra alterations, through the SEM analysis performed, the co-particles showed a dimpled spherical structure, showing less aggregation than DEX co-particles (Annex D.2). Comparing the obtained images with the literature, it seems that the spray-dried MAN does not have a pure crystalline structure (confirmed by the WAXS, which shows a mixture of crystalline and amorphous structures) (Koner et al., 2015).

The structural changes, in addition to the loss of activity, the increase in the number of particles and the high correlation in the correlation matrix (from the PCA), corroborate the effect of the processing on the enzyme´s performance.

Compared with the DEX mixtures after SD, MAN seems a better stabilizer because even though in the DEX mixtures, the number of particles is lower, in the MAN mixtures, the activity is almost twice higher. Furthermore, compared with the non-spray-dried MAN mixtures, the

activity is slightly lower, showing more instability, however, when compared with the CAT SD, the activity increases, suggesting that MAN is stabilizing CAT during the SD.

The structural changes of the sugar are related to the process conditions of the SD. Furthermore, the protein that is being co-produced with MAN by SD influences the form of the sugar after the process (Hulse et al., 2009). The change of polymorphism can occur even though the β form is the most stable polymorphic form (Penha et al., 2021). Moreover, MAN has a lower T_g, and with the SD conditions, the temperature during the process is higher than T_g, which in turn changes from the crystalline structure to a hybrid structure or amorphous can occur. The differences seen in the ATR-FTIR spectra were confirmed by WAXS, in line with the changes on Amide I and II peaks (from ATR-FTIR), in which MAN has a hybrid structure (semi-crystalline structure), and it seems to occur a transition from the β to the α form, existing as a mixture of both forms (Cares-Pacheco et al., 2014; Zellnitz et al., 2019).

Amorphous MAN can form hydrogen bonds, while in the crystalline phase, this is not so common (Chen et al., 2021). However, considering the results, the possibility of a higher number of hydrogen bonds did not increase the stability of CAT. Besides MAN has six O-H that can form hydrogen bonds, when there is a mixture of forms, some of these atoms can be occupied or rearranged in a position that cannot form other bonds. It has been described that sugars stabilize proteins via O-H bonding, thus, during the ATR-FTIR experiments, it was aimed to observe if it would be possible to identify any O-H bonding by the shift in the peak around 3300 cm^{-1}. However, it was not observed any shift, being only seen changes in the peak intensity, likewise, to further understand if there were changes in the chemical bonding and if the sugar is stabilizing the protein via O-H bonding, supplementary techniques such as hydrogen nuclear magnetic resonance or X-ray diffraction techniques should be applied (Cheng et al., 2020).

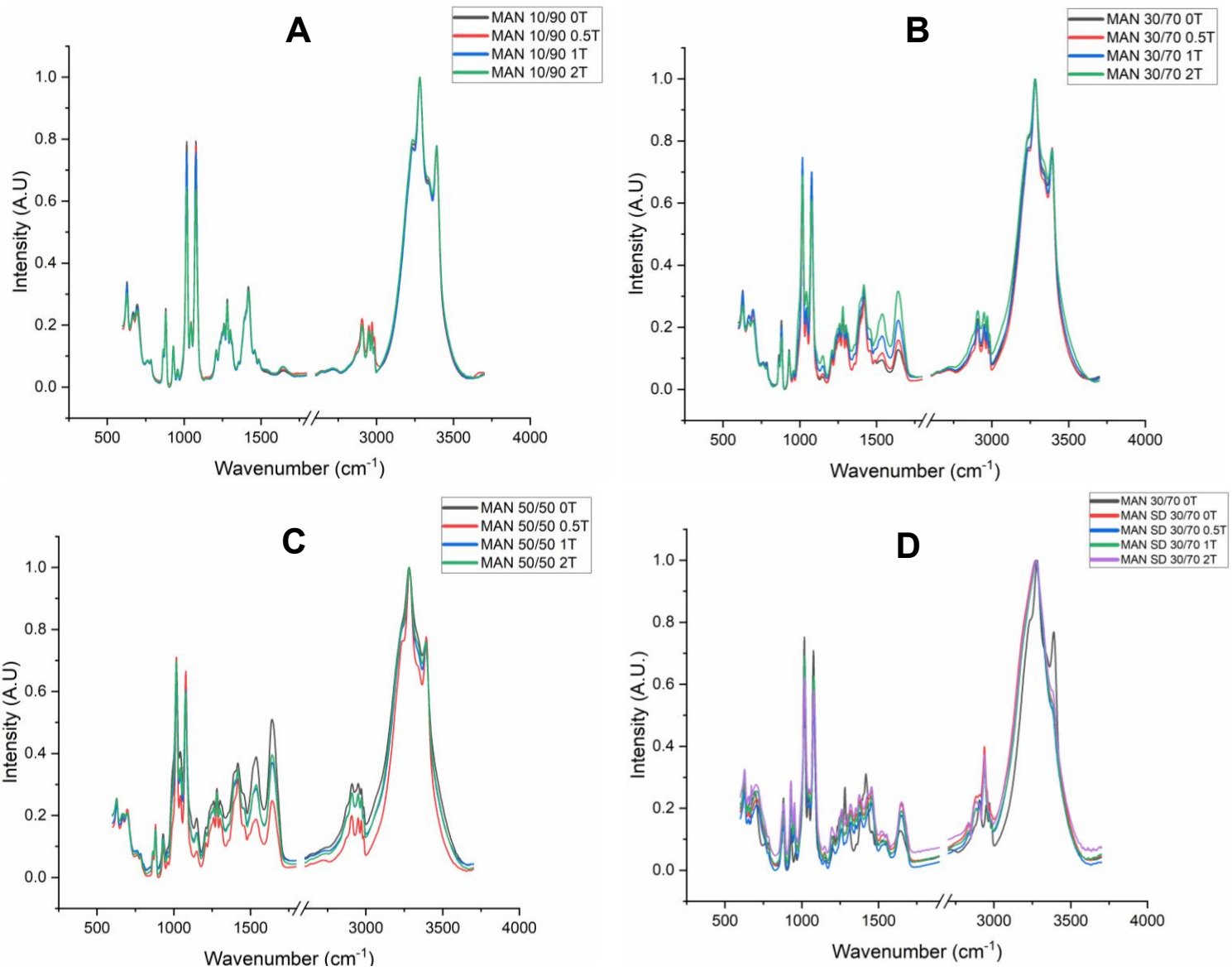

Figure 31 - ATR-FTIR spectrums (600-3700 cm^{-1}) non-spray-dried and spray-dried MAN mixtures, as a blend, co-particle and after compression. *Legend: A – 10/90 ratio; B – 30/70 ratio; C – 50/50 ratio; D – 30/70 spray-dried ratio.*

3.3.4 Tablets with Catalase and Trehalose

As in the previous saccharides, the increase of the CAT loading in the formulation causes an increase in the intensity of the peaks of Amide I and II. The characteristic peaks of the sugar are not affected by the decrease in its amount. In the case of TRH, it is present the dihydrate form (Annex B.3 and C.2). The main characteristic of this form is the large peak and around 3300 cm^{-1}, in addition to the three peaks in the region from 2800 to 3000 cm^{-1} (Grdadolnik & Hadži, 1998). In the region between 900 and 1200 cm^{-1} are present the signal of the C-O-C

and C-O ring vibrations characteristics of carbohydrates (Faghihzadeh et al., 2016) (Figure 32).

Lastly, the increase of the Amide I and II peaks is observed again with the increase of the quantity of CAT in the formulation (Figure 33), as in the TRH blends. To TRH 10/90, the spectra are similar, indicating that there might not be a significant change in the structure. To the remaining ratios, it is possible to observe changes in the intensity of the peaks (Amide I and II), probably due to changes in the secondary structure (Faghihzadeh et al., 2016). In the mixtures with the 30/70 ratio, the TRH 30/70 2T was the most affected by force since no differences in the peaks are only observed in the characteristic region of carbohydrates. In the 30/70 ratio, at the two highest forces, changes can be observed in the peak of Amide II, suggesting changes in the secondary structure of the protein. Furthermore, changes in the O-H bonding peaks are observed.

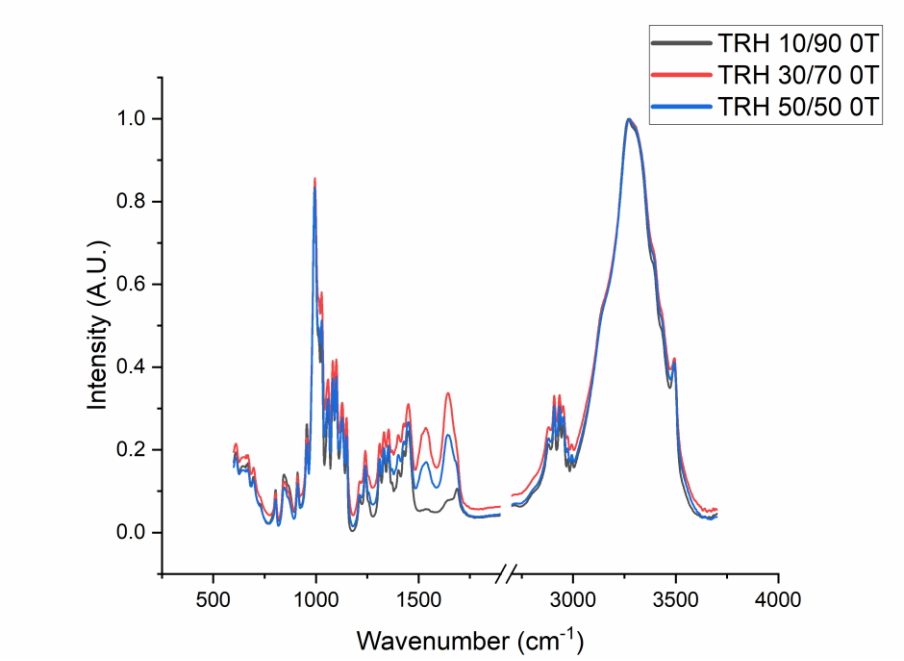

Figure 32 - ATR-FTIR spectrum (600-3700 cm^{-1}) of TRH mixtures as a blend.

To this saccharide was possible to determine that the application of compression forces leads to changes in the activity and number of particles, as well as in the secondary structure of the protein (as shown by the changes in the Amide I and II). This suggests that the secondary structure is changing and, in its turn, this is affecting the activity and aggregation.

The ATR-FTIR spectra of TRH mixtures show similar intensities (Figure 33 - D). Compared with the TRH 30/70 0T, the spray-dried mixtures have a different peak in the region of 1250-1500 $cm^{-1,}$ and in the region of 2900 cm^{-1}, the peaks are more intense and larger. This can suggest that alterations in the structure of CAT and the polymorphism of the sugar might be

occurring. From the WAXS analysis, compared with literature, it was observed that after SD, TRH became amorphous (Annex C.4) (Aziz et al., 2020). Regarding the secondary structure of CAT, the decrease of intensity of the peak of Amide I, with the application of force, can mean that the secondary structure is affected after tableting.

Furthermore, to complement the ATR-FTIR spectra, SEM analysis showed that the co-particles formed in the SD have a dimpled spherical structure. Also, it suggested that this sugar is observed with the lowest level of aggregation between the sugar and the protein (Annex D.3). The spherical morphology of the particles confirms the amorphous structure of TRH after the SD (Koner et al., 2015).

The changes in the spectra through the ATR-FTIR technique corroborate the alterations in both activity and number of particles.

Comparing the results of the techniques, despite not being observed that in the dry-state TRH is stabilizing CAT during the tableting, it seems that it is stabilizing the protein during the SD, in which the characteristics of CAT look similar to the characteristics in the non-spray-dried tablets. This stabilization can be due to the formation of hydrogen bonds during the SD between TRH and the protein (Chen et al., 2021). The hydroxyl groups can form these bonds on the rings of TRH, and then inter-molecular hydrogen bonds can be formed (Shao et al., 2019). The hydrogen bonds can be facilitated since this work is being used TRH dihydrate, in which the water from the composition can help during the hydrogen bonding since, generally, saccharides protect proteins by acting as a water substitute for the structure (Kaushik & Bhat, 2003). Studies showed that TRH can substitute the water molecules from the surface of proteins during dehydration (during SD), and the results suggest that the same is occurring with CAT and TRH (Liao et al., 2002). Again, this explanation is based on the O-H bonding that should be confirmed as described in Section 3.3.3 since the changes in the characteristic peaks of the O-H bonding might not be directly related to the increase of the O-H bondings.

Moreover, the stabilization can be due to the reduced water dynamics because the addition of TRH molecules leads to the slowing of the protein residues, which causes a stabilization of the structure due to the hydrogen bonds (Olsson et al., 2019). Although no more O-H bonds were visible in the spectra (as mentioned in Section 3.3.3), it might be that is not chemical interaction at play. Likewise, it might be that the beneficial effect of TRH is due to the glass dynamics. The glass transition temperature of TRH also plays an important role in CAT's stabilization against denaturation. It is reported that higher T_g (as TRH's T_g) improves stability due to vitrification (Grasmeijer et al., 2013). This theory suggests that a glassy state, with high-temperature tolerance and high stability, is formed, in which the glassy matrix can hold and protect the protein's structure and, thus, avoid the loss of biological activity (Burek et al., 2015).

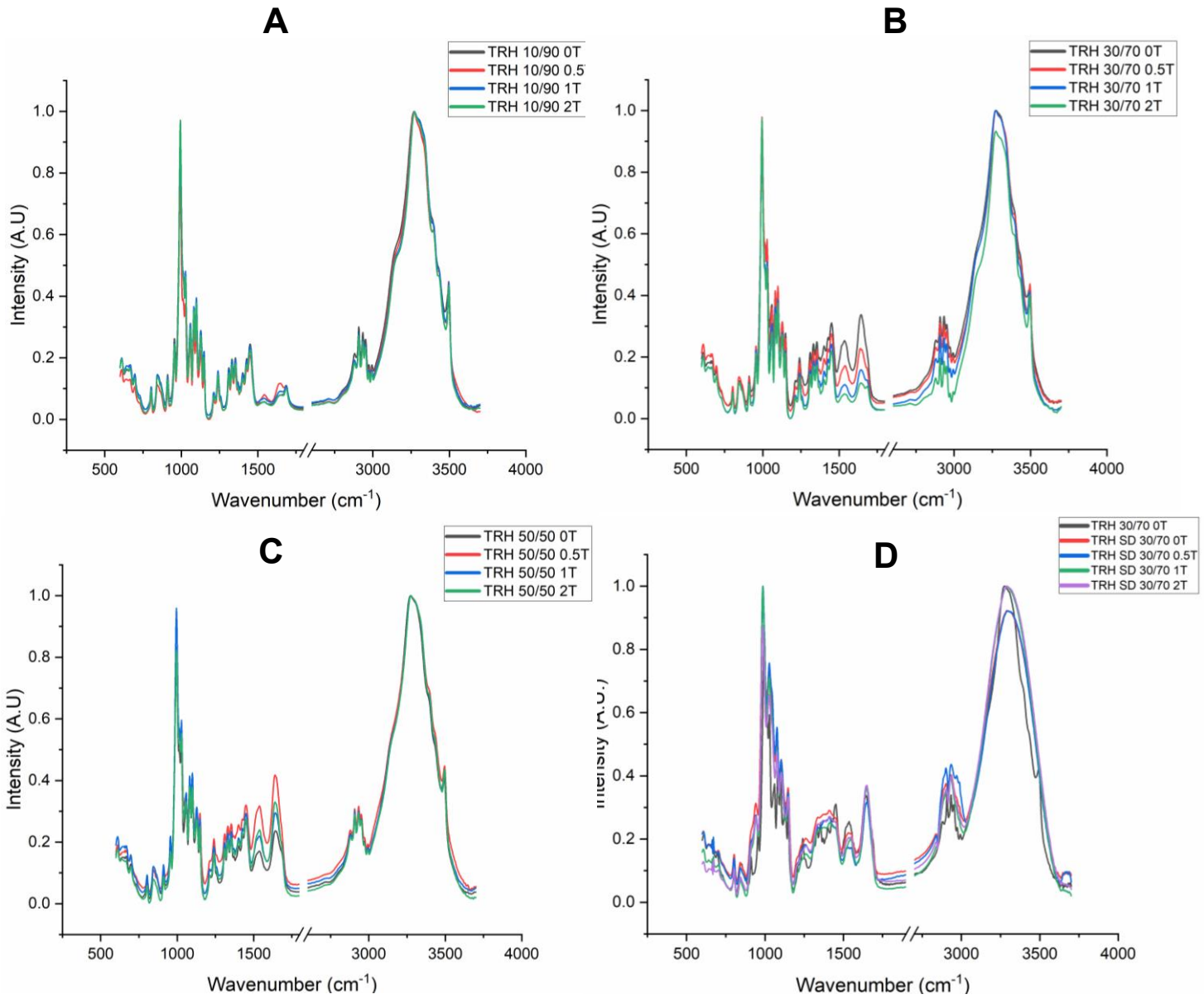

Figure 33 - ATR-FTIR spectrums (600-3700 cm^{-1}) non-spray-dried and spray-dried TRH mixtures, as a blend, co-particle and after compression. *Legend: A – 10/90 ratio; B – 30/70 ratio; C – 50/50 ratio; D – 30/70 spray-dried ratio.*

3.4 Principal Component Analysis

3.4.1 Principal Component Analysis of Non-spray-dried Mixtures

The results were analysed by PCA to reveal the correlations between the compression force used during tableting and CAT´s properties (activity and aggregates).

The PCA contained 40 observations (produced samples) and 18 variables (process and material characteristics). Not normally distributed variables (13 out of the total 18) were transformed using a logarithmic function. More specifically, the variables transformed were the Abs_{180s}, all the particle size ranges (from MFI), and their respective STD. Two principal components were considered, leading to the overall performance of an R^2 of 0.628 and a Q^2 of 0.355. Although the Q^2 is rather low (suggesting a poor predictive ability), the developed PCA was only used to identify correlations and thus, it is still expected to provide valuable information.

From the loading plot (Figure 34), it is observed almost all the variables are predominantly represented by PC1 (Principal Component 1), and only CAT loading, Abs_{180s} (STD) and 300≤x≤MAX and the respective STD are mainly represented by PC2 (Principal Component 2). It is also possible to observe that Abs_{180s} are positively correlated with the compression force and with the number of particles measured by MFI (variables located in close vicinity in the loading plot), whereas CAT loading is not correlated with the other variables. The class of 300≤x≤MAX is also not correlated with the other variables since the class always has a value of zero particles. From the score plot, colored by the saccharide's types, it can be observed that the observations are distributed across the entire plot, and it is not possible to identify any trend related to the type of saccharide used (Annex E.1).

However, when the score plot is colored according to the force (Figure 35), it is possible to visualize a trend where samples produced at progressively higher force move from the first quadrant to the third in line with the position of the pressure in the loading plot. Moreover, different mixtures are correlated with the same forces due to the existing clusters and division by the zone of the score plot (Bro & Smilde, 2014), suggesting that the applied force has a larger impact compared to the saccharide used. The formulation TRH 10/90 2T is detected as an outlier (out of the 95 % confidence level limit).

The results described above are reflected in the correlation matrix of the PCA (Table 7), showing the strength of the correlation (from -1 to 1) between all the variables of the investigated dataset. The higher values (with a darker color) show the strongest correlations (positive or negative). The matrix analysis shows that CAT loading does not correlate with the

variables, as mentioned above. The most important correlations considered in the data analysis were: (I) Force and Abs_{180s} (0.743); (II) Force and range 25≤x≤50 (0.719); and (III) Abs_{180s} and range 25≤x≤50 (0.831). Thus, it is possible to conclude that there is a relation between tableting (forces used), the activity, and the number of particles in the aforementioned range. Also, based on this table, the class of 25≤x≤50 μm in the MFI technique was chosen for the Bonferroni statistical analysis since it has the strongest correlation with the activity and the force applied.

Figure 34 - Loading Plot of the PCA of the non-spray-dried mixtures.

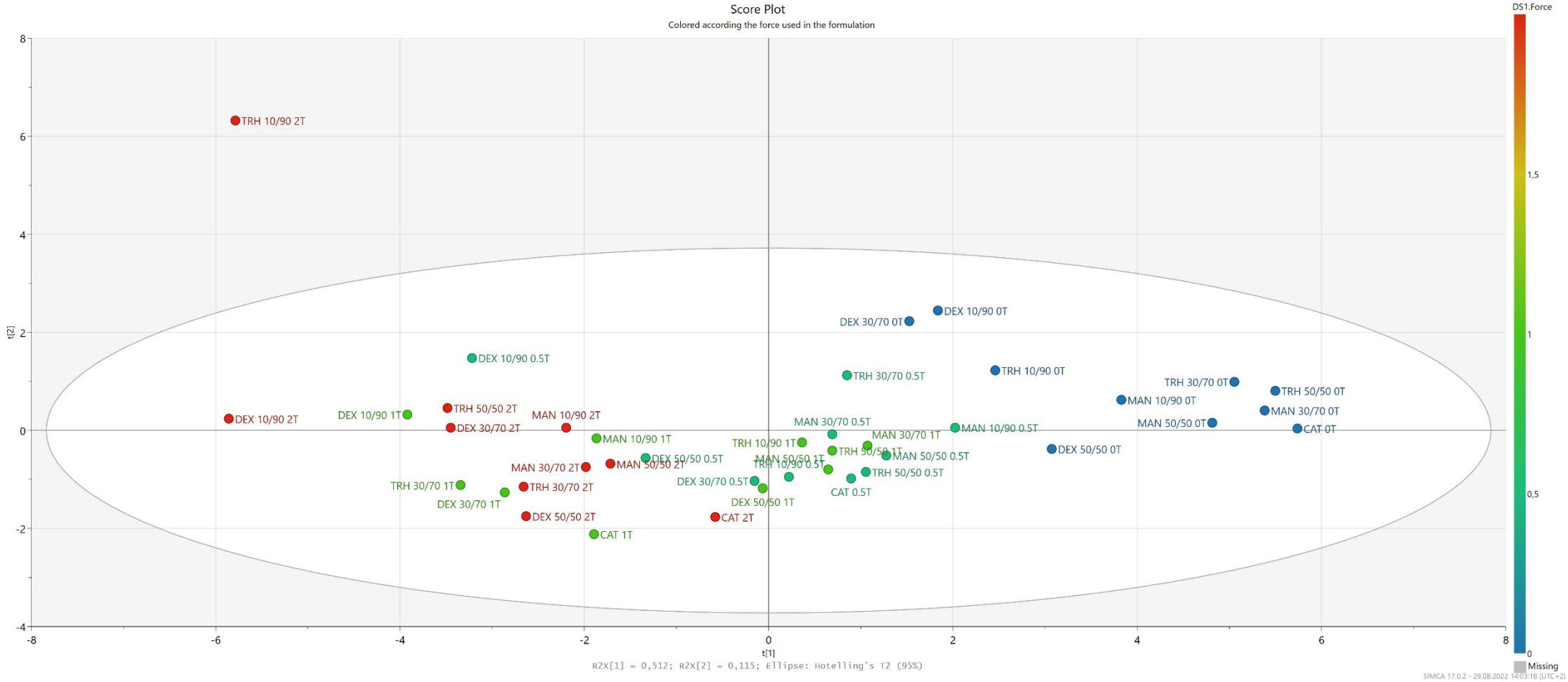

Figure 35 - Score Plot of the PCA of the non-spray-dried mixtures (colored according to the force used in the formulation).

Table 7 - Correlation matrix of PCA of all the non-spray-dried mixtures.

	CAT Loading	Force	Abs_{180s}	Abs_{180s} (STD)	5≤x≤10	10≤x≤25	25≤x≤50	50≤x≤75	75≤x≤100	100≤x≤300	300≤x≤MAX	5≤x≤10 (STD)	10≤x≤25 (STD)	25≤x≤50 (STD)	50≤x≤75 (STD)	75≤x≤100 (STD)	100≤x≤300 (STD)	300≤x≤MAX (STD)
CAT Loading	1.000	-0.001	-0.215	-0.024	-0.046	-0.063	-0.124	-0.203	-0.208	-0.308	-0.324	-0.065	-0.167	-0.082	-0.016	-0.107	-0.274	-0.295
Force		1.000	0.743	0.084	0.687	0.674	0.719	0.586	0.558	0.624	0.241	0.674	0.642	0.395	0.454	0.539	0.654	0.255
Abs_{180s}			1.000	-0.001	0.720	0.699	0.831	0.728	0.667	0.631	0.337	0.540	0.545	0.320	0.403	0.519	0.612	0.311
Abs_{180s} (STD)				1.000	-0.101	-0.067	-0.013	-0.027	-0.011	-0.055	0.265	-0.073	0.021	-0.061	-0.055	0.127	-0.095	0.286
5≤x≤10					1.000	0.984	0.903	0.808	0.707	0.633	0.237	0.574	0.639	0.476	0.391	0.415	0.536	0.187
10≤x≤25						1.000	0.889	0.810	0.709	0.651	0.292	0.580	0.628	0.493	0.388	0.422	0.546	0.232
25≤x≤50							1.000	0.869	0.789	0.717	0.298	0.610	0.616	0.481	0.394	0.492	0.641	0.257
50≤x≤75								1.000	0.897	0.753	0.349	0.518	0.536	0.311	0.571	0.523	0.600	0.297
75≤x≤100									1.000	0.821	0.339	0.497	0.445	0.315	0.562	0.708	0.675	0.299
100≤x≤300										1.000	0.517	0.533	0.518	0.499	0.530	0.606	0.912	0.483
300≤x≤MAX											1.000	0.216	0.257	0.363	0.184	0.189	0.392	0.982
5≤x≤10 (STD)												1.000	0.748	0.421	0.507	0.537	0.565	0.218
10≤x≤25 (STD)													1.000	0.496	0.512	0.484	0.565	0.275
25≤x≤50 (STD)														1.000	0.314	0.390	0.524	0.340
50≤x≤75 (STD)															1.000	0.617	0.508	0.178
75≤x≤100 (STD)																1.000	0.625	0.198
100≤x≤300 (STD)																	1.000	0.394
300≤x≤MAX (STD)																		1.000

3.4.2 Principal Component Analysis of Spray-dried Mixtures

After the SD, two analyses were performed, by PCA, containing only the spray-dried samples and another with all the samples (non-spray-dried and spray-dried).

For the analysis by PCA containing only the spray-dried mixtures (Figure 36), 2 PCs were retained, and 10 out of 18 variables (with 17 observations each) were logarithmically transformed, leading to a performance of an R^2 of 0.685 and a Q^2 of 0.266. The variables transformed were: all the MFI ranges and respective STDs, with the exception of 300≤x≤MAX, 5≤x≤10 (STD), 25≤x≤50 (STD), 75≤x≤100 (STD), and 300≤x≤MAX (STD). From the score plot colored according to the applied forces, a trend of change is visible in which there is a displacement of the observations from the right side to the left. This trend is taking a different direction from one of the PCAs without SD due to the different positions of the force variable in the loading plot (Annex E.2). No correlation between the CAT loading and the sugar used was observed since CAT loading is a fixed variable. Moreover, no significant changes were observed among the correlations of the variables in comparison to the previous PCA. The only exception was the sharp decrease of correlation between the Abs_{180s} with the range 25≤x≤50 µm and force (see correlation matrix in Annex E.3). This decrease may be related to the sharp increase in the number of particles after SD.

Two principal components were used in the fitting with all the mixtures (spray-dried and non-spray-dried), and 15 out of 18 variables (with 56 observations each) were transformed using a logarithmic function. The variables transformed were all the variables except the CAT loading, the force, and the Abs_{180s}. The PCA had an R^2 of 0.610 and a Q^2 of 0.337. A slight decrease in the R^2 and an increase in the Q^2 compared with the PCA before the SD is observed.

With the inclusion of the SD data, an inversion of the variables' positions in the loading plot occurred (Annex E.4). The same type of correlation as before (Section 3.1.5) between the variables is observed. Moreover, the existing cluster of the force, Abs_{180s} and the MFI classes are wider than before the addition of the new data.

From the score plot colored by force used in the formulation (Figure 37), it is observed a pattern of the distribution of the observations in the score plot, in which the spray-dried samples follow the same pattern as the non-spray-dried. The outlier TRH 10/90 2T stands outside the 95 % confidence interval as in the previous PCA. To this analysis, the increased applied force makes the scores move in the horizontal direction (along PC1).

The correlation matrix (Table 8) shows a change in the correlation strength. The most relevant correlations were: (I) Force and Abs_{180s}, which changed from 0.743 in the first PCA to 0.520; (II) Force and range 25≤x≤50 µm, which changed from 0.719 to 0.720; and (III) Abs_{180s} and

range 25≤x≤50, that changed from 0.831 to 0.577. The addition of the data after SD increases the variability of the data, and then an impact in the correlation matrix is observed. Besides the decreases, the variables kept correlated between them. Furthermore, the CAT loading is not correlated with any variable, so it does not have an impact on the alterations of CAT's characteristics after tableting. Generally, those results suggest that an increase in the force applied during compression results in reduced activity and a higher number of aggregates (particularly seen in the dimension range of 25≤x≤50 μm).

Concluding, changes in the correlation between the variables after the addition of the data regarding the SD are observed. The SD data seems to follow the same behaviour as the non-spray-dried data, showing that with this process, the differences are not significant in the results of the characterization methods

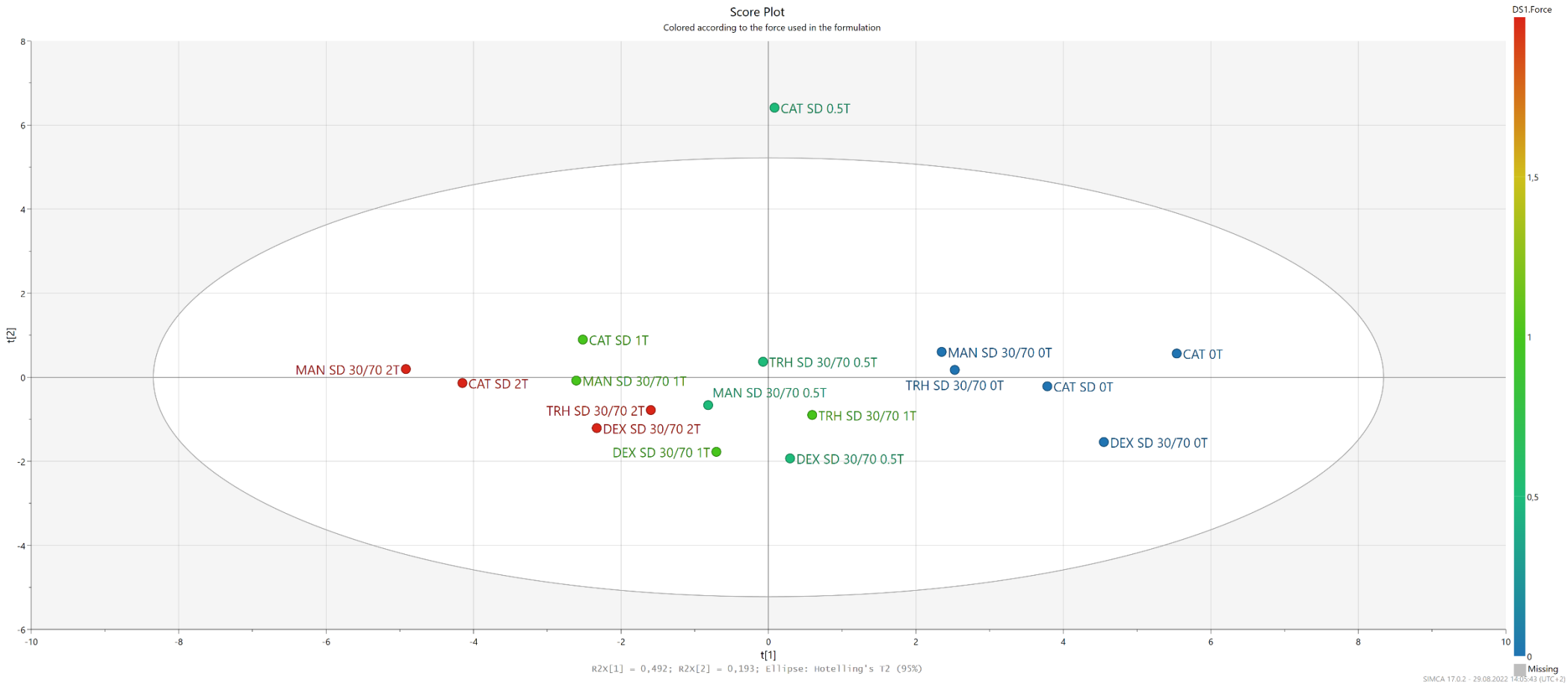

Figure 36 - Score Plot of the PCA only of the spray-dried mixtures (colored according to the force used in the formulation).

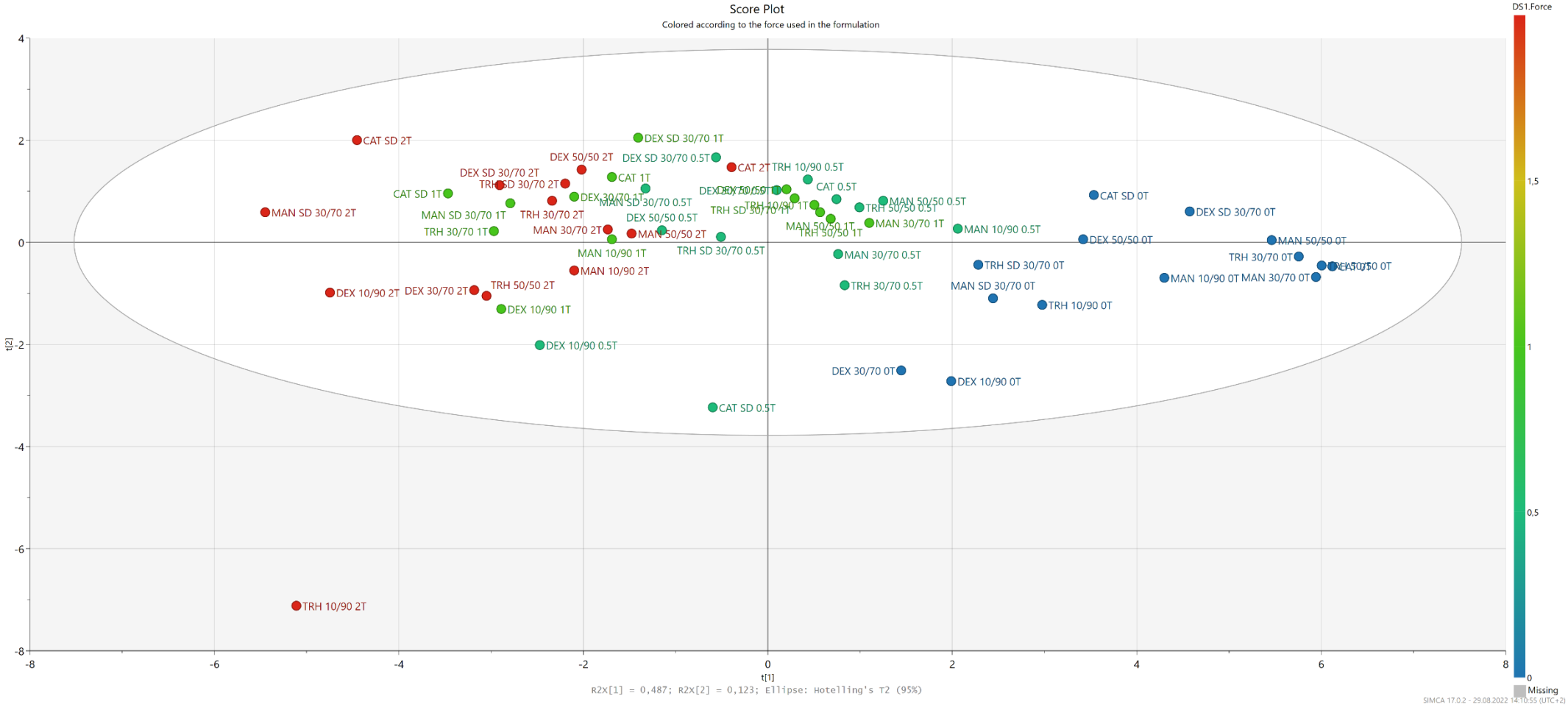

Figure 37 - Score Plot of the PCA of all the mixtures (colored according to the force used in the formulation).

.

Table 8 - Correlation matrix of PCA of all the mixtures

	CAT Loading	Force	Abs_{180s}	Abs_{180s} (STD)	5≤x≤10	10≤x≤25	25≤x≤50	50≤x≤75	75≤x≤100	100≤x≤300	300≤x≤MAX	5≤x≤10 (STD)	10≤x≤25 (STD)	25≤x≤50 (STD)	50≤x≤75 (STD)	75≤x≤100 (STD)	100≤x≤300 (STD)	300≤x≤MAX (STD)
CAT Loading	1.000	0.000	-0.014	0.044	0.026	0.028	-0.018	-0.083	-0.076	-0.207	-0.157	0.018	-0.096	-0.056	0.008	0.040	-0.206	-0.124
Force		1.000	0.520	0.126	0.730	0.738	0.720	0.620	0.575	0.628	0.180	0.699	0.648	0.450	0.385	0.486	0.560	0.189
Abs_{180s}			1.000	-0.085	0.648	0.628	0.577	0.507	0.387	0.335	0.156	0.469	0.501	0.372	0.458	0.215	0.326	0.146
Abs_{180s} (STD)				1.000	-0.008	0.019	0.098	0.098	0.133	0.053	0.252	0.036	0.070	-0.056	0.029	0.269	-0.007	0.272
5≤x≤10					1.000	0.992	0.967	0.877	0.770	0.627	0.158	0.666	0.630	0.522	0.505	0.485	0.453	0.138
10≤x≤25						1.000	0.982	0.874	0.763	0.624	0.163	0.677	0.630	0.547	0.479	0.487	0.465	0.142
25≤x≤50							1.000	0.884	0.766	0.649	0.219	0.651	0.616	0.599	0.451	0.476	0.467	0.189
50≤x≤75								1.000	0.885	0.734	0.273	0.570	0.558	0.431	0.626	0.553	0.492	0.236
75≤x≤100									1.000	0.827	0.307	0.534	0.463	0.274	0.563	0.764	0.610	0.278
100≤x≤300										1.000	0.453	0.503	0.471	0.346	0.509	0.649	0.876	0.426
300≤x≤MAX											1.000	0.174	0.168	0.132	0.088	0.189	0.367	0.984
5≤x≤10 (STD)												1.000	0.753	0.445	0.431	0.500	0.426	0.175
10≤x≤25 (STD)													1.000	0.500	0.455	0.436	0.435	0.180
25≤x≤50 (STD)														1.000	0.358	0.186	0.252	0.116
50≤x≤75 (STD)															1.000	0.548	0.399	0.094
75≤x≤100 (STD)																1.000	0.574	0.201
100≤x≤300 (STD)																	1.000	0.369
300≤x≤MAX (STD)																		1.000

4. Conclusion

It was demonstrated that the compression force resulted in changes in the CAT characteristics (i.e., loss of activity, increase of aggregates and structural changes). On the one hand side, the addition of saccharides in the dry state was not found to stabilize the protein during the tableting, probably due to only mechanical stabilization occurring. On the other hand, even if the use of spray-dried saccharides also did not help in improving the enzyme stability during tableting, its ability to protect CAT during spray drying was observed. Particularly MAN and TRH showed some stabilizer effect compared to the CAT SD mixtures, contrary to what is observed in DEX SD mixtures.

In the non-spray-dried mixtures, after the compression force applied, even with saccharides in the formulation, changes in the spectra (particularly, in Amide peaks) and an increase in the number of particles (due to aggregation) were observed. In addition, a decrease in activity was observed to all the mixtures. Even if no protection during tableting occurred (due to the decrease of activity from the blends to the tablets), it was possible to show that DEX mixtures in a 30/70 ratio were the most stable mixtures within the applied forces (similar activities), followed by TRH that showed a decrease in activity to the highest force used. Generally, from the results it is possible to conclude that the activity gradually decreases with the increase of force. From the PCA of the results of these mixtures was not found a relation between the saccharides used and the changes after the tableting.

Concerning the spray-dried mixtures, again changes in the structure, number of particles and a consequent loss of activity occurred. The number of particles was significantly higher than in the non-spray-dried formulations and the changes in the ATR-FTIR spectra more visible, due to the inclusion of the SD. Moreover, due to the SD, MAN suffered a transition of the structure from crystalline to a mixture of amorphous and crystalline structure as well as a transition from β form to a mixture of α and β form, while TRH transited to an amorphous structure. To the spray-dried mixtures, TRH seems to be the saccharide that best protected the enzyme against the SD due to the similar activities to the non-spray-dried mixtures and DEX, the worst additive to this end. In these mixtures, the PCA showed that after SD, the mixtures have the same behaviour, indicating that there is no correlation between the SD and the changes occurring, meaning that the tableting is what is causing the negative impact on CAT.

The results suggest that spray-dried materials are not advantageous for a stabilized enzyme with similar characteristics to the raw protein. So, the interactions between the protein and

saccharides and the processing conditions need to be improved in order to have a stable protein at the end of the processing.

The analysis of the results by PCA helped to visualize and quantify the level of correlation between the compression force and the variables. The PCA showed a correlation between the quantitative variables considered, in which was confirmed that the compression force has an effect on CAT´s properties, particularly in the activity that is inversional proportional to the applied compression force. It also corroborated that the loading or type of saccharide used did not influence the outcome of the tableting process. This allows to conclude that the stability of CAT is detrimentally affected by the compression forces, regardless of the excipient used or its load.

Thus, the work focused on the effect of tableting on catalase and investigated the use of different sugar types and concentrations in the tablets. In this work, the biological activity of CAT complemented with the number of aggregates and structural changes was assessed to allow a more in-depth investigation of the impact of the compression force on catalase, which has not been previously reported in the literature. Concluding, a correlation between the applied compression force, the loss of activity, the increase in the number of particles (due to the aggregation) and structural changes was found. The activity of CAT was not preserved during tableting in all the mixtures with the different saccharides (non-spray-dried and spray-dried). This conclusion reports contrasting evidence with the literature where the stabilization of biologics with the use of these saccharides was demonstrated.

5. Future Work

Tablets containing biologics have become of big interest, and it is expected that this interest will continue growing in the coming years.

Thus, in addition to the experimental work done during the Master Thesis, it would be interesting to: (I) use different stabilizing techniques, such as encapsulation by spray-congealing or emulsion-based techniques; (II) perform analyses such as differential scanning calorimetry to a better characterize the polymorphism of the saccharides after SD and size-exclusion chromatography to characterize the aggregates; (III) produce tablets with different proteins (e.g., lactase or naringinase); (IV) use a wider interval of compression forces, in order to better understand how the protein behaves with the stresses; (V) use more materials in the formulation, such as stabilizer additives and other excipients (e.g., lubricant, disintegrant, etc); (VI) perform the scale-up of the tableting step from a single-punch tableting press to a rotary tablet press and perform a more in-depth analysis of the compression behaviour (e.g., compaction simulator to determine if the material is plastic or undergoes fragmentation); and lastly (VII) after a good understanding of the behaviour of a few model compounds, a predictive model could be developed to predict the behaviour of proteins in the production of oral solid dosage forms.

These additional points could allow a better understanding of the stabilizing capacity of other saccharides, as well as the changes in the polymorphism of the materials after the processing conditions, their effect during the production of different tablets of biologics and an eventual scale-up of production.

6. Bibliography

A Guide to Tablet Presses - Fette America. Fette America. (2022). Retrieved 6 June 2022, from https://www.fette-compacting-parts.com/guide-to-tablet-presses/

Ahn, J. (2006). Associations between Catalase Phenotype and Genotype: Modification by Epidemiologic Factors. Cancer Epidemiology Biomarkers & Amp; Prevention, 15(6), 1217-1222. https://doi.org/10.1158/1055-9965.epi-06-0104

Ajito, S., Iwase, H., Takata, S., & Hirai, M. (2018). Sugar-Mediated Stabilization of Protein against Chemical or Thermal Denaturation. The Journal Of Physical Chemistry B, 122(37), 8685-8697. https://doi.org/10.1021/acs.jpcb.8b06572

Albert, V., Lanz, M., Imanidis, G., Hersberger, K., & Arnet, I. (2017). Stability of medicines after repackaging into multicompartment compliance aids: eight criteria for detection of visual alteration. Drugs &Amp; Therapy Perspectives, 33(10), 487-496. https://doi.org/10.1007/s40267-017-0431-9

Alfonso-Prieto, M., Biarnés, X., Vidossich, P., & Rovira, C. (2009). The Molecular Mechanism of the Catalase Reaction. Journal Of The American Chemical Society, 131(33), 11751-11761. https://doi.org/10.1021/ja9018572

Allison, S. D., Chang, B., Randolph, T. W., & Carpenter, J. F. (1999). Hydrogen Bonding between Sugar and Protein Is Responsible for Inhibition of Dehydration-Induced Protein Unfolding. Archives of Biochemistry and Biophysics, 365(2), 289–298. https://doi.org/10.1006/ABBI.1999.1175

Allison, S., Manning, M., Randolph, T., Middleton, K., Davis, A., & Carpenter, J. (2000). Optimization of Storage Stability of Lyophilized Actin Using Combinations of Disaccharides and Dextran. Journal Of Pharmaceutical Sciences, 89(2), 199-214. https://doi.org/10.1002/(sici)1520-6017(200002)89:2<199::aid-jps7>3.0.co;2-b

Almukainzi, M., Bou-Chacra, N., Walker, R., & Löbenberg, R. (2014). Biorelevant Dissolution Testing. *Therapeutic Delivery Solutions*, 335-365. https://doi.org/10.1002/9781118903681.ch12

Alothman, M., Ispas-Szabo, P., & Mateescu, M. (2021). Design of Catalase Monolithic Tablets for Intestinal Targeted Delivery. *Pharmaceutics*, *13*(1), 69. https://doi.org/10.3390/pharmaceutics13010069

Antikainen, O., & Yliruusi, J. (2003). Determining the compression behaviour of pharmaceutical powders from the force–distance compression profile. International Journal Of Pharmaceutics, 252(1-2), 253-261. https://doi.org/10.1016/s0378-5173(02)00665-8

Area, ECD and Intensity: Micro-Flow Imaging. Lobsteroverseas.net. (2022). Retrieved 13 March 2022, from https://lobsteroverseas.net/technology-overview/size-and-morphology/area-ecd-and-intensity/index.html.

Armstrong, R. (2014). When to use the Bonferroni correction. Ophthalmic And Physiological Optics, 34(5), 502-508. https://doi.org/10.1111/opo.12131

Asensio, J., Ardá, A., Cañada, F., & Jiménez-Barbero, J. (2012). Carbohydrate–Aromatic Interactions. Accounts Of Chemical Research, 46(4), 946-954. https://doi.org/10.1021/ar300024d

Ayenew, Z., Paudel, A., & Van den Mooter, G. (2012). Can compression induce demixing in amorphous solid dispersions? A case study of naproxen–PVP K25. European Journal Of Pharmaceutics And Biopharmaceutics, 81(1), 207-213. https://doi.org/10.1016/j.ejpb.2012.01.007

Ayenew, Z., Paudel, A., Rombaut, P., & Van den Mooter, G. (2012). Effect of Compression on Non-isothermal Crystallization Behaviour of Amorphous Indomethacin. Pharmaceutical Research, 29(9), 2489-2498. https://doi.org/10.1007/s11095-012-0778-5

Aziz, S., Scherlieβ, R., & Steckel, H. (2020). Development of High Dose Oseltamivir Phosphate Dry Powder for Inhalation Therapy in Viral Pneumonia. Pharmaceutics, 12(12), 1154. https://doi.org/10.3390/pharmaceutics12121154

Balbás, P., & Lorence, A. (2004). Recombinant gene expression (2nd ed., p. 241). Humana Press.

Basu, A., De, A., & Dey, S. (2013). Techniques of Tablet Coating: Concepts and Advancements: A Comprehensive Review. Journal of Pharmacy and Pharmaceutical Sciences, 2(4), 1–6.

Bauer, H., Herkert, T., Bartels, M., Kovar, K., Schwarz, E., & Schmidt, P.C. (2000). Investigations on polymorphism of mannitol/ sorbitol mixtures after spray-drying using Differential scanning calorimetry, X-ray diffraction and Near-Infrared spectroscopy. Pharmazeutische Industrie, 62, 231-235.

Baysan, U., Elmas, F., & Koç, M. (2019). The effect of spray drying conditions on physicochemical properties of encapsulated propolis powder. Journal Of Food Process Engineering, 42(4). https://doi.org/10.1111/jfpe.13024

Bekard, I., Asimakis, P., Bertolini, J., & Dunstan, D. (2011). The effects of shear flow on protein structure and function. Biopolymers, n/a-n/a. https://doi.org/10.1002/bip.21646

Bogda, M.J. (2013). Tablet Compression: Machine Theory, Design and Process Troubleshooting. 3494-3510. https://doi.org/10.1081/E-EPT4-100200019

Boonyaratanakornkit, B., Park, C., & Clark, D. (2002). Pressure effects on intra- and intermolecular interactions within proteins. Biochimica Et Biophysica Acta (BBA) - Protein Structure And Molecular Enzymology, 1595(1-2), 235-249. https://doi.org/10.1016/s0167-4838(01)00347-8

Bovine liver catalase without NADPH. *RCSB-PDB* (2022). *1TGU: The crystal structure of bovine liver catalase without NADPH*. Rcsb.org. Retrieved 26 February 2022, from https://www.rcsb.org/structure/1tgu.

Brader, M., Estey, T., Bai, S., Alston, R., Lucas, K., & Lantz, S. et al. (2015). Examination of Thermal Unfolding and Aggregation Profiles of a Series of Developable Therapeutic Monoclonal Antibodies. Molecular Pharmaceutics, 12(4), 1005-1017. https://doi.org/10.1021/mp400666b

Bro, R., & Smilde, A. (2014). Principal component analysis. Anal. Methods, 6(9), 2812-2831. https://doi.org/10.1039/c3ay41907j

Burek, M., Waskiewicz, S., Wandzik, I., & Kaminska, K. (2015). Trehalose – properties, biosynthesis and applications.

Burger, A., Henck, J., Hetz, S., Rollinger, J., Weissnicht, A., & Stöttner, H. (2000). Energy/Temperature Diagram and Compression Behaviour of the Polymorphs of d-Mannitol. Journal Of Pharmaceutical Sciences, 89(4), 457-468. https://doi.org/10.1002/(sici)1520-6017(200004)89:4<457::aid-jps3>3.0.co;2-g

Busignies, V., Arruda, D., Charrueau, C., Ribeiro, M., Lachagès, A., & Malachias, A. et al. (2020). Compression of Vectors for Small Interfering RNAs Delivery: Toward Oral Administration of siRNA Lipoplexes in Tablet Forms. Molecular Pharmaceutics, 17(4), 1159-1169. https://doi.org/10.1021/acs.molpharmaceut.9b01190

Cares-Pacheco, M., Vaca-Medina, G., Calvet, R., Espitalier, F., Letourneau, J., Rouilly, A., & Rodier, E. (2014). Physicochemical characterization of d-mannitol polymorphs: The challenging surface energy determination by inverse gas chromatography in the infinite dilution region. International Journal Of Pharmaceutics, 475(1-2), 69-81. https://doi.org/10.1016/j.ijpharm.2014.08.029

Casettari, L., Bonacucina, G., Morris, G., Perinelli, D., Lucaioli, P., Cespi, M., & Palmieri, G. (2015). Dextran and its potential use as tablet excipient. Powder Technology, 273, 125-132. https://doi.org/10.1016/j.powtec.2014.12.030

Charm, S., & Wong, B. (1981). Shear effects on enzymes. Enzyme And Microbial Technology, 3(2), 111-118. https://doi.org/10.1016/0141-0229(81)90068-5

Chauhan, V., Zhang, H., Dalby, P., & Aylott, J. (2020). Advancements in the co-formulation of biologic therapeutics. *Journal Of Controlled Release*, *327*, 397-405. https://doi.org/10.1016/j.jconrel.2020.08.013

Chen, P., & Hub, J. (2015). Interpretation of Solution X-Ray Scattering by Explicit-Solvent Molecular Dynamics. Biophysical Journal, 108(10), 2573-2584. https://doi.org/10.1016/j.bpj.2015.03.062

Chen, W., Wang, J., Desai, D., Chang, S., Kiang, S., & Lyngberg, O. (2017). A Strategy for Tablet Active Film Coating Formulation Development Using a Content Uniformity Model and Quality by Design Principles. Comprehensive Quality By Design For Pharmaceutical Product Development And Manufacture, 193-233. https://doi.org/10.1002/9781119356189.ch8

Chen, Y., Ling, J., Li, M., Su, Y., Arte, K., & Mutukuri, T. et al. (2021). Understanding the Impact of Protein–Excipient Interactions on Physical Stability of Spray-Dried Protein Solids. Molecular Pharmaceutics, 18(7), 2657-2668. https://doi.org/10.1021/acs.molpharmaceut.1c00189

Cheng, H., Wei, Y., Wang, S., Qiao, Q., Heng, W., & Zhang, L. et al. (2020). Improving Tabletability of Excipients by Metal-Organic Framework-Based Cocrystallization: a Study of Mannitol and CaCl2. Pharmaceutical Research, 37(7). https://doi.org/10.1007/s11095-020-02850-8

Chiti, F., & Dobson, C. (2006). Protein Misfolding, Functional Amyloid, and Human Disease. Annual Review Of Biochemistry, 75(1), 333-366. https://doi.org/10.1146/annurev.biochem.75.101304.123901

Cruz-Angeles, J., Martínez, L., & Videa, M. (2015). Application of ATR-FTIR spectroscopy to the study of thermally induced changes in secondary structure of protein molecules in solid state. Biopolymers, 103(10), 574-584. https://doi.org/10.1002/bip.22664

de Backere, C., De Beer, T., Vervaet, C., & Vanhoorne, V. (2022). Effect of feed frame on lubricant sensitivity during upscaling from a compaction simulator to a rotary tablet press. International Journal Of Pharmaceutics, 616, 121562. https://doi.org/10.1016/j.ijpharm.2022.121562

Dobson, C. (2003). Protein folding and misfolding. Nature, 426(6968), 884-890. https://doi.org/10.1038/nature02261

Dunford, H. (1982). The biological chemistry of iron (pp. 439-457). D. Reidel, published in cooperation with NATO Scientific Affairs Division.

Emami, F., Vatanara, A., Park, E., & Na, D. (2018). Drying Technologies for the Stability and Bioavailability of Biopharmaceuticals. Pharmaceutics, 10(3), 131. https://doi.org/10.3390/pharmaceutics10030131

Enzymatic Assay of Catalase (EC 1.11.1.6). Sigmaaldrich.com. (2022). Retrieved 8 March 2022, from https://www.sigmaaldrich.com/PT/en/technical-

documents/protocol/protein-biology/enzyme-activity-assays/enzymatic-assay-of-catalase.

Faghihzadeh, F., Anaya, N., Schifman, L., & Oyanedel-Craver, V. (2016). Fourier transform infrared spectroscopy to assess molecular-level changes in microorganisms exposed to nanoparticles. Nanotechnology For Environmental Engineering, 1(1). https://doi.org/10.1007/s41204-016-0001-8

Fonteyne, M., Vercruysse, J., Díaz, D., Gildemyn, D., Vervaet, C., Remon, J., & Beer, T. (2011). Real-time assessment of critical quality attributes of a continuous granulation process. Pharmaceutical Development And Technology, 18(1), 85-97. https://doi.org/10.3109/10837450.2011.627869

Glorieux, C. & Calderon, P. (2017). Catalase, a remarkable enzyme: targeting the oldest antioxidant enzyme to find a new cancer treatment approach. Biological Chemistry, 398(10), 1095-1108. https://doi.org/10.1515/hsz-2017-0131

Golovina, E., Golovin, A., Hoekstra, F., & Faller, R. (2009). Water Replacement Hypothesis in Atomic Detail—Factors Determining the Structure of Dehydrated Bilayer Stacks. Biophysical Journal, 97(2), 490-499. https://doi.org/10.1016/j.bpj.2009.05.007

Goyal, M., & Basak, A. (2010). Human catalase: looking for complete identity. Protein &Amp; Cell, 1(10), 888-897. https://doi.org/10.1007/s13238-010-0113-z

Grasmeijer, N., Stankovic, M., de Waard, H., Frijlink, H., & Hinrichs, W. (2013). Unraveling protein stabilization mechanisms: Vitrification and water replacement in a glass transition temperature controlled system. Biochimica Et Biophysica Acta (BBA) - Proteins And Proteomics, 1834(4), 763-769. https://doi.org/10.1016/j.bbapap.2013.01.020

Grdadolnik, J., & Hadži, D. (1998). FT infrared and Raman investigation of saccharide–phosphatidylcholine interactions using novel structure probes. Spectrochimica Acta Part A: Molecular And Biomolecular Spectroscopy, 54(12), 1989-2000. https://doi.org/10.1016/s1386-1425(98)00111-5

Hagelstein, V., Gerhart, M., & Wagner, K. (2018). Tricalcium citrate – a new brittle tableting excipient for direct compression and dry granulation with enormous hardness yield. Drug Development And Industrial Pharmacy, 44(10), 1631-1641. https://doi.org/10.1080/03639045.2018.1483389

Haque, M., Chen, J., Aldred, P., & Adhikari, B. (2015). Denaturation and Physical Characteristics of Spray-Dried Whey Protein Isolate Powders Produced in the Presence and Absence of Lactose, Trehalose, and Polysorbate-80. Drying Technology, 33(10), 1243-1254. https://doi.org/10.1080/07373937.2015.1023311

Hegedűs, Á., & Pintye-Hódi, K. (2007). Comparison of the effects of different drying techniques on properties of granules and tablets made on a production scale. International Journal Of Pharmaceutics, 330(1-2), 99-104. https://doi.org/10.1016/j.ijpharm.2006.09.001

Hulse, W., Forbes, R., Bonner, M., & Getrost, M. (2009). Influence of protein on mannitol polymorphic form produced during co-spray drying. International Journal Of Pharmaceutics, 382(1-2), 67-72. https://doi.org/10.1016/j.ijpharm.2009.08.007

Hulse, W., Forbes, R., Bonner, M., & Getrost, M. (2009). The characterization and comparison of spray-dried mannitol samples. Drug Development And Industrial Pharmacy, 35(6), 712-718. https://doi.org/10.1080/03639040802516491

Izutsu, K., Yoshioka, S., & Terao, T. (1994). Effect of Mannitol Crystallinity on the Stabilization of Enzymes during Freeze-Drying. Chemical And Pharmaceutical Bulletin, 42(1), 5-8. https://doi.org/10.1248/cpb.42.5

Jain, N., & Roy, I. (2008). Effect of trehalose on protein structure. Protein Science, 24-36. https://doi.org/10.1002/pro.3

Jain, S. (1999). Mechanical properties of powders for compaction and tableting: an overview. Pharmaceutical Science &Amp; Technology Today, 2(1), 20-31. https://doi.org/10.1016/s1461-5347(98)00111-4

Jolliffe, I., & Cadima, J. (2016). Principal component analysis: a review and recent developments. Philosophical Transactions Of The Royal Society A: Mathematical, Physical And Engineering Sciences, 374(2065), 20150202. https://doi.org/10.1098/rsta.2015.0202

Kaialy, W., Khan, U., & Mawlud, S. (2016). Influence of mannitol concentration on the physicochemical, mechanical and pharmaceutical properties of lyophilized mannitol. International Journal Of Pharmaceutics, 510(1), 73-85. https://doi.org/10.1016/j.ijpharm.2016.05.052

Kasper, J., Winter, G., & Friess, W. (2013). Recent advances and further challenges in lyophilization. European Journal Of Pharmaceutics And Biopharmaceutics, 85(2), 162-169. https://doi.org/10.1016/j.ejpb.2013.05.019

Kaushik, J., & Bhat, R. (2003). Why Is Trehalose an Exceptional Protein Stabilizer?. Journal Of Biological Chemistry, 278(29), 26458-26465. https://doi.org/10.1074/jbc.m300815200

Kazarian, S., & Chan, K. (2006). Applications of ATR-FTIR spectroscopic imaging to biomedical samples. Biochimica Et Biophysica Acta (BBA) - Biomembranes, 1758(7), 858-867. https://doi.org/10.1016/j.bbamem.2006.02.011

Kazarian, S., & Chan, K. (2013). ATR-FTIR spectroscopic imaging: recent advances and applications to biological systems. The Analyst, 138(7), 1940. https://doi.org/10.1039/c3an36865c

Klukkert, M., van de Weert, M., Fanø, M., Rades, T., & Leopold, C. (2015). Influence of Tableting on the Conformation and Thermal Stability of Trypsin as a Model Protein. Journal Of Pharmaceutical Sciences, 104(12), 4314-4321. https://doi.org/10.1002/jps.24672

Köhn, B., & Kovermann, M. (2019). Macromolecular Crowding Tunes Protein Stability by Manipulating Solvent Accessibility. Chembiochem, 20(6), 759-763. https://doi.org/10.1002/cbic.201800679

Kokaly, R. (2001). Investigating a Physical Basis for Spectroscopic Estimates of Leaf Nitrogen Concentration. Remote Sensing Of Environment, 75(2), 153-161. https://doi.org/10.1016/s0034-4257(00)00163-2

Koner, J., Rajabi-Siahboomi, A., Bowen, J., Perrie, Y., Kirby, D., & Mohammed, A. (2015). A Holistic Multi Evidence Approach to Study the Fragmentation Behaviour of Crystalline Mannitol. Scientific Reports, 5(1). https://doi.org/10.1038/srep16352

Lee, S., Hafeman, A., Debenedetti, P., Pethica, B., & Moore, D. (2006). Solid-State stabilization of α-Chymotrypsin and Catalase with Carbohydrates. Industrial &Amp; Engineering Chemistry Research, 45(14), 5134-5147. https://doi.org/10.1021/ie0513503

Lennarz, W., & Lane, M. (2013). *Encyclopedia of biological chemistry*. Elsevier/Academic Press.

Liao, Y. H., Brown, M. B., Nazir, T., Quader, A., & Martin, G. P. (2002). Effects of sucrose and trehalose on the preservation of the native structure of spray-dried lysozyme. Pharmaceutical research, 19(12), 1847–1853. https://doi.org/10.1023/a:1021445608807

Liu, X., & Kokare, C. (2017). Chapter 11 - Microbial Enzymes of Use in Industry. In G. Brahmachari (Ed.), Biotechnology of Microbial Enzymes (pp. 267–298). https://doi.org/https://doi.org/10.1016/B978-0-12-803725-6.00011-X

Makurvet, F. (2021). Biologics vs. small molecules: Drug costs and patient access. *Medicine In Drug Discovery*, *9*, 100075. https://doi.org/10.1016/j.medidd.2020.100075

Marvin, L., Paiva, W., Gill, N., Morales, M., Halpern, J., Vesenka, J., & Balog, E. (2019). Flow imaging microscopy as a novel tool for high-throughput evaluation of elastin-like polymer coacervates. PLOS ONE, 14(5), e0216406. https://doi.org/10.1371/journal.pone.0216406

Mazel, V., Busignies, V., Diarra, H., & Tchoreloff, P. (2015). Lamination of pharmaceutical tablets due to air entrapment: Direct visualization and influence of the compact thickness. International Journal Of Pharmaceutics, 478(2), 702-704. https://doi.org/10.1016/j.ijpharm.2014.12.023

Mensink, M., Frijlink, H., van der Voort Maarschalk, K., & Hinrichs, W. (2017). How sugars protect proteins in the solid state and during drying (review): Mechanisms of stabilization in relation to stress conditions. European Journal Of Pharmaceutics And Biopharmaceutics, 114, 288-295. https://doi.org/10.1016/j.ejpb.2017.01.024

Mishra, S., Sarkar, U., Taraphder, S., Datta, S., Swain, D., & Saikhom, R. et al. (2017). Principal Component Analysis. International Journal Of Livestock Research, 1. https://doi.org/10.5455/ijlr.20170415115235

Mofidi Najjar, F., Taghavi, F., Ghadari, R., Sheibani, N., & Moosavi-Movahedi, A. (2017). Destructive effect of non-enzymatic glycation on catalase and remediation via curcumin. Archives Of Biochemistry And Biophysics, 630, 81-90. https://doi.org/10.1016/j.abb.2017.06.018

Nagar, M., Singhai, S.K., Chopra, V., Bala, I., & Trivedi, P. (2010). A study over effects of process parameters on quality attributes of a tablet by applying quality by design.

Nandi, A., Yan, L. J., Jana, C. K., & Das, N. (2019). Role of Catalase in Oxidative Stress- And Age-Associated Degenerative Diseases. Oxidative Medicine and Cellular Longevity, 2019. https://doi.org/10.1155/2019/9613090

New, R. (2020). Oral Delivery of Biologics via the Intestine. *Pharmaceutics*, *13*(1), 18. https://doi.org/10.3390/pharmaceutics13010018

Ngo, H., & Garneau-Tsodikova, S. (2018). What are the drugs of the future? Medchemcomm, 9(5), 757-758. https://doi.org/10.1039/c8md90019a

Ngono, F., Cuello, G., Jiménez-Ruiz, M., Willart, J., Guerain, M., & Wildes, A. et al. (2019). Morphological and Structural Properties of Amorphous Lactulose Studied by Scanning Electron Microscopy, Polarized Neutron Scattering, and Molecular Dynamics Simulations. Molecular Pharmaceutics,17(1),10-20. https://doi.org/10.1021/acs.molpharmaceut.9b00767

Nunes, C., Suryanarayanan, R., Botez, C., & Stephens, P. (2004). Characterization and Crystal Structure of D-Mannitol Hemihydrate. Journal Of Pharmaceutical Sciences, 93(11), 2800-2809. https://doi.org/10.1002/jps.20185

Olsson, C., Genheden, S., García Sakai, V., & Swenson, J. (2019). Mechanism of Trehalose-Induced Protein Stabilization from Neutron Scattering and Modeling. The Journal Of Physical Chemistry B, 123(17), 3679-3687. https://doi.org/10.1021/acs.jpcb.9b01856

Olsson, C., Zangana, R., & Swenson, J. (2020). Stabilization of proteins embedded in sugars and water as studied by dielectric spectroscopy. Physical Chemistry Chemical Physics, 22(37), 21197-21207. https://doi.org/10.1039/d0cp03281f

Oral solid dosage manufacturing. CRB. (2022). Retrieved 2 April 2022, from https://www.crbgroup.com/insights/oral-solid-dosage-manufacturing.

Pasieka, A. (2016). Immunoglobulin G Antibody Molecule. Fine Art America. Retrieved 7 June 2022, from https://fineartamerica.com/featured/9-immunoglobulin-g-antibody-molecule-alfred-pasieka.html.

Patel, S., Kaushal, A., & Bansal, A. (2006). Compression Physics in the Formulation Development of Tablets. Critical Reviews In Therapeutic Drug Carrier Systems, 23(1), 1-66. https://doi.org/10.1615/critrevtherdrugcarriersyst.v23.i1.10

Penha, F., Gopalan, A., Meijlink, J., Ibis, F., & Eral, H. (2021). Selective Crystallization of d-Mannitol Polymorphs Using Surfactant Self-Assembly. Crystal Growth &Amp; Design, 21(7), 3928-3935. https://doi.org/10.1021/acs.cgd.1c00243

Pinto, J., Faulhammer, E., Dieplinger, J., Dekner, M., Makert, C., Nieder, M., & Paudel, A. (2021). Progress in spray-drying of protein pharmaceuticals: Literature analysis of trends in formulation and process attributes. Drying Technology, 39(11), 1415-1446. https://doi.org/10.1080/07373937.2021.1903032

Poornachary, S., Parambil, J., Chow, P., Tan, R., & Heng, J. (2013). Nucleation of Elusive Crystal Polymorphs at the Solution–Substrate Contact Line. Crystal Growth &Amp; Design, 13(3), 1180-1186. https://doi.org/10.1021/cg301597d

Porter, S. (2021). Coating of pharmaceutical dosage forms. Remington, 551-564. https://doi.org/10.1016/b978-0-12-820007-0.00027-1

Qiu, Y., Chen, Y., Zhang, G., Yu, L., & Mantri, R. (2017). Developing Solid Oral Dosage Forms (2nd ed., p. 418). Pharmaceutical Theory and Practice.

Rasool, S., Mir, B., Rehman, M., Amin, I., Mir, M., & Ahmad, S. (2019). Abiotic Stress and Plant Senescence. Senescence Signalling And Control In Plants, 15-27. https://doi.org/10.1016/b978-0-12-813187-9.00002-0

Ratanji, K., Derrick, J., Dearman, R., & Kimber, I. (2013). Immunogenicity of therapeutic proteins: Influence of aggregation. Journal Of Immunotoxicology, 11(2), 99-109. https://doi.org/10.3109/1547691x.2013.821564

Rohs, R., Etchebest, C., & Lavery, R. (1999). Unraveling Proteins: A Molecular Mechanics Study. Biophysical Journal, 76(5), 2760-2768. https://doi.org/10.1016/s0006-3495(99)77429-1

Rostiashvili, V., & Vilgis, T. (2014). Statistical Thermodynamics of Polymeric Networks. Encyclopedia Of Polymeric Nanomaterials, 1-18. https://doi.org/10.1007/978-3-642-36199-9_308-1

Sajna, K., Gottumukkala, L., Sukumaran, R., & Pandey, A. (2015). White Biotechnology in Cosmetics. Industrial Biorefineries &Amp; White Biotechnology, 607-652. https://doi.org/10.1016/b978-0-444-63453-5.00020-3

Sanchez-Castillo, F., Anwar, J., & Heyes, D. (2003). Molecular dynamics simulations of granular compaction: The single granule case. The Journal Of Chemical Physics, 118(10), 4636-4648. https://doi.org/10.1063/1.1543982

Santos, D., Maurício, A., Sencadas, V., Santos, J., Fernandes, M., & Gomes, P. (2018). Spray Drying: An Overview. Biomaterials - Physics And Chemistry - New Edition. https://doi.org/10.5772/intechopen.72247

Sasahara, K., McPhie, P., & Minton, A. (2003). Effect of Dextran on Protein Stability and Conformation Attributed to Macromolecular Crowding. Journal Of Molecular Biology, 326(4), 1227-1237. https://doi.org/10.1016/s0022-2836(02)01443-2

Schaefer, J., & Lee, G. (2015). Arrhenius activation energy of damage to catalase during spray-drying. International Journal Of Pharmaceutics, 489(1-2), 124-130. https://doi.org/10.1016/j.ijpharm.2015.04.078

Scibior, D., & Czeczot, H. (2006). [Catalase: structure, properties, functions]. Postepy higieny i medycyny doswiadczalnej (Online), 60, 170–180.

Sedlock, R. (2016). A tabletting Tabletability , compactibility , and compressibility : What's the difference?. Tablets & Capsules.

Sefidani Forough, A., Lau, E., Steadman, K., Cichero, J., Kyle, G., Serrano Santos, J., & Nissen, L. (2018). A spoonful of sugar helps the medicine go down? A review of strategies for making pills easier to swallow. *Patient Preference And Adherence*, *Volume 12*, 1337-1346. https://doi.org/10.2147/ppa.s164406

Sepasi Tehrani, H., & Moosavi-Movahedi, A. (2018). Catalase and its mysteries. Progress In Biophysics And Molecular Biology, 140, 5-12. https://doi.org/10.1016/j.pbiomolbio.2018.03.001

Shah, j. (2017). Effect of bulk density on tensile strength of tablets prepared by using hiceltmmcc (microcrystalline cellulose) and hiceltmsmcc (silicified microcrystalline cellulose). World Journal of Pharmaceutical Research, 841-852. https://doi.Org/10.20959/wjpr201710-9377

Shao, Q., Wang, J., & Zhu, W. (2019). Trehalose Stabilizing Protein in a Water Replacement Scenario: Insights from Molecular Dynamics Simulation. https://doi.org/10.1101/2019.12.27.889063

Shawkat, H., Westwood, M., & Mortimer, A. (2012). Mannitol: a review of its clinical uses. Continuing Education In Anaesthesia Critical Care &Amp; Pain, 12(2), 82-85. https://doi.org/10.1093/bjaceaccp/mkr063

Siddiqui, N., Aman, A., Silipo, A., Qader, S., & Molinaro, A. (2014). Structural analysis and characterization of dextran produced by wild and mutant strains of Leuconostoc mesenteroides. Carbohydrate Polymers, 99, 331-338. https://doi.org/10.1016/j.carbpol.2013.08.004

Simon, H. (2014). Human growth hormone. Chemistry World. Retrieved 7 April 2022, from https://www.chemistryworld.com/podcasts/humangrowthhormone/7912.article

Singh, S., & Singh, J. (2003). Effect of polyols on the conformational stability and biological activity of a model protein lysozyme. AAPS Pharmscitech, 4(3), 101-109. https://doi.org/10.1208/pt040342

Skelbæk-Pedersen, A., Vilhelmsen, T., Wallaert, V., & Rantanen, J. (2019). Quantification of Fragmentation of Pharmaceutical Materials After Tableting. Journal Of Pharmaceutical Sciences, 108(3), 1246-1253. https://doi.org/10.1016/j.xphs.2018.10.040

Starciuc, T., Malfait, B., Danede, F., Paccou, L., Guinet, Y., Correia, N., & Hedoux, A. (2020). Trehalose or Sucrose: Which of the Two Should be Used for Stabilizing Proteins in the Solid State? A Dilemma Investigated by In Situ Micro-Raman and Dielectric Relaxation Spectroscopies During and After Freeze-Drying. Journal Of Pharmaceutical Sciences, 109(1), 496-504. https://doi.org/10.1016/j.xphs.2019.10.055

Su, W., Jia, N., Li, H., Hao, H., & Li, C. (2017). Polymorphism of D-mannitol: Crystal structure and the crystal growth mechanism. Chinese Journal Of Chemical Engineering, 25(3), 358-362. https://doi.org/10.1016/j.cjche.2016.09.002

Sussich, F., Urbani, R., Princivalle, F., & Cesàro, A. (1998). Polymorphic Amorphous and Crystalline Forms of Trehalose. Journal Of The American Chemical Society, 120(31), 7893-7899. https://doi.org/10.1021/ja9800479

Talari, A., Martinez, M., Movasaghi, Z., Rehman, S., & Rehman, I. (2016). Advances in Fourier transform infrared (FTIR) spectroscopy of biological tissues. Applied Spectroscopy Reviews, 52(5), 456-506. https://doi.org/10.1080/05704928.2016.1230863

Tatulian, S. (2012). Structural Characterization of Membrane Proteins and Peptides by FTIR and ATR-FTIR Spectroscopy. Methods In Molecular Biology, 177-218. https://doi.org/10.1007/978-1-62703-275-9_9

Thipparaboina, R., Kumar, D., Chavan, R., & Shastri, N. (2016). Multidrug co-crystals: towards the development of effective therapeutic hybrids. Drug Discovery Today, 21(3), 481-490. https://doi.org/10.1016/j.drudis.2016.02.001

Tom, J. (2021). UV-Vis Spectroscopy: Principle, Strengths and Limitations and Applications. Analysis & Separations from Technology Networks. Retrieved 20 May

2022, from https://www.technologynetworks.com/analysis/articles/uv-vis-spectroscopy-principle-strengths-and-limitations-and-applications-349865.

Tonnis, W., Mensink, M., de Jager, A., van der Voort Maarschalk, K., Frijlink, H., & Hinrichs, W. (2015). Size and Molecular Flexibility of Sugars Determine the Storage Stability of Freeze-Dried Proteins. Molecular Pharmaceutics, 12(3), 684-694. https://doi.org/10.1021/mp500423z

Tusé, D., Tu, T., & McDonald, K. (2014). Manufacturing Economics of Plant-Made Biologics: Case Studies in Therapeutic and Industrial Enzymes. Biomed Research International, 2014, 1-16. https://doi.org/10.1155/2014/256135

Tye, C., Sun, C., & Amidon, G. (2005). Evaluation of the effects of tableting speed on the relationships between compaction pressure, tablet tensile strength, and tablet solid fraction. Journal Of Pharmaceutical Sciences, 94(3), 465-472. https://doi.org/10.1002/jps.20262

Ubbink, J. (2016). Structural and thermodynamic aspects of plasticization and antiplasticization in glassy encapsulation and biostabilization matrices. Advanced Drug Delivery Reviews, 100, 10-26. https://doi.org/10.1016/j.addr.2015.12.019

Ubhe, T. S., & Gedam, P. (2020). A Brief Overview on Tablet and Its Types. Journal of Advancement in Pharmacology, 1(1).

Vagenende, V., Yap, M., & Trout, B. (2009). Mechanisms of Protein Stabilization and Prevention of Protein Aggregation by Glycerol. Biochemistry, 48(46), 11084-11096. https://doi.org/10.1021/bi900649t

van Beers, M., Slooten, C., Meulenaar, J., Sediq, A., Verrijk, R., & Jiskoot, W. (2017). Micro-Flow Imaging as a quantitative tool to assess size and agglomeration of PLGA microparticles. European Journal Of Pharmaceutics And Biopharmaceutics, 117, 91-104. https://doi.org/10.1016/j.ejpb.2017.04.002

Vernon-Parry, K. (2000). Scanning electron microscopy: an introduction. III-Vs Review, 13(4), 40-44. https://doi.org/10.1016/s0961-1290(00)80006-x

Wang, W., Nema, S., & Teagarden, D. (2010). Protein aggregation—Pathways and influencing factors. International Journal Of Pharmaceutics, 390(2), 89-99. https://doi.org/10.1016/j.ijpharm.2010.02.025

Wei, Y., Wang, C., Jiang, B., Sun, C., & Middaugh, C. (2019). Developing Biologics Tablets: The Effects of Compression on the Structure and Stability of Bovine Serum Albumin and Lysozyme. Molecular Pharmaceutics, 16(3), 1119-1131. https://doi.org/10.1021/acs.molpharmaceut.8b01118

Wilkinson, L. (1971). William Brockedon, F.R.S. (1787-1854). *Notes and Records of the Royal Society of London*, *26*(1), 65–72. http://www.jstor.org/stable/531053

Wurster, D., & Ternik, R. (1995). Pressure-Induced Activity Loss in Solid State Catalase. Journal Of Pharmaceutical Sciences, 84(2), 190-194. https://doi.org/10.1002/jps.2600840213

Xie, R., Chung, J., Ylaya, K., Williams, R., Guerrero, N., & Nakatsuka, N. et al. (2011). Factors Influencing the Degradation of Archival Formalin-Fixed Paraffin-Embedded Tissue Sections. Journal Of Histochemistry & Amp; Cytochemistry, 59(4), 356-365. https://doi.org/10.1369/0022155411398488

Yan, Y., Wang, Q., He, H., & Zhou, H. (2004). Protein Thermal Aggregation Involves Distinct Regions: Sequential Events in the Heat-Induced Unfolding and Aggregation of Hemoglobin. Biophysical Journal, 86(3), 1682-1690. https://doi.org/10.1016/s0006-3495(04)74237-x

Yoshinari, T., Forbes, R., York, P., & Kawashima, Y. (2002). Moisture induced polymorphic transition of mannitol and its morphological transformation. International Journal Of Pharmaceutics, 247(1-2), 69-77. https://doi.org/10.1016/s0378-5173(02)00380-0

Yuzugullu Karakus, Y. (2020). Typical Catalases: Function and Structure. Glutathione System And Oxidative Stress In Health And Disease. https://doi.org/10.5772/intechopen.90048

Zeeshan, F., Tabbassum, M., & Kesharwani, P. (2019). Investigation on Secondary Structure Alterations of Protein Drugs as an Indicator of Their Biological Activity Upon Thermal Exposure. The Protein Journal, 38(5), 551-564. https://doi.org/10.1007/s10930-019-09837-4

Zellnitz, S., Pinto, J., Brunsteiner, M., Schroettner, H., Khinast, J., & Paudel, A. (2019). Tribo-Charging Behaviour of Inhalable Mannitol Blends with Salbutamol Sulphate. Pharmaceutical Research, 36(6). https://doi.org/10.1007/s11095-019-2612-9

Zhu, M., & Yu, L. (2017). Polyamorphism of D-mannitol. The Journal Of Chemical Physics, 146(24), 244503. https://doi.org/10.1063/1.4989961

Zhu, M., Mollet, M., Hubert, R., Kyung, Y., & Zhang, G. (2017). Industrial Production of Therapeutic Proteins: Cell Lines, Cell Culture, and Purification. Handbook Of Industrial Chemistry And Biotechnology, 1639-1669. https://doi.org/10.1007/978-3-319-52287-6_29

Zimmermann, M., Schaldach, G., Thommes, M., Bauer-Brandl, A., & Kleinebudde, P. (2018). Comparison of the Performance of Single Punch and Rotary Tablet Presses from Different Vendors. TechnoPharm, 8(2), 96-103.

7. Annexes

Annex A – Biological Activity Characterization Graphs: UV/Vis

Annex A.1 - Absorbance of non-spray-dried CAT mixtures in function of time

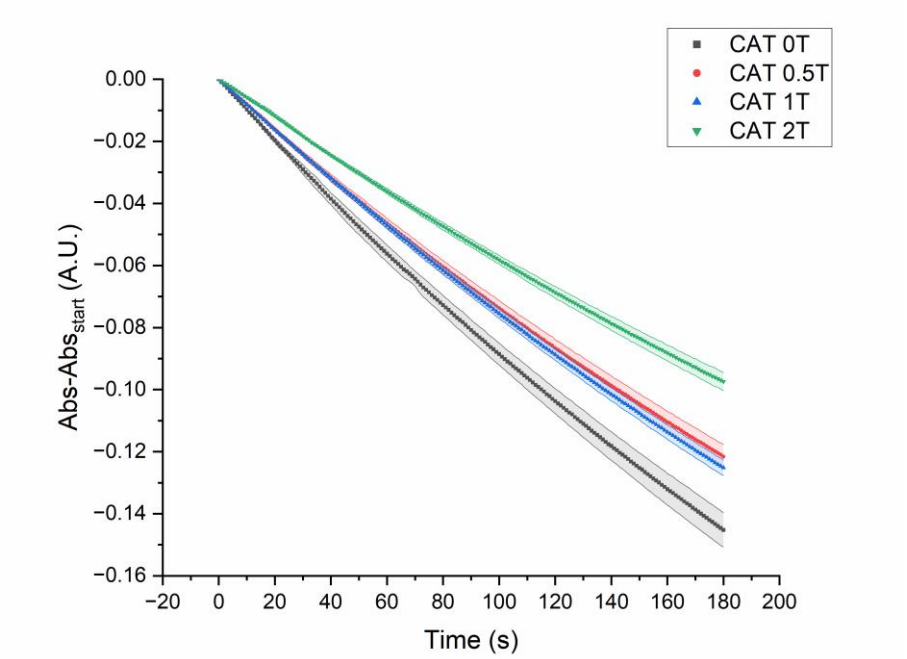

Figure A.1 - Error band graph of CAT blend and tablets. *The colored transparent area represents the standard variation of the relative activity of the formulation.*

Annex A.2 – Absorbance of spray-dried CAT mixtures in function of time

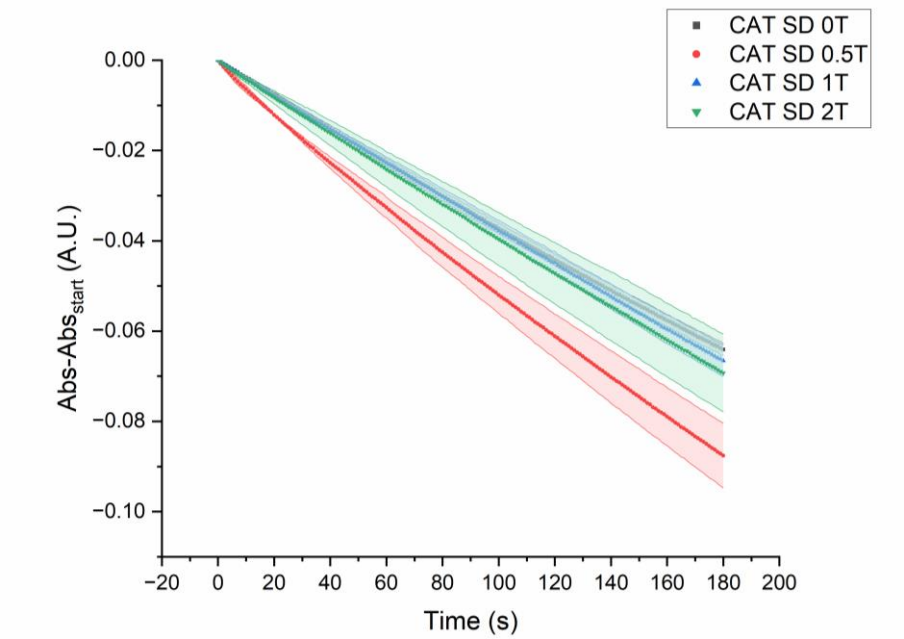

Figure A.2 - Error band graph of spray-dried CAT co-particle and tablets. *The colored transparent area represents the standard variation of the relative activity of the formulation.*

Annex A.3 – Absorbance of non-spray-dried DEX mixtures in function of time

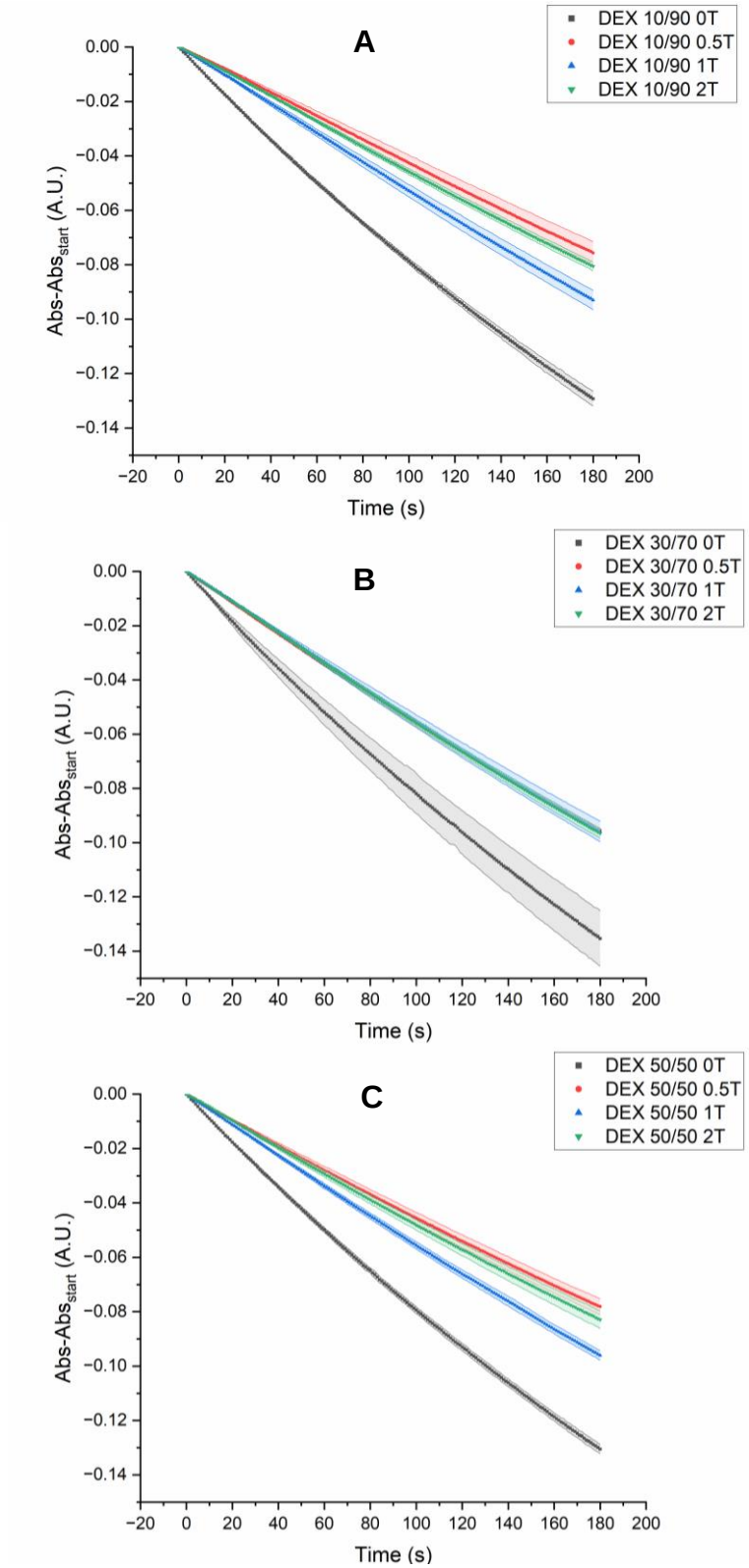

Figure A.3 - Error band graph of DEX mixtures with different ratios. *The colored transparent area represents the standard variation of the relative activity of the formulation. Legend: A – DEX 10/90 ratio; B – DEX 30/70 ratio; C – DEX 50/50 ratio.*

Annex A.4 – Absorbance of spray-dried DEX mixtures in function of time

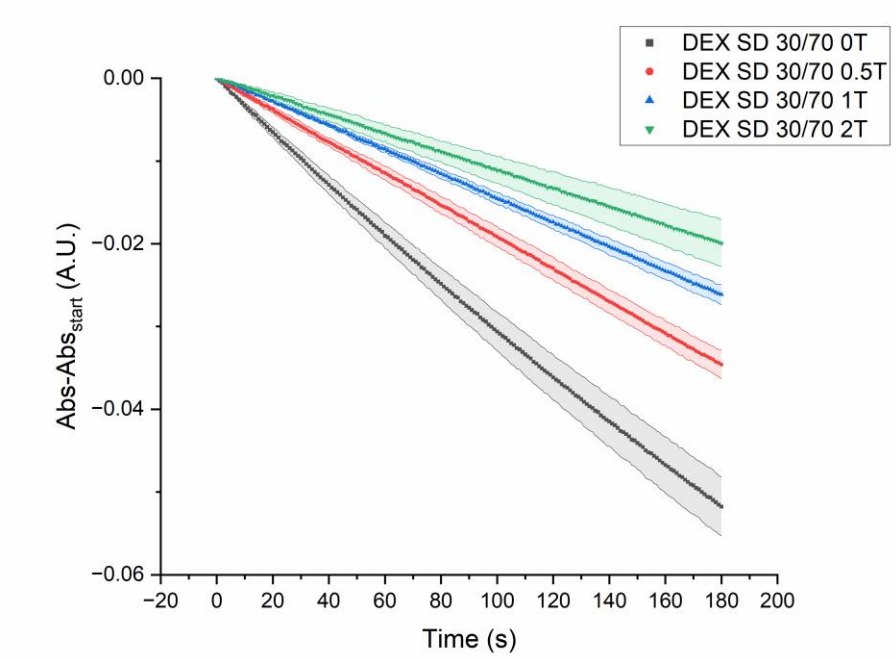

Figure A.4 - Error band graph of spray-dried DEX co-particle and tablets. *The colored transparent area represents the standard variation of the relative activity of the formulation.*

Annex A.5 – Absorbance of non-spray-dried MAN mixtures in function of time

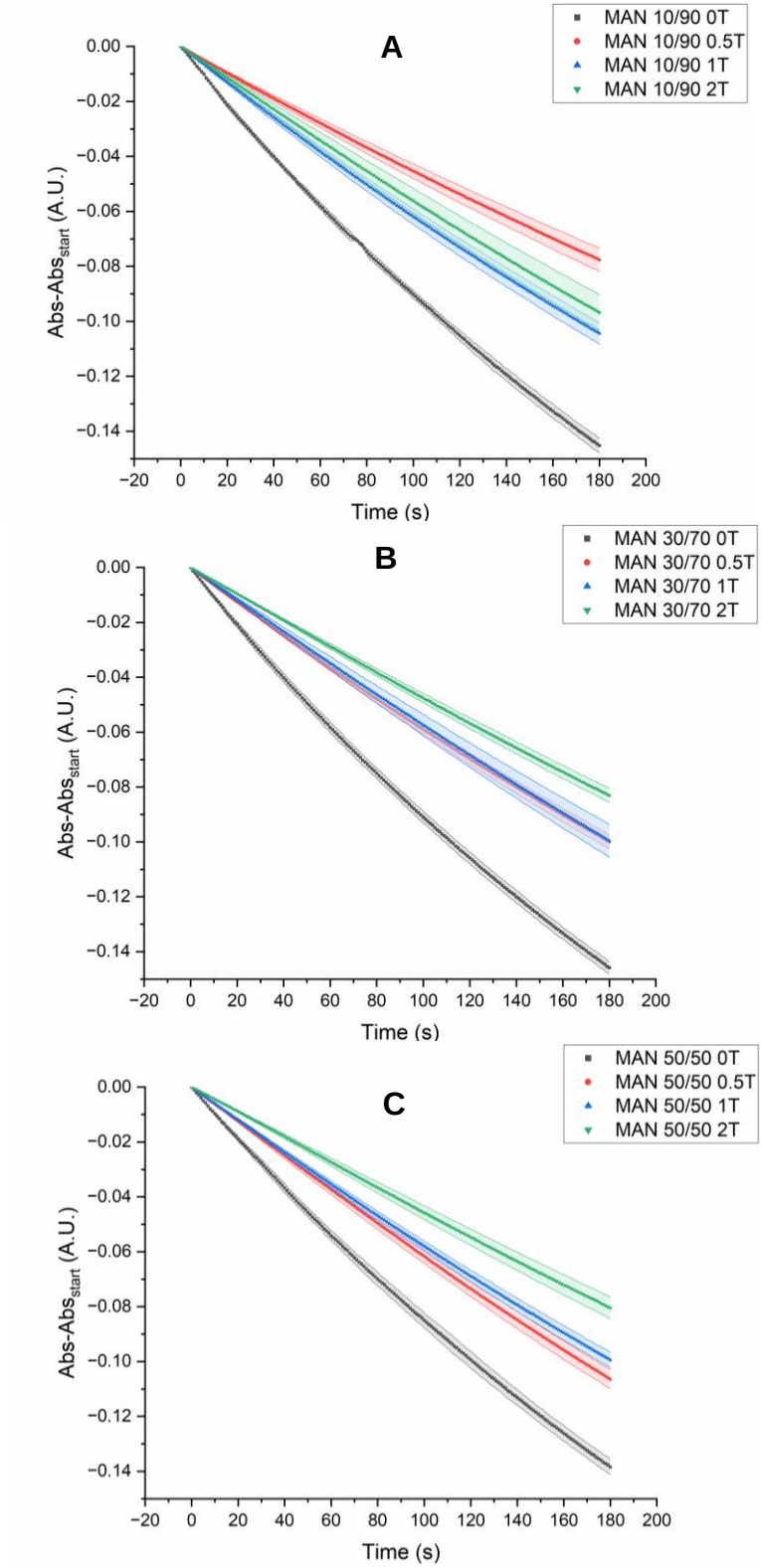

Figure A.5 - Error band graph of MAN blend and tablets with different ratios. *The colored transparent area represents the standard variation of the relative activity of the formulation. Legend: A – MAN 10/90 ratio; B – MAN 30/70 ratio; C – MAN 50/50 ratio.*

Annex A.6 - Absorbance of spray-dried MAN mixtures in function of time

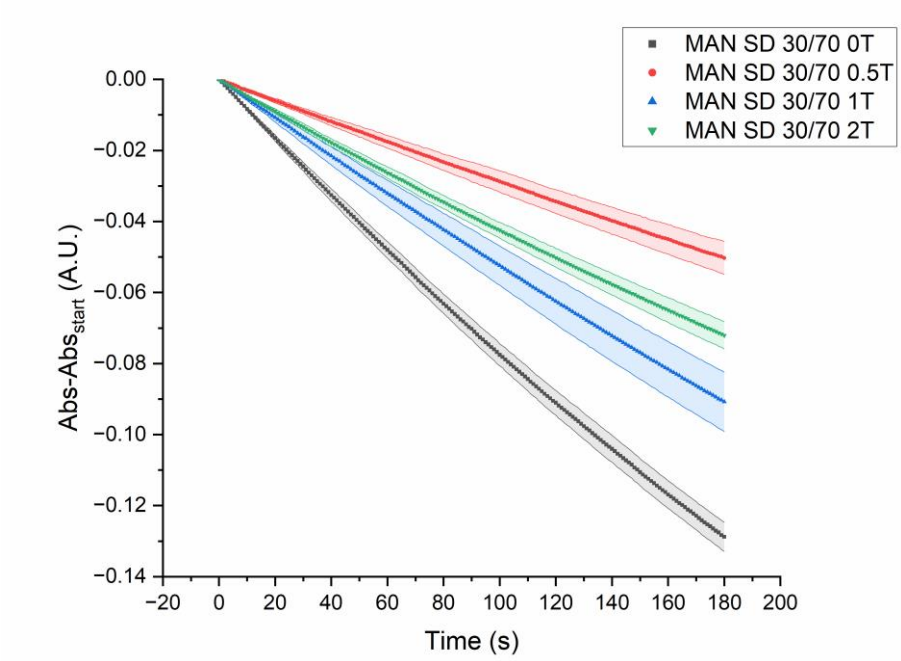

Figure A.6 - Error band graph of spray-dried MAN co-particle and tablets. *The colored transparent area represents the standard variation of the relative activity of the formulation.*

Annex A.7 - Absorbance of non-spray-dried TRH mixtures in function of time

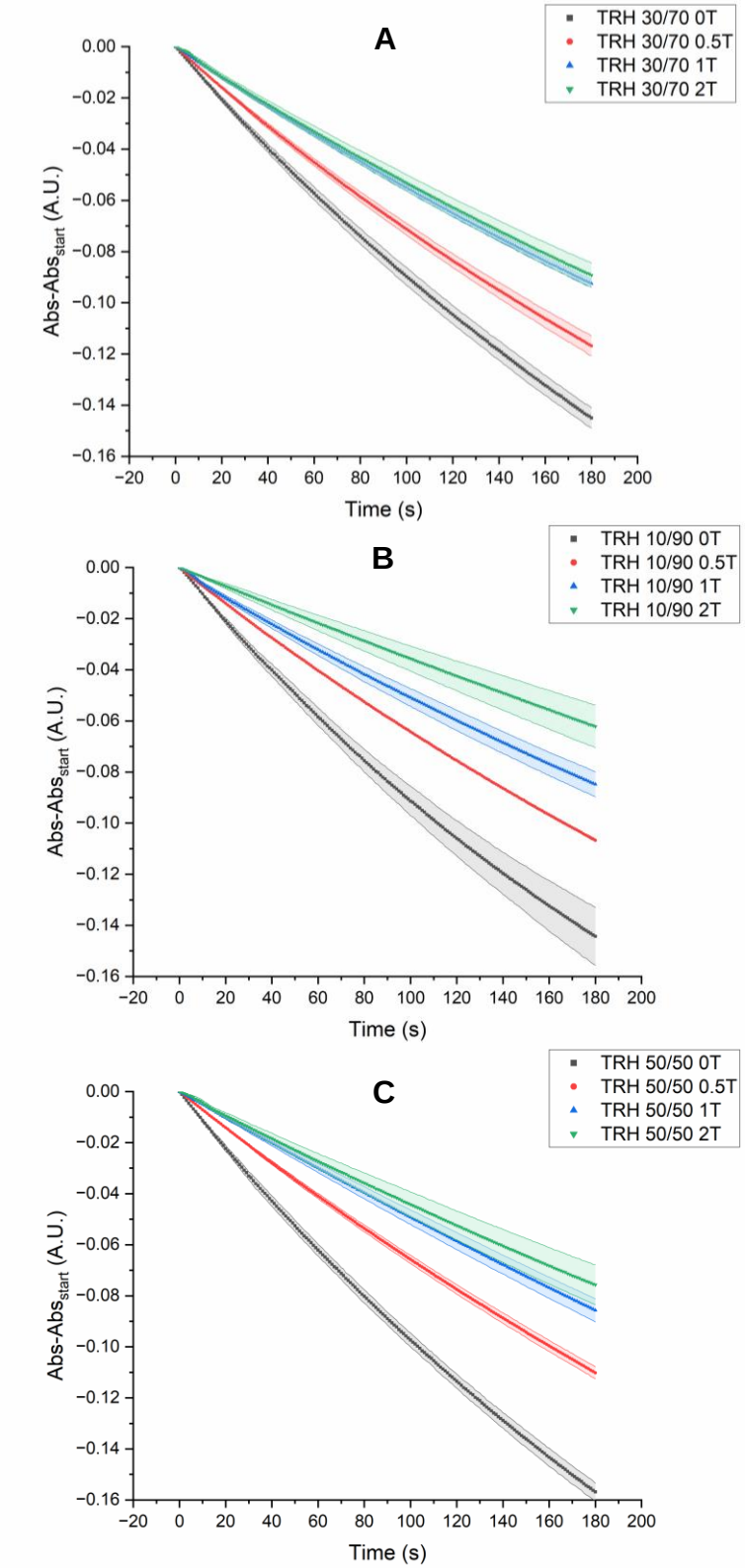

Figure A.7 - Error band graph of TRH tablets with different ratios. *The colored transparent area represents the standard variation of the relative activity of the formulation. Legend: A – TRH 10/90 ratio; B – TRH 30/70 ratio; C – TRH 50/50 ratio.*

Annex A.8 - Absorbance of spray-dried TRH tablets in function of time

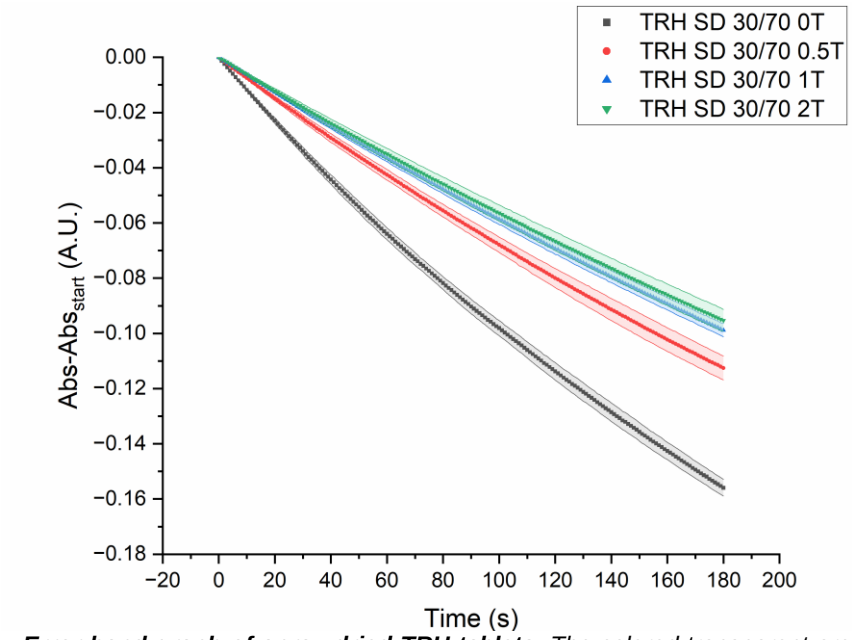

Figure A.8 - Error band graph of spray-dried TRH tablets. *The colored transparent area represents the standard variation of the relative activity of the formulation.*

Annex B – Structural Characterization Graphs: ATR-FTIR

Annex B.1 – Infrared Absorbance Intensity in function of the wavenumber of raw DEX

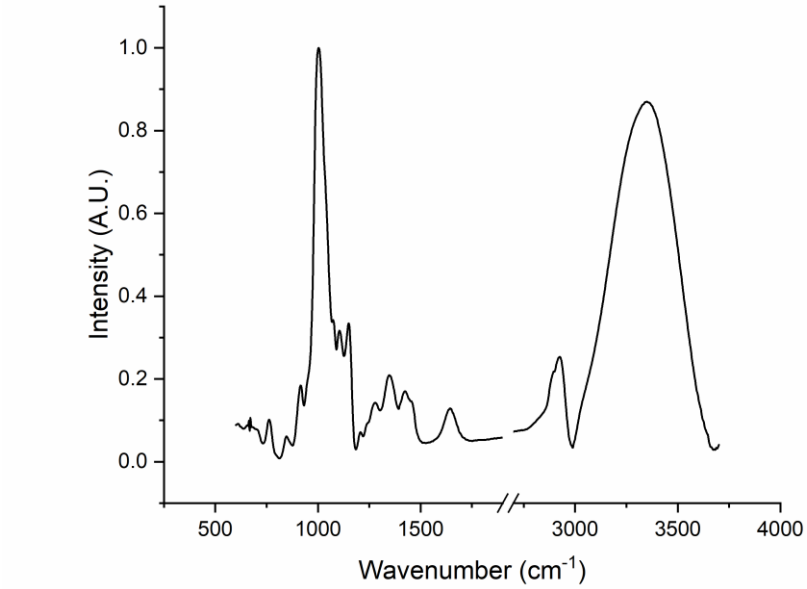

Figure B.1 - ATR-FTIR spectra of DEX (raw material).

Annex B.2 – Infrared Absorbance Intensity in function of the wavenumber of raw MAN

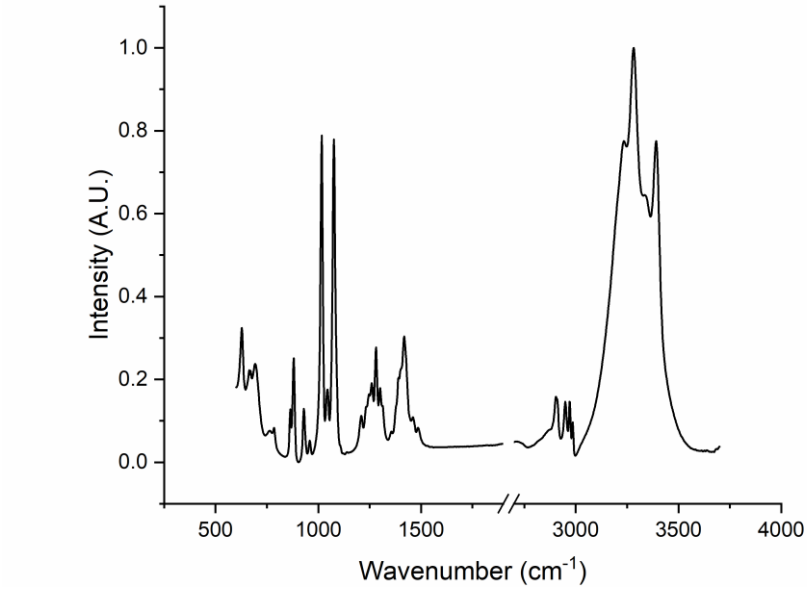

Figure B.2 - ATR-FTIR spectra of MAN (raw material).

Annex B.3 - Infrared Absorbance Intensity in function of the wavenumber of raw TRH

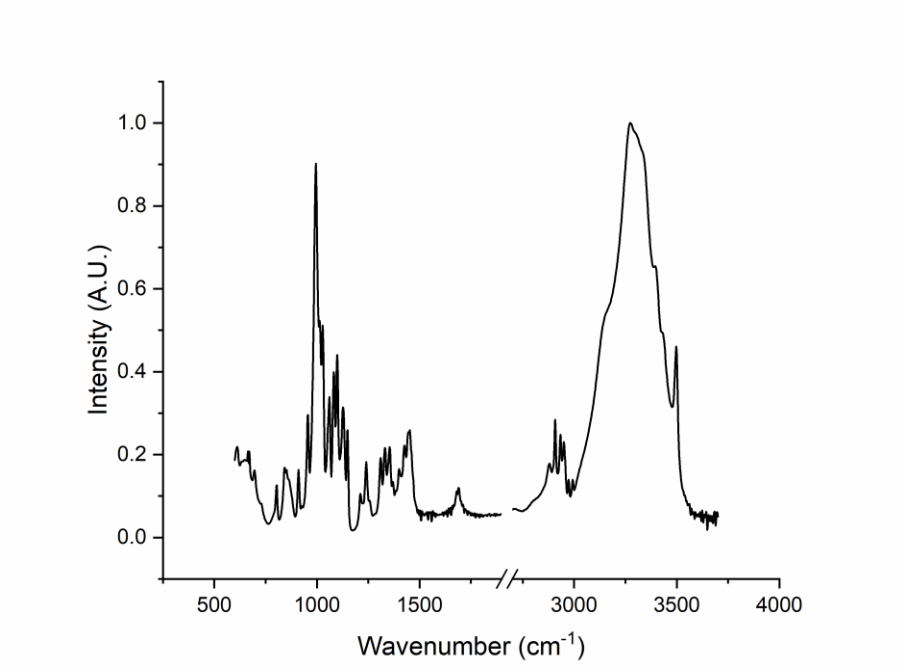

Figure B.3 - ATR-FTIR spectra of TRH (raw material).

Annex C – Structural Characterization Graphs: SWAXS

Annex C.1 – Intensity (counts) in function of 2θ (°) of raw MAN.

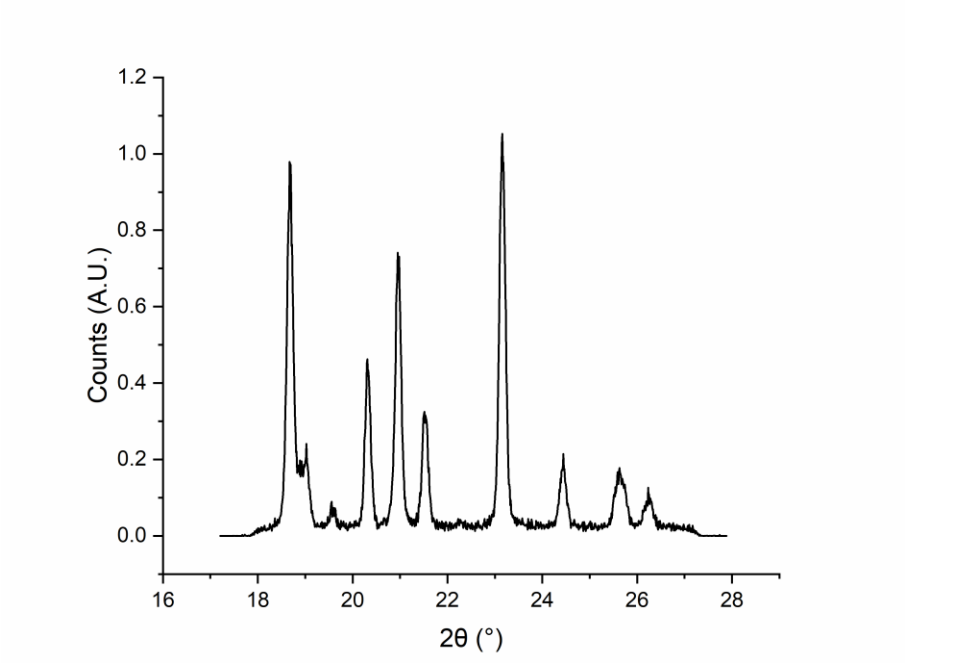

Figure C.1 - WAXS spectra of MAN (raw material).

Annex C.2 - Intensity (counts) in function of 2θ (°) of raw TRH.

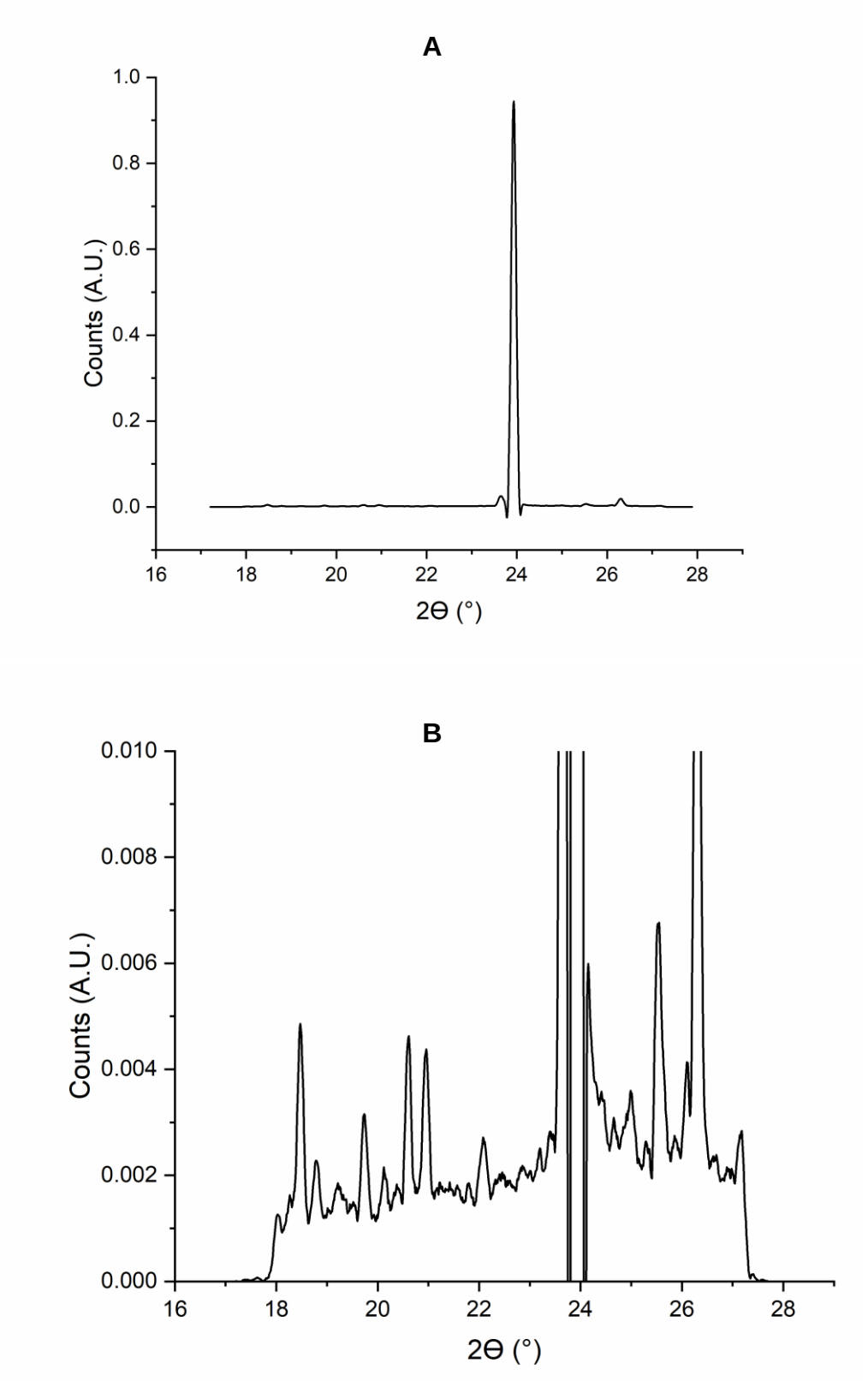

Figure C.2 - WAXS spectra of TRH (raw material). *Legend: A – Zoomed out plot; B – Zoomed in plot.*

Annex C.3 - Intensity (counts) in function of 2θ (°) of spray-dried CAT and MAN co-particles.

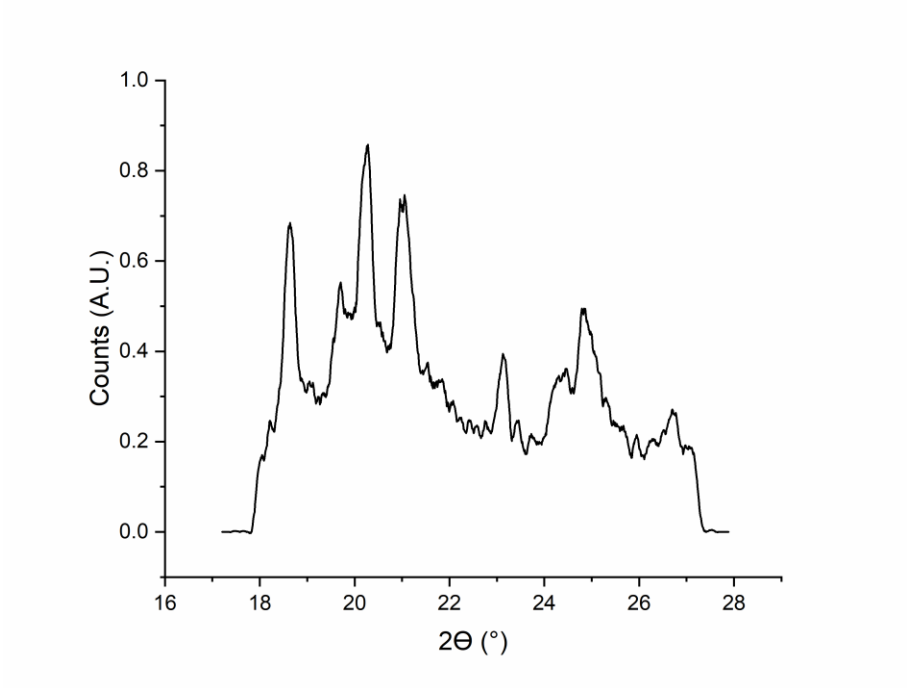

Figure C.3 - WAXS spectra of CAT and MAN co-particles (after SD).

Annex C.4 - Intensity (counts) in function of 2θ (°) of spray-dried CAT and TRH co-particles.

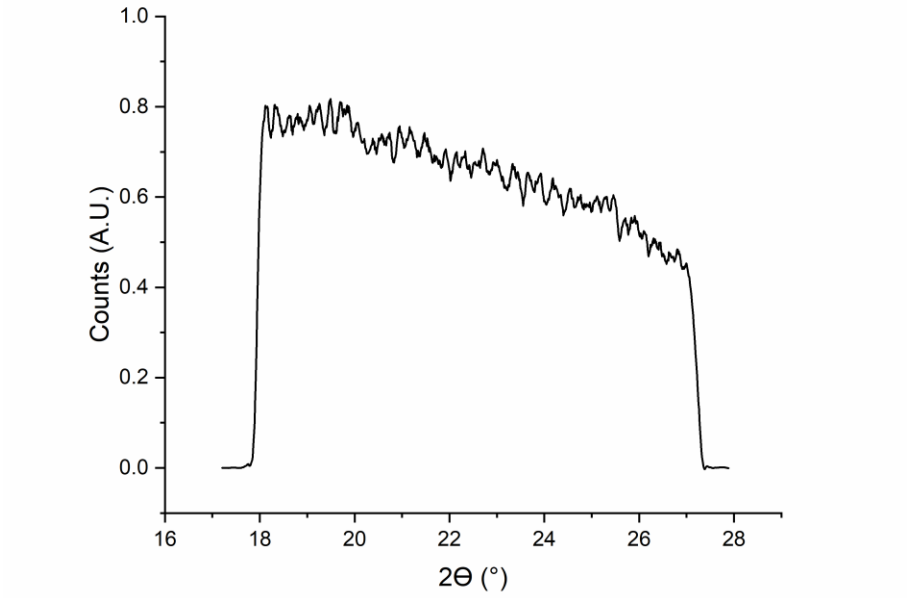

Figure C.4 - WAXS spectra of CAT and TRH co-particles (after SD).

Annex D – Structural Characterization Graphs: SEM

Annex D.1 – SEM images of the CAT and DEX after Spray-drying.

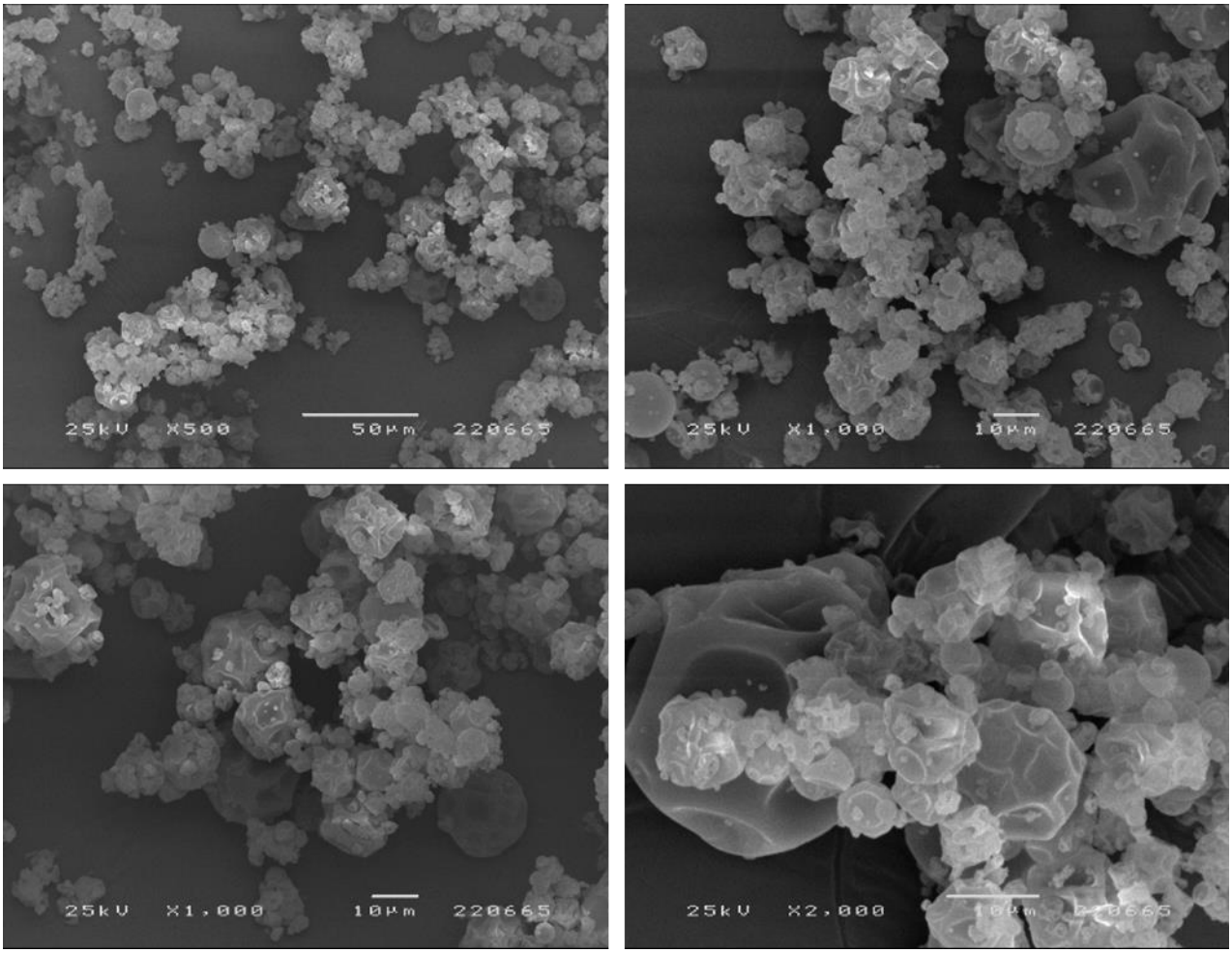

Figure D.1 - SEM images of the CAT and DEX co-particles (after SD).

Annex D.2 - SEM images of the CAT and MAN after Spray-drying.

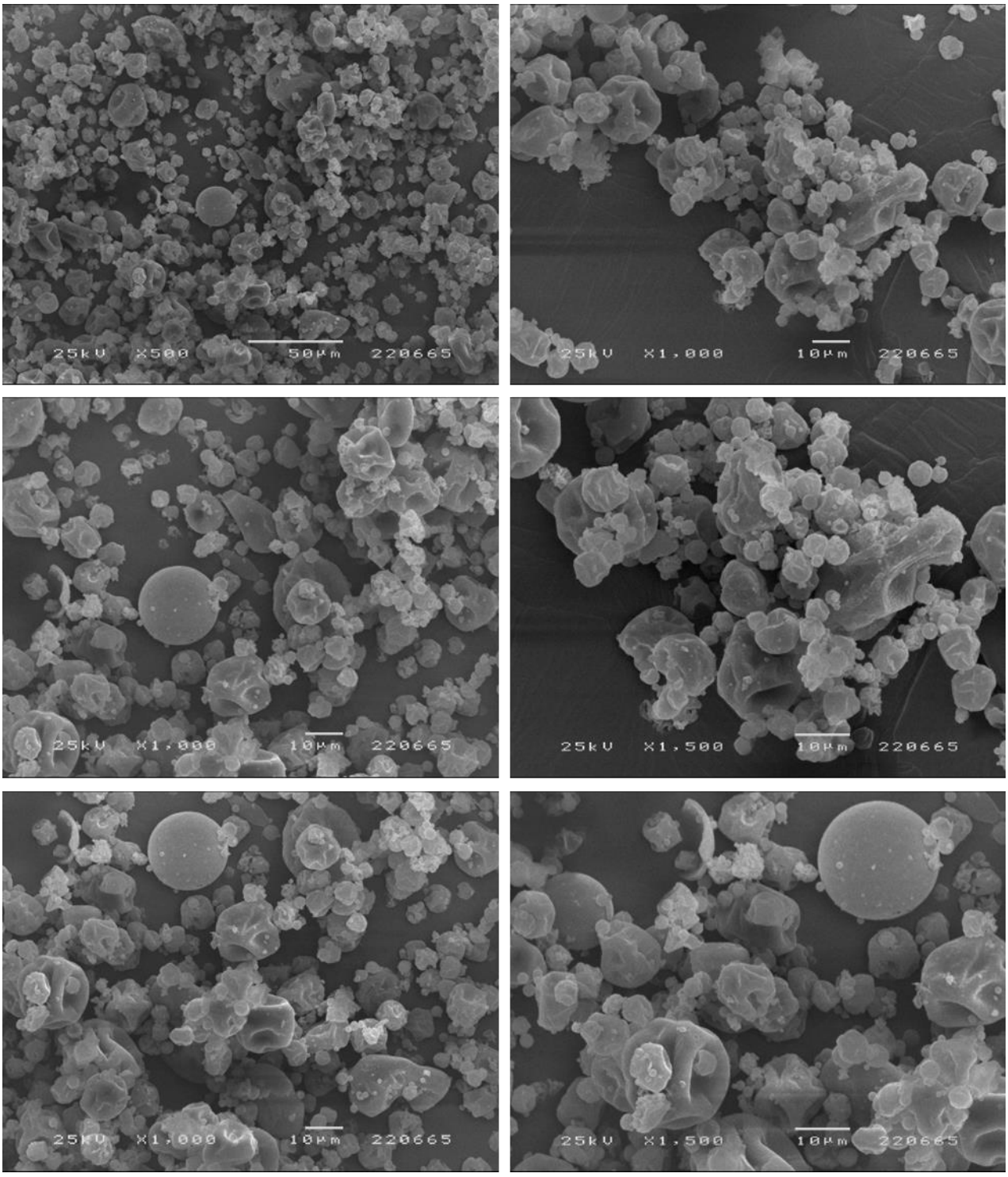

Figure D.2 - SEM images of the CAT and MAN co-particles (after SD).

Annex D.3 - SEM images of the CAT and TRH after Spray-drying.

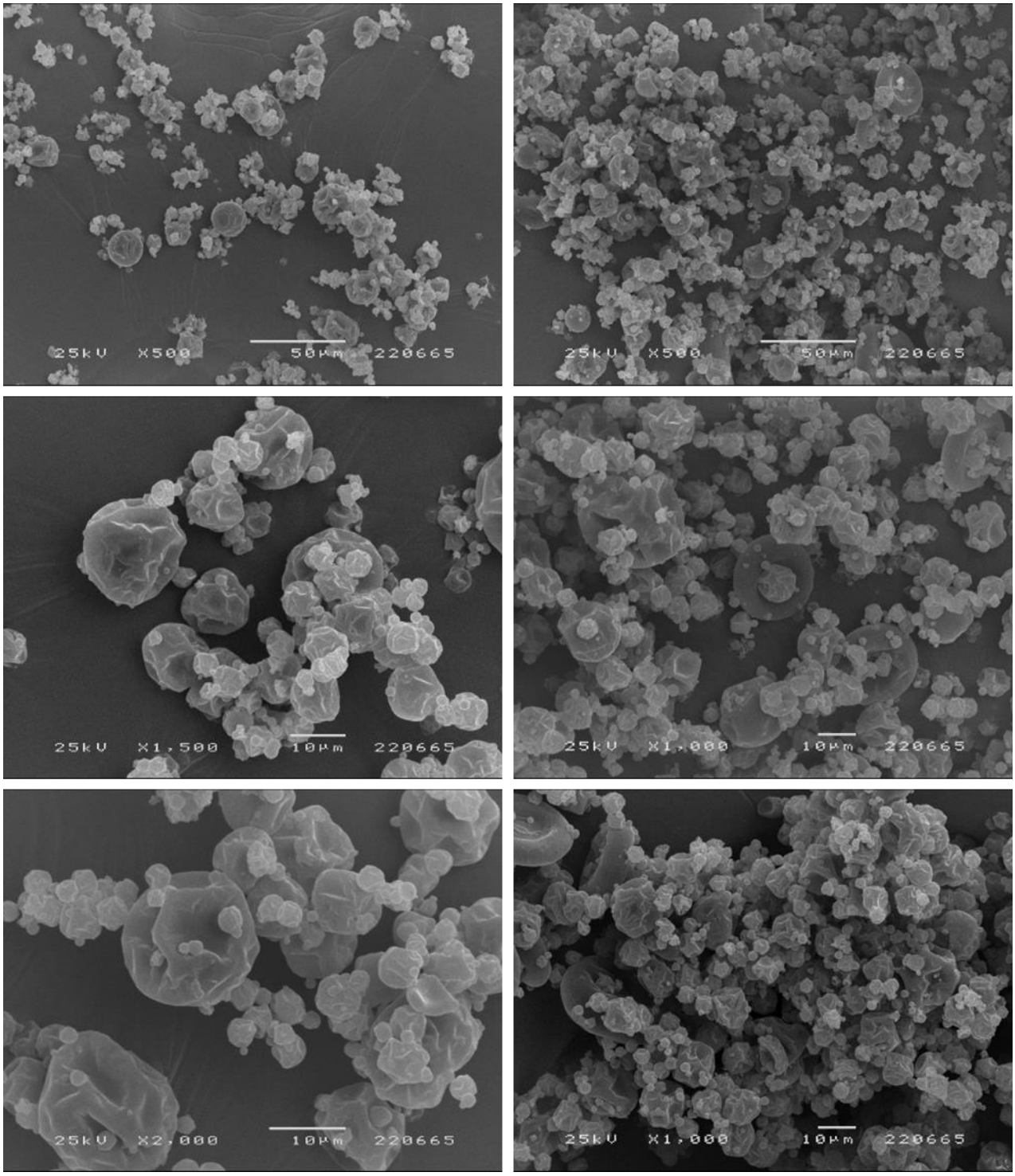

Figure D.3 - SEM images of the CAT and TRH co-particles (after SD).

Annex E – Multivariate analysis: PCA

Annex E.1 – Score Plot of the non-spray-dried mixtures, colored according to the saccharide used in the formulation.

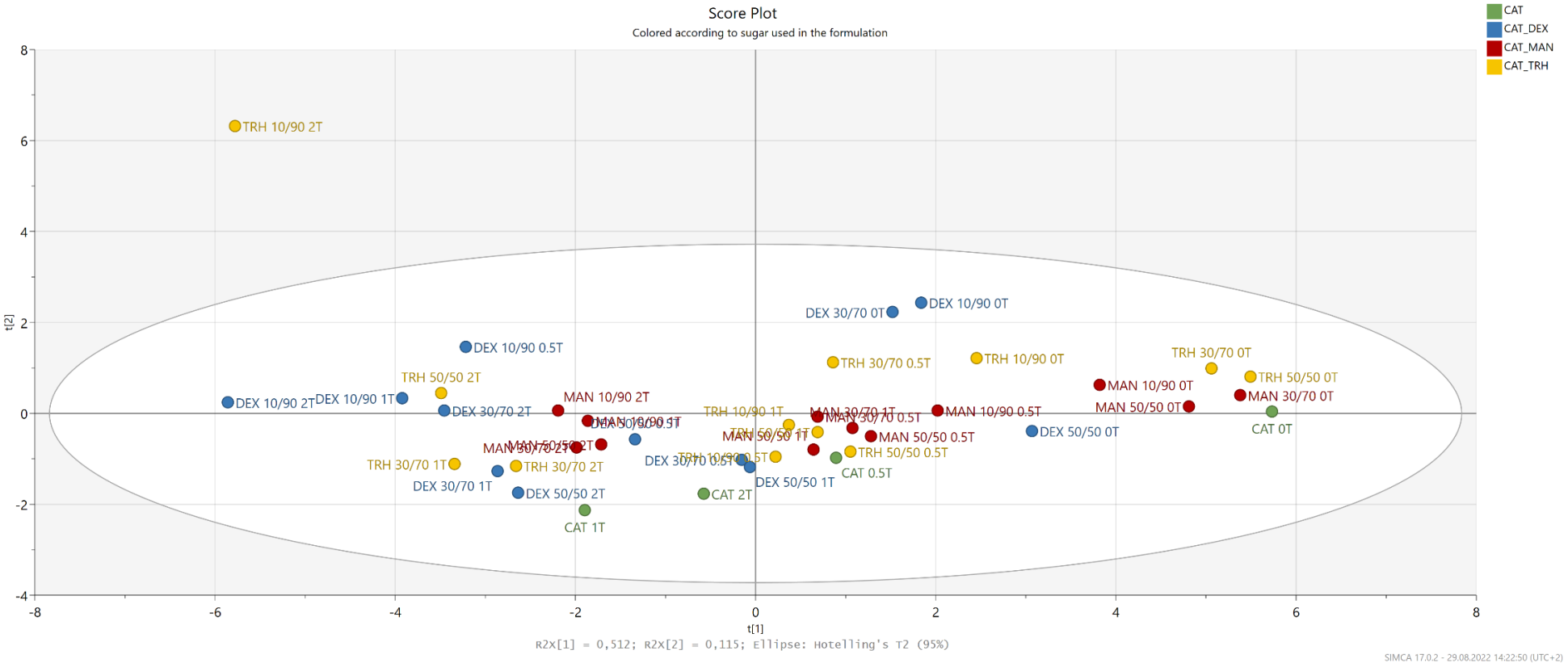

Figure E.1 - Score plot colored according to the saccharides used in the formulation*. Only quantitative data, of the non-spray-dried mixtures, was used to perform the PCA.*

Legend: Green – Catalase; Blue – Catalase and Dextran; Red – Catalase and Mannitol; Yellow – Catalase and Trehalose-

Annex E.2 - Loading plot of the spray-dried mixtures.

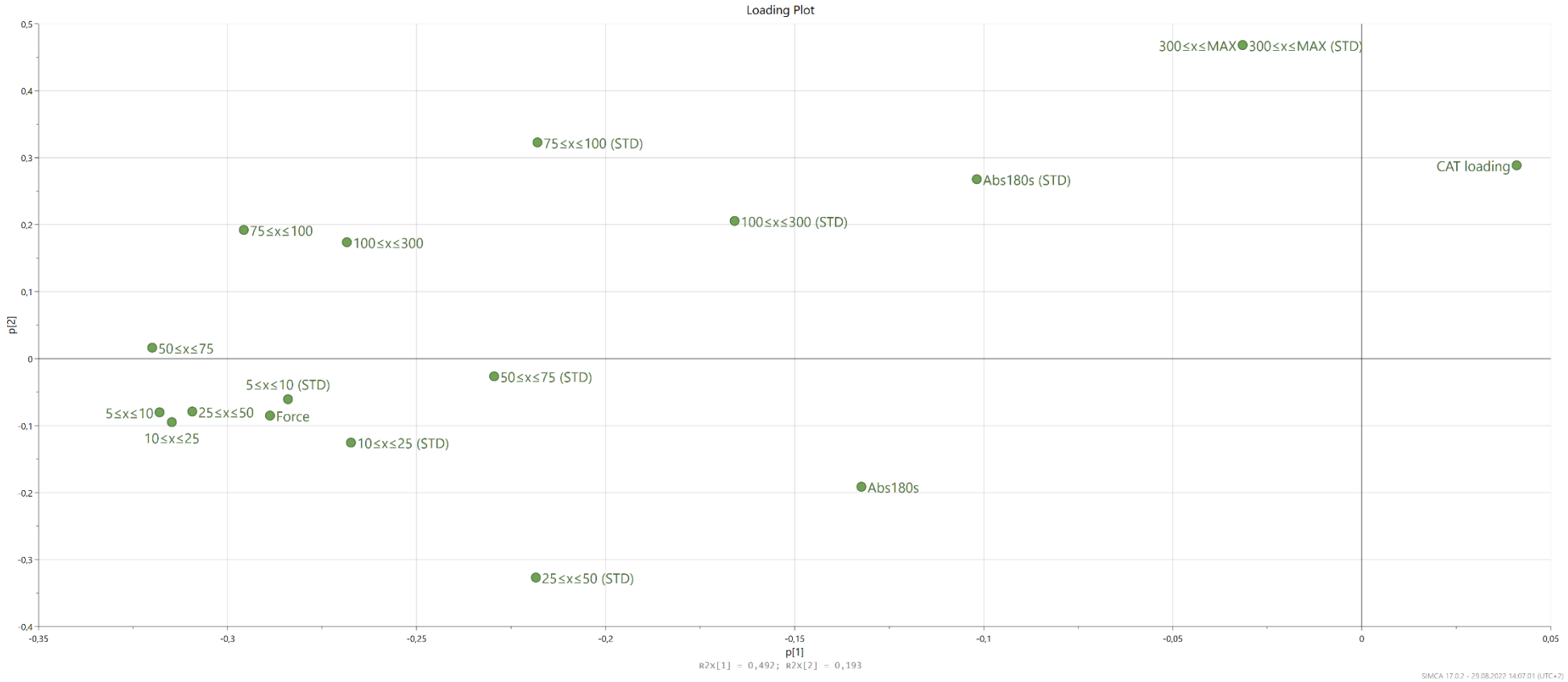

Figure E.2 - Loading plot of the spray-dried mixtures. *Only quantitative data, of the spray-dried mixtures, was used to perform the PCA.*

Annex E.3 - Correlation matrix of only the spray-dried mixtures.

Table E.1 - Correlation matrix of the spray-dried mixtures.

	CAT Loading	Force	Abs_{180s}	Abs_{180s} (STD)	5≤x≤10	10≤x≤25	25≤x≤50	50≤x≤75	75≤x≤100	100≤x≤300	300≤x≤MAX	5≤x≤10 (STD)	10≤x≤25 (STD)	25≤x≤50 (STD)	50≤x≤75 (STD)	75≤x≤100 (STD)	100≤x≤300 (STD)	300≤x≤MAX (STD)
CAT Loading	1.000	-0.107	-0.100	0.333	-0.133	-0.120	-0.120	-0.127	-0.020	-0.146	0.533	0.054	-0.100	-0.224	-0.345	0.123	-0.180	0.533
Force		1.000	0.390	0.192	0.806	0.798	0.769	0.774	0.671	0.673	-0.072	0.778	0.740	0.630	0.503	0.423	0.375	-0.072
Abs_{180s}			1.000	-0.280	0.454	0.400	0.329	0.234	0.054	0.075	0.000	0.541	0.483	0.411	0.464	-0.164	0.152	0.000
Abs_{180s} (STD)				1.000	0.176	0.204	0.226	0.287	0.413	0.228	0.294	0.286	0.371	-0.108	0.043	0.569	0.127	0.294
5≤x≤10					1.000	0.985	0.973	0.932	0.776	0.623	0.043	0.836	0.714	0.766	0.563	0.488	0.261	0.043
10≤x≤25						1.000	0.994	0.919	0.749	0.599	0.000	0.812	0.724	0.806	0.530	0.467	0.263	0.000
25≤x≤50							1.000	0.926	0.754	0.595	0.017	0.782	0.677	0.796	0.489	0.474	0.254	0.017
50≤x≤75								1.000	0.886	0.776	0.125	0.756	0.661	0.646	0.622	0.623	0.393	0.125
75≤x≤100									1.000	0.883	0.306	0.676	0.571	0.301	0.564	0.900	0.537	0.306
100≤x≤300										1.000	0.245	0.487	0.515	0.257	0.629	0.781	0.811	0.245
300≤x≤MAX											1.000	0.015	-0.220	-0.390	0.053	0.406	0.319	1.000
5≤x≤10 (STD)												1.000	0.732	0.569	0.536	0.472	0.167	0.015
10≤x≤25 (STD)													1.000	0.608	0.542	0.420	0.346	-0.220
25≤x≤50 (STD)														1.000	0.356	-0.043	0.022	-0.390
50≤x≤75 (STD)															1.000	0.362	0.537	0.053
75≤x≤100 (STD)																1.000	0.549	0.406
100≤x≤300 (STD)																	1.000	0.319
300≤x≤MAX (STD)																		1.000

Annex E.4 - Loading Plot of non-spray-dried and spray-dried mixtures.

Figure E.3 - Loading Plot of all the mixtures (non-spray-dried and spray-dried mixtures.